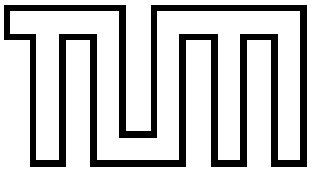

FAKULTÄT FÜR INFORMATIK

Lehrstuhl für Echtzeitsysteme und Robotik

DER TECHNISCHEN UNIVERSITÄT MÜNCHEN

Automation of a Portable Heart-Lung Machine and Patient Monitoring with Data Mining Methods

Benedikt Michael Baumgartner

Vollständiger Abdruck der von der Fakultät für Informatik der Technischen Universität München zur Erlangung des akademischen Grades eines Doktors der Naturwissenschaften (Dr. rer. nat.) genehmigten Dissertation.

Vorsitzender:	Univ.-Prof. Gudrun J. Klinker
Prüfer der Dissertation:	1. Univ.-Prof. Dr. Alois Knoll
	2. apl. Prof. Dr. Robert Franz Bauernschmitt

Die Dissertation wurde am 28.06.2013 bei der Technischen Universität München eingereicht und durch die Fakultät für Informatik am 08.02.2014 angenommen.

Ich versichere, dass ich diese Dissertation selbständig verfasst und nur die angegebenen Quellen und Hilfsmittel verwendet habe.

München, den 25. März 2013 Benedikt Michael Baumgartner

Zusammenfassung

Ein kardiogener Schock ist mit einer hohen Sterberate assoziiert. Meist leiden Patienten schon an irreversiblen Organschäden bevor ein Krankenhaus zur professionellen Behandlung erreicht wird. In den letzten Jahren erhöhten miniaturisierte extrakorporale Kreislauf-Unterstützungssysteme die Überlebenschancen durch eine Erstversorgung des Patienten am Unfallort und während des Transports. Dennoch verhindern Platzmangel in Krankenwagen, Fachkräftemangel und finanzielle Überlegungen den flächendeckenden Einsatz solcher Systeme.

Ein automatisch gesteuertes Unterstützungssystem könnte den Patienten optimal perfundieren, wodurch die Patientensicherheit erhöht und das Notarztteam entlastet wird. Diese Arbeit beleuchtet 2 Aspekte bei der Automatisierung einer portablen Herz-Lungen Maschine: Die Entwicklung robuster Regler für die Steuerung der Herz-Lungen Maschine, sowie die Anwendung von Data Mining Methoden für intelligentes Patientenmonitoring. Tierexperimente ermöglichten die Aufzeichnung von Vitalparametern des Patienten und ihrem Zusammenspiel mit der Herz-Lungen Maschine in verschiedenen Szenarien. Basierend auf diesen Daten wird ein Simulationsmodell und ein hydraulisches Kreislaufmodell erstellt. Das hydraulische Modell bildet das kardiovaskuläre System nach und wird dazu verwendet, robuste Regler für die Pumpgeschwindigkeit der Herz-Lungen Maschine, in Abhängigkeit von Blutdruck und -fluss, zu entwickeln. Vier konkurrierende Regelstrategien wurden implementiert: ein PI-Regler, ein H_∞-Regler, ein Fuzzy-Regler und ein modellbasierter adaptiver Regler. Die Regler werden robust eingestellt und in mehreren Szenarien evaluiert.

Autonome Kreislauf-Unterstützungssysteme erfordern kontinuierliches und ausfallsicheres Patienten-Monitoring. Gewöhnlich entscheidet der Arzt über die Behandlung aufgrund aktueller Patientenparameter und seiner Erfahrung. Erst in den vergangenen Jahren wurden Data Mining und Knowledge Discovery Methoden in medizinischen Fragestellungen untersucht. In dieser Arbeit werden Data Mining Methoden für eine Online-Bewertung des Patientenzustands besprochen. In einer Benchmark-Studie wird gezeigt, wie entsprechende Algorithmen dabei helfen können, die Fehlalarmrate von Patientenmonitoren zu verringern. Hierdurch wird die Behandlungsqualität verbessert und der Einsatz autonomer medizinischer Geräte, wie der geregelten Herz-Lungen Maschine, wird unterstützt.

Abstract

A cardiogenic shock is associated with a high mortality rate. Often, patients suffer from irreversible organ damage before they reach a hospital for professional therapy. In recent years miniaturized extracorporeal circulatory support systems increased the survivor rate by providing primary care for the patient at the emergency site and during transportation. Nevertheless, the limited space in ambulances, the lack of trained staff and financial considerations constrain an area-wide employment of such systems.

An automatically regulated support system could provide optimal perfusion, increasing patient safety and reducing the workload of the emergency team. This work examines two aspects of the automation of a portable heart-lung machine: The design of robust controllers for the regulation of the heart-lung machine, and the application of Data Mining methods for intelligent patient monitoring.

Animal experiments allowed to collect vital patient parameters and their interaction with the heart-lung machine in distinct scenarios. Based on this data a simulation model and a hydraulic circulatory model are established. The hydraulic model replicates the cardiovascular system and is used to design robust controllers, regulating the pump speed of the heart-lung machine dependent on blood pressure and flow. Four concurrent control strategies were implemented: a PI Controller, a H_∞-Controller, a Fuzzy Controller and a Model Reference Adaptive Controller. The controllers are tuned robustly and evaluated in several scenarios.

Autonomous circulatory support systems require continuous and failure-safe patient monitoring. Usually, the medical practitioner decides on the choice of treatment, based on current patient parameters and his experience. Only in recent years Data Mining and Knowledge Discovery methods found their way into medical research. In this work Data Mining methods for the online assessment of the patient's condition are reviewed. In a benchmark study it is shown how such algorithms are able to reduce the false alarm rate of patient monitors. This increases the quality of care and supports the application of autonomous medical devices such as the controlled heart-lung machine.

Acknowledgments

I would like to thank my supervisors Prof. Dr. Alois Knoll and Prof. Dr. Robert Bauernschmitt for giving me the opportunity to work on this thesis, for reviewing my work and for their encouraging support.
After more than four years at the I6 chair, special thanks go to Dr. Gerhard Schrott, Dr. Reinhard Lafrenz and the *Secretoids* for their open ears and support in every matter.
I would also like to thank my colleagues at the German Heart Center for their collaboration, fruitful discussions and for the fun working environment, namely Dr. Ulrich Schreiber, Dr. Stefan Eichhorn, Alejandro Mendoza and Nicole Sprunk.
During the last couple of years, I was given the opportunity to supervise several students for their Master's and Bachelor's thesis. I very much appreciate the contributions of Stefan Drexler, Chris Becker and Kolja Rödel to this work.
I am happy that I have met Lukas Gorzelniak and Christoph Staub. Not only did they proofread this thesis, but they also shared the good and bad times in doing a PhD and became reliable companions.
I say thank you to my close friends Stefan Synek and Dr. Tobias Schmidt for distracting me with skiing trips, safaris or alike and for their honest support and advices concerning all aspects of life.
Last but not least I am deeply grateful for my family's support. My parents and brothers and sisters always give me orientation and confidence when needed. I know, that I will never be able to pay back their encouragement and trust in me.

Contents

Abstract . . . . . **vii**

Abbreviations. . . . . . **xix**

I Introduction **1**
1 Motivation and Goals 1
2 Methodology and Contribution 3
3 Organization 6

II Medical Background and Extracorporeal Circulation **9**
1 The Heart 9
2 The Circulatory System 10
2.1 Hemodynamics. 11
3 The Heart-Lung Machine 13
3.1 Venous Reservoir. 14
3.2 Blood Pumps 15
3.3 Oxygenators 15
3.4 Cannulation. 15
3.5 Miniaturization and Application outside Operating Rooms 16
4 Perfusion during Extracorporeal Circulation 16
4.1 Pulsatile vs Constant Flow Perfusion 17
4.2 Patient Monitoring during Extracorporeal Circulation 18
4.3 Mean Arterial Pressure 18
4.4 Central Venous Pressure. 19
4.5 Pump Flow 19
4.6 Hematocrit and Hemodilution 20
4.7 Oxygen Delivery 20

III State of the Art **23**
1 Hydraulic Mock Circulation Systems 23
2 Mathematical Models and Circulatory System Simulations 29
3 Automatic Control of Heart-Lung Machines 32

IV Animal Experiments 35
1 Overview 35
2 Anaesthesia, Preparation and Sensor Placement 36
3 Experimental Procedure and Results 37
3.1 Steady State with and without ECCS 37
3.2 Medication: Vasoconstriction and Vasodilation 38
3.3 Pump Speed Variation 39
3.4 Cannula Obstruction 40
4 Prototype Controller Test 42
5 Summary 44

V Development and Automation of a Hydraulic Circulatory Mock Model. 45
1 Hydraulic Circulatory Model 45
1.1 Layout and Components 46
1.2 Model Aggregation 52
1.3 Model Validation 55
2 Proportional-Integral-Controller 57
2.1 Control Design 58
3 H_∞-Controller 60
3.1 Control Design 62
4 Model Reference Adaptive Controller 63
4.1 Control Design 64
5 Fuzzy–Controller 66
5.1 Control Design 67
6 Results 68
6.1 Changes of Target Value 68
6.2 External Perturbations 69
6.3 System Parameter Variation 71
6.4 Discussion 75
7 Summary 77

VI Medical Data Mining for Intelligent Patient Monitoring 79
1 Motivation and General Approach 79
1.1 Requirements for Automated ECCSs in Non-Clinical Environments . . 80
1.2 The Clinical Decision Support Approach 80
2 Data Mining and Knowledge Discovery 81
2.1 Data Mining in Medical Applications 82
2.2 Discretization Methods 84
2.3 Feature Selection Approaches 85
2.4 Data Mining Algorithms 86
2.5 Performance Analysis 92
3 Related Work 93

VII Case Study: False Alarm Rate Reduction of Patient Monitors 97
1 Case Study: Reducing False Alarm Rates of Patient Monitors 97
2 Persitency of False Alarms in Patient Monitoring 98

3 Data Source and Selection Criteria . . . 99
4 Preprocessing and Feature Design . . . 100
4.1 Scope-based Features . . . 101
4.2 Interval-based Features . . . 101
4.3 Sample-based Features . . . 102
4.4 Feature Overview . . . 103
5 Classification and Evaluation Criteria . . . 104
6 Results and Discussion . . . 104

VIII Conclusion . . . 109
1 Summary . . . 109
2 Future Work . . . 110

A Appendix . . . 113
1 Classification of Complete Training Sets . . . 113
2 Classification of Asystole Alarms . . . 114
3 Classification of Brady Alarms . . . 114
4 Classification of Tachy Alarms . . . 115
5 Classification of V-Fib/Tach Alarms . . . 115
6 Classification of V-Tach Alarms . . . 116

Publications . . . 117

Bibliography . . . 119

List of Figures

I-1 Application fields of the Lifebridge HLM. 3

II-1 The human circulatory system 10
II-2 Perfusion in the cardiovascular system 11
II-3 State of the art HLMs 13
II-4 HLM components and connection to the patient 14
II-5 Roller and centrifugal pump 15
II-6 Multiple influences on a patient under ECC support 17
II-7 Oxyhemoglobin dissociation curve 21

III-1 Three- and four-element Windkessel models 25
III-2 Schematic of hydraulic mock model. 26
III-3 Hydraulic mock circulation loops. 27
III-4 Structured representation of the arterial circulatory system. 29

IV-1 Experimental protocol 36
IV-2 Experimental setup 37
IV-3 Steady state measurements. 38
IV-4 Medication 39
IV-5 Pump speed variation. 40
IV-6 Cannula obstruction 41
IV-7 Fuzzy sets for prototype controller 42
IV-8 Control during application of vasoactive drugs 43

V-1 Schematic and physical layout of mock model 47
V-2 Comparison of measured and simulated motor speed 49
V-3 Collected data for pump identification 49
V-4 Comparison of predicted and measured pump values 50
V-5 Network representation of the three-element Windkessel model. 51
V-6 Comparison of linear and nonlinear system representation. 56
V-7 Comparison of simulation model and hydraulic model. 57
V-8 Comparison of hydraulic model and animal experiments 58
V-9 PI-Controller structure diagram. 58

V-10 Stability boundaries for PI parameters . . . 59
V-11 System's step response for different PI parameters. . . . 60
V-12 Simple control loop and H_∞-standard-problem. . . . 61
V-13 Standard H-∞ weighting scheme. . . . 61
V-14 Amplitude response of plant for H_∞-Control design . . . 62
V-15 Amplitude response of W_S and W_T for H_∞-Control. . . . 63
V-16 H_∞-Control step response . . . 63
V-17 Direct Adaptive Control loop. . . . 64
V-18 Direct MRAC loop. . . . 64
V-19 Step response of the MRAC reference model . . . 65
V-20 MRAC identification process. . . . 66
V-21 General structure of a Fuzzy-Controller. . . . 67
V-22 Fuzzy sets for controller variables . . . 68
V-23 Control during changes of target value (scenario 1). . . . 70
V-24 Control during external perturbation (scenario 2). . . . 72
V-25 Plant characteristics during variation of R_p. . . . 73
V-26 Control during variation of peripheral resistance (scenario 3). . . . 74

VI-1 The knowledge discovery process . . . 83
VI-2 Risk level assessment applying K-Means clustering . . . 95

VII-1 Sample from the training set . . . 100
VII-2 Morphological features of blood pressure waveform . . . 102

VIII-1 Supervising Unit Layout . . . 111

List of Tables

II.1 Indications for the application of Heart-Lung Machines 17
II.2 Arterial Pressure Management 19
II.3 Recommended flow rates per BSA 20

III.1 Comparison of selected hydraulic mock circulation loops 28

V.1 Capacity measurements of the closed chamber 52
V.2 Direct MRAC scheme for second-order SISO plants 65
V.3 IAE during changes in the target value 69
V.4 IAE during external perturbations 71
V.5 IAE under system parameter variation 75

VI.1 Confusion matrix 92

VII.1 Distribution of the training set over class and alarm type 99
VII.2 Thresholds for the normality range feature 103
VII.3 Physiological signals and applied features 104
VII.4 Applied discretization, feature selection and classification methods 105
VII.5 Classification results and alarm suppression rates 106

Abbreviations

ABP Arterial Blood Pressure

ANN Artificial Neural Network

BSA Body Surface Area

CDSS Clinical Decision Support System

CDS Clinical Decision Support

CPB Cardiopulmonary Bypass

CPR Cardiopulmonary Resuscitation

CVP Central Venous Pressure

CVS Cardiovascular System

DM Data Mining

DT Decision Tree

ECC Extracorporeal Circulation

ECCS Extracorporeal Circulation Support System

ECG Electrocardiogram

ECMO Extracorporeal Membrane Oxygenation

EFR Extracorporeal Flow Rate

FiO$_2$ Fraction of inspired Oxygen

FUZZYC Fuzzy Controller

GPC General Predictive Controller

HINFC H_∞-Controller

HLM Heart-Lung Machine

HR Heart Rate

HRV Heart Rate Variability

IAE Integral of Absolute Error

ICU Intensive Care Unit

IVC Inferior Vena Cava

kNN k-Nearest-Neighbor

KD Knowledge Discovery

LVAD Left Ventricular Assist Device

MAP Mean Arterial Pressure

MRAC Model Reference Adaptive Controller

NB Naive Bayes

NEP Norepinephrine

PAP Pulmonary Arterial Pressure

PIC Proportional-Integral Controller

RA Right Atrium

RMSE Root-Mean-Square Error

SNP Sodium Nitroprusside

SpO_2 Oxygen Saturation

SU Supervising Unit

SVC Superior Vena Cava

SVM Support Vector Machine

TPR Total Peripheral Resistance

VAD Ventricular Assist Device

Chapter I

Introduction

Contents

1 **Motivation and Goals** 1
2 **Methodology and Contribution** 3
3 **Organization** 6

1. Motivation and Goals

The World Health Organization assumes that by 2015 cardiovascular diseases will be the number one cause of death worldwide. Each year approximately 12 million people die due to cardiovascular diseases [16]. In Germany cardiovascular diseases were the most common cause of death in 2011 (40.2% from a total of 852.328). The predominant group suffered from an ischemic heart disease (127.101), followed by acute and recurring myocardial infarct (55.286)[17].
Cardiac insufficiency or myocardial infarcts can cause a cardiogenic shock, associated with a mortality of up to 75% [18]. With the malfunction of the heart, cardiac output is decreased, leading to hypoxia and, eventually, organ failure. The high rate of mortalitity could be decreased with an early application of an Extracorporeal Circulation Support System (ECCS). An ECCS pumps venous blood from the body through the external device, where it is enriched with oxygen, and back into the human circulatory system again. I.e., the ECCS takes over the function of the heart and the lungs. By providing a sufficient blood flow and oxygenation, patients can be stabilized until they reach a cardiac center for in-depth care and therapy. Cardiopulmonary Bypass (CPB) with a Heart-Lung Machine (HLM) is routine practice in cardiac surgery, but rarely for patients undergoing emergency resuscitation, due to the large size and complicated set-up of currently available systems [19]. Only in recent years companies started to develop compact and portable ECCSs, that, together with defibrillators and mechanical cardiopulmonary resuscitation devices, complement the family of emergency cardiac support systems.
In clinical settings HLMs allow operations at the rested heart and guarantee sufficient organ perfusion for the patient. They are operated by trained perfusionists in cooperation

with anaesthesiologists and cardiac surgeons. Monitoring systems constantly observe vital parameters during the operation. Miniaturized monitoring systems, the construction of smaller and more efficient pumps and oxygenators facilitated the development of portable systems, intended for both clinical and emergency applications. With such portable ECCSs patients can already be perfused during transportation to the clinic, increasing the survivor rate.

However, the shift from clinical to emergency applications holds some obstacles and has special requirements. First, space in ambulances or helicopters is limited. Therefore, additional staff (perfusionist, surgeon) might not be available. And second, financial considerations limit the availability of additional manpower. According to Feindt et al. [20], at least two trained medical practitioners are required: One experienced surgeon, that is able to perform the percutaneous cannulation and one perfusionist, operating the HLM.
Apart from the organizational problems, also safety aspects can constrain the application of an ECCS as an emergency device. A comprehensive patient monitoring system, comparable to those applied in operating rooms, is not available. Furthermore, sensor data can be disturbed more easily, for example by vibrations during transportation. And the emergency staff might be stressed in critical situations and not able to take care of the patient and the machine at the same time.
Therefore, an autonomous device, providing optimal perfusion, based on online data of the patient, is desirable. It could reduce the workload of the paramedics in stressful situations and increase the patient safety and quality of care, by continuous observation of vital patient parameters, and according adjustments of machine parameters. Still, the automation task is intrinsically complex: Until now, the regulation and control of characteristic and critical variables are managed by human decisions and actions, dependent on the perfusionist experience, sensibility and habits [21]. Schwarzhaupt et al. identified the need for an objective observer for automated HLM operation and suggested decision trees and neural networks for the assessment of the physiological patient status and the detection of particular events, such as loss of volume or stenosis [22].

This work shall contribute to medical device automation in non-clinical applications. The control of a portable HLM, the Lifebridge B_2T system [23] (see Figure I-1), serves as a real-world application. A particular focus of this thesis is on the design and evaluation of control strategies for robust pump speed control. The pump speed of the HLM has direct impact on two major perfusion parameters, the blood pressure and the blood flow in the patient's Cardiovascular System (CVS).
The context of HLM applications in emergency situations is different from the standard clinical setting. For a secure and robust control system, a closed-loop control is favorable. Perfusion will be more adequate, if the autonomous HLM is aware of the situational requirements, the physical and the physiological conditions of the patient. Therefore, Data Mining (DM) methods in medical applications are examined and applied to the well-known problem of false alarm rate reduction in patient monitoring.
Two major goals can be formulated for autonomous Extracorporeal Circulation (ECC) during emergency situations or transportation:

1. **Adequate Perfusion:** Based on the current state of the patient an adequate perfusion shall be provided. Optimal perfusion depends on multiple parameters, including age, height, sex and more (see Chapter 4). A certain blood pressure and blood flow

needs to be maintained in order to deliver oxygen to organs and tissue.

2. **Robust Patient Monitoring:** In order to provide adequate perfusion the patient and the HLM must be continuously monitored. Patient and machine data must be verified and analyzed, since this data is the basis for autonomous HLM control. Also, due to the special requirements in non-clinical applications (sensor malfunction, detachment etc.), robust monitoring of vital patient parameters is needed.

(a) Cardiac surgery at the German Heart Center Munich.

(b) Emergency transportation. From [23].

Figure I-1.: The Lifebridge B_2T is a portable HLM designed for two fields of applications: for cardiac surgery (a) and for emergency transportation (b).

2. Methodology and Contribution

This thesis looks into two aspects of ECCS automation for non-clinical applications: (i) The design and evaluation of robust pump speed controllers and (ii) the potentials of DM methods for intelligent patient monitoring. The automation of a HLM serves as a real world application. A holistic approach was chosen to design and to examine pump speed controllers. This approach included animal experiments, a hydraulic circulatory mock model and a virtual model of the CVS and the HLM.
Literature shows, that each of the three approaches had been applied before. Exemplarily, Meyrowitz [24] developed a computer model of the CVS and a HLM and also conducted a trial animal experiment, but misses out a hydraulic model. Misgeld [25] on the other hand built up a hydraulic model and a system simulation, but did not conduct animal experiments. Each method is justified on its own, but has limitations. For example, animal experiments do not allow the repetition of specific procedures or tests with the same

setting, such as a computer simulation or a hydraulic model allows. A hydraulic model is helpful for hardware and software tests in a standardized in-vitro setting, but cannot simulate oxygen delivery. And finally a computer simulation can be close to reality but, exemplarily, is unable to include unpredictable events, such as human interventions, as they can happen during animal experiments. Only the combination of all approaches gives a comprehensive overview on HLM automation and, at the same time, a deeper insight into control engineering in the medical field. Together with DM methods for patient monitoring, a better understanding of the possibilities and obstacles in medical device automation is elaborated.

Animal Experiments: The major goal of the experiments was to record reference data of a patient (pig) under ECC. Vital parameters of the patient and important parameters of the HLM were recorded. This data served as ground truth data for both the hydraulic mock model and the simulation. Furthermore, the animal experiments allowed the evaluation of several sensor and data acquisition devices. And finally, a prototype controller for automated pump speed control of the HLM could be tested during one experiment. A tailor-made software was developed in order to aggregate and visualize the parameters from different devices in one place. In total, 10 experiments were conducted, in accordance with legal and ethical guidelines, following a specific protocol (see Chapter IV).

Hydraulic Mock Model: The circulatory mock model was needed in order to design, test and evaluate control strategies for pump speed control in a standardized physical setting. The model represents the CVS under ECC and was validated with data from animal experiments. The design of the model followed the well-known Westerhof model [26], which is said to give the best trade-off between simplicity and accuracy by many researchers (see Chapter III). Since the components of the mock circulation can be represented in a mathematical way, a complete analytical model of the system (patient and HLM) was derived and transfered to a state space representation, which is the most common system description in control engineering. Four state-of-the-art controllers were designed and evaluated in several test cases (see Chapter V).

Simulation: A mathematical description also serves as the basis for the simulation approach. The heart, lungs, venous and arterial trees can be represented by electrical circuits, consisting of resistors, capacitors and inductances. A network of those basic elements is able to replicate the complete human CVS. Also models for temperature or oxygen delivery under ECC can be implemented in a computer simulation. During this project a CVS simulation was extended with components of a HLM, such that it replicated the CVS under ECC. Again, the simulation can be validated with animal data and eases the design and evaluation of control strategies. The simulation approach is thoroughly described in the dissertation of Alejandro Mendoza [27].

Patient Monitoring: An autonomously operating HLM can only be successful with reliable patient and device data. Therefore, secure and robust patient monitoring is needed. The vision of intelligent monitoring, i.e. the automatic assessment of the patient state,

requires fast and accurate algorithms, detecting significant events and changes in the patient's vital parameters. Only in recent years, researchers think about applying Machine Learning and DM algorithms in medical applications. Especially the area of alarm management on Intensive Care Units (ICUs) has become a major focus of interest. In this work DM methods for monitoring in medical applications are reviewed and a benchmark test is performed on a well-known database from ICU monitoring.

This work evolved from contributions of several project collaborators. Particularly, it complements the dissertation of Alejandro Mendoza [27]. While he focuses on the simulation approach and control with (adaptive) Fuzzy Controllers (FUZZYCs), central topics of this work are the hydraulic mock model, the design and evaluation of robust pump speed controllers, and DM methods for patient monitoring. In particular, contributions to the following aspects are made:

Medical Data Fusion: The *AutoMedic* software-framework [2] was co-developed. It manages the aggregation of data streams of multiple sensors and was predominantly developed for animal experiments. With different interfaces such as RS232, Ethernet, analog inputs or CAN-Bus, vital patient parameters (blood pressure, oxygen saturation, ECG, heart rate, ...) and key data from the Lifebridge HLM (pump speed, produced flow, inlet and outlet pressure) were recorded and visualized. Due to its modular design, the library also served as a basis for the simulation and hydraulic model. With a communication module channel data can be streamed and also processed by third-party software such as Matlab.

Circulatory Mock Model: A physical replication of the CVS under ECC was set-up. The CVS is represented by two resistors and an air chamber to replicate the peripheral and aortic resistance and capacity. After an extensive literature research the three-element Westerhof model [26] was chosen as a basis for the layout and design. A complete mathematical description of physical CVS representation and a centrifugal pump, replicating the ECCS, is derived. The model is validated with data from animal experiments and the analytical description is also verified. The differential equations, representing the mock model, are transfered to a linearized state space representation, which is used for the design of pump speed controllers. Both resistance elements and the pump speed can be controlled by the *AutoMedic* framework, or alternatively, the real-time environment of Matlab/Simulink.

Robust Pump Speed Controllers: Based on the mathematical model, several pump speed controllers for flow and pressure control were implemented. As a classical feedback controller a Proportional-Integral Controller (PIC) was chosen. From the field of Adaptive Control a Model Reference Adaptive Controller (MRAC) was designed. The H_∞-Controller (HINFC) represents the Robust Control family and, finally, a FUZZYC was selected from Intelligent Control approaches. The controllers were tuned robustly and tested in three scenarios, including step changes of the target values, external perturbations and variations of the peripheral resistance. The design process is described thoroughly and results are compared to other works in HLM automation.

Medical Data Mining: As mentioned before, an ideal HLM controller would have knowledge about the current constitution of the patient, so that it is able to recognize and cope with contextual events, such as sensor failure or intervention of the staff. Motivated from Clinical Decision Support Systems (CDSSs), the challenges of automated ECC and medical DM are identified. Related work is reviewed and commonly used DM algorithms are introduced. Finally, those algorithms are tested on a well-known ICU database [28] and contribute to

False Alarm Rate Reduction in Patient Monitoring: The high FA rate is a persistent problem in patient monitoring and DM or Machine Learning algorithms are rarely applied, due to the lack of publicly available large-scale databases. During this work an online survey on monitoring alarms was developed and 23 surgeons from the *German Heart Center Munich* contributed to an alarm database. A classical DM approach, including feature extraction, learning and classification, is followed and state of the art algorithms are applied in a benchmark test with the goal to correctly classify alarm situations. Instead of only observing one parameter, a multimodal approach is followed, considering data from multiple sources at the same time. Surprisingly, literature is sparse in this field. The results are quantitatively compared to data from another study [29] and also discussed qualitatively.

3. Organization

This work resulted from a cooperative project between the *Department of Informatics, Technische Universität München* and the *German Heart Center Munich*. The project team included computer scientists, electrical and mechanical engineers and cardiac surgeons. There was also a close collaboration with industry (*Lifebridge Medizintechnik AG*, *Sorin Group*). This means, that some contributions of this thesis are the result of teamwork. It also means, that some results have been published in journals or have been presented at conferences already. This will be clearly indicated at the beginning of a section. The thesis is structured as follows:

Chapter II describes the medical fundamentals needed to understand this work. First, an introduction to the human CVS is given (sections 1 and 2) and hemodynamic aspects are described mathematically (2.1). In the following, the evolution of the HLM is outlined and main components are described (3). Finally, major perfusion strategies and parameters are described with a focus on hemodynamic aspects (4).

Chapter III gives an overview on the state of the art. Previous physical setups for CVS modeling are described, starting in the 1970ies, including 3 and 4-element Windkessel models (section 1). The models are reviewed in terms of accuracy and complexity. Section 2 introduces mathematical CVS models and simulation approaches, which are predominantly based on the model of Avolio [30]. The chapter ends with a summary of the few previous approaches towards HLM automation (3).

Chapter IV describes the animal experiments as the first approach towards HLM automation. First, an overview is given, introducing the experimental protocol as well as general preparations and sensor placement (section 1 and 2). Section 3 reports the experimental procedures in more detail and their results. In section 4 a prototype controller is introduced which was tested during one experiment, counteracting the effects of vasoactive drugs.

Chapter V is a core part of this thesis and introduces the physical setup of the CVS under ECC. First, the layout and components of the circulatory mock model are depicted and, at the same time, a mathematical describtion is derived. Differential equations are formed, that describe the relationships between the pump speed of the HLM, the produced flow and the pressure difference between pump inlet and outlet. The analytical model is transfered to a linearized state space representation and both, the physical setup and its analytical representation, are validated with data from animal experiments (section 1). In the following, four state-of-the-art controllers are designed, based on the mathematical system description. The control task is to regulate the pump speed, based on pressure or flow. A PIC (section 2), a HINFC (section 3), a MRAC (section 4) and a FUZZYC (section 5) were designed robustly and tested in three scenarios. Results are presented (section 6), followed by a discussion (section 6.4) and a summary (section 7).

Chapter VI motivates the application of DM and Knowledge Discovery algorithms in medical control applications. Considering the special requirements of automated ECCSs in non-clinical environments, goals for a CDSS are formulated (section 1). Section 2 summarizes standard DM algorithms and highlight the challenges in medical DM (section 2.1). Finally, section 3 summarizes the related work in medical DM and Knowledge Discovery (KD), with a focus on the classification of online patient data.

Chapter VII shows the applicability of DM methods for patient monitoring with a benchmark study on a well-known database from ICU monitoring. First, the problem of false alarm rates is described (section 2). Sections 3 – 5 follow the classical machine learning process and explain the training data and selected features, as well as the classification process. The chapter closes with the achieved results and a discussion (section 6).

Chapter VIII concludes this thesis and gives an outlook on future work.

Chapter II

Medical Background and Extracorporeal Circulation

Contents

1	**The Heart**	9
2	**The Circulatory System**	10
3	**The Heart-Lung Machine**	13
4	**Perfusion during Extracorporeal Circulation**	16

This chapter starts with a short introduction of the human circulatory system. Only the aspects needed to understand this work will be mentioned. Detailed information on the human physiology can be found in medical textbooks [31–33]. After an introduction to ECC and HLMs the physiological and hemodynamic aspects of ECC will be illustrated in Section 4. Again, only the mechanisms relevant for this work are described.

1. The Heart

The human heart is a muscular organ pump, which pumps blood through the systemic and pulmonary circuit. The heart is divided into a left and right heart, separated by the septum (see Figure II-1). Both parts are again divided into an atrium for blood collection and a ventricle chamber for blood ejection. The chambers are connected by valves, preventing the backflow of blood. Blood flow in the heart is achieved by rhythmic contraction of the left and right ventricles. The heart is connected to the vascular system by the aorta ascendens and the arteria pulmonalis on the arterial side, and the vena cava superior/inferior and vena pulmonalis on the venous side.
Oxygen-poor blood from the vascular system is collected in the right atrium and, after opening of the tricuspid valve, enters the right ventricle. After the contraction of the heart, the pulmonary valve opens and the blood is pumped into the lungs, where a gas exchange takes place. Carbon dioxide (CO_2) is exhaled and the blood is enriched with oxygen (O_2) again. The oxygen-rich blood enters the left atrium and, passing the mitral valve, the left

ventricle. When finally the aortic valve opens, the blood enters the aorta from where it is delivered into the vascular system. Blood supply for the heart itself is delivered by coronary arteries.

During standard CPB applications in an operating room, the heart is decoupled from the circulatory system and the pumping function is taken over by an ECCS. Since this thesis deals with the automation of a *portable* HLM, the preconditions are slightly different. In situations where the portable HLM is used, cannulation is done via the femoral artery and femoral vein. This means, that the heart is still connected to the circulatory system, however, is not able to produce enough cardiac output for adequate perfusion.

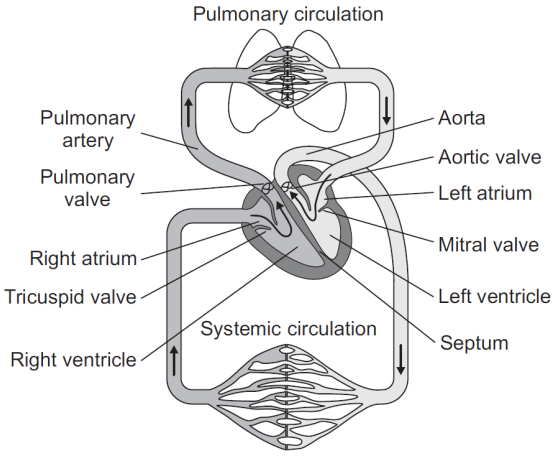

Figure II-1.: Schematic representation of the human circulatory system with the heart, pulmonary and systemic circulation. From [25].

2. The Circulatory System

The circulatory system can be divided into the pulmonary circulation and the systemic (body) circulation, connected by the heart (see Figure II-1). The main purpose of the circulatory system is the delivery of oxygen, nutrients and other substances to organs and different tissue areas and the removal of CO_2. The vessels leading away from the heart are called arteries, the ones leading towards the heart are called veins. Arteries, except for the pulmonary arteries, transport oxygen-rich blood from the heart to organs and tissue. Veins, except for pulmonary veins, carry oxygen-poor blood from the vascular system back to the heart.

The vascular system can be also regarded as an arterial high-pressure and a venous low-pressure system. The mean blood pressure in the low-pressure system does usually not exceed 20 mmHg while the pressure of the high-pressure system is between 60 and 100 mmHg. About 85% of the total blood volume is in the low-pressure system [32]. Figure II-2 shows the perfusion in human pulmonary and systemic circulation under normal physiological conditions. From the left ventricle the blood is transported through the aorta, which separates into big arteries going to organ and tissue areas. Arteries are separated again into

arterioles and capillaries, where blood gases, nutrients etc. are exchanged between the blood and interstitial spaces.

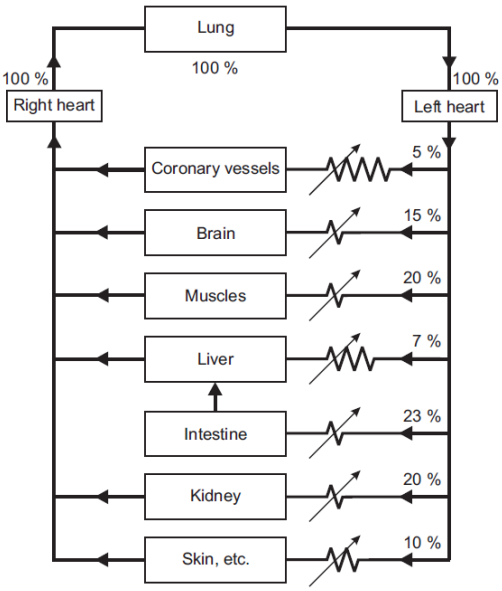

Figure II-2.: Perfusion in the CVS during rest. Shown is the distribution of the cardiac output on major body organs depending on different vascular resistances. From [25], modified from [32].

2.1. Hemodynamics

Blood flow is caused by pressure differences in the circulatory system. Blood flows from areas with high pressure into areas with low pressure. Thereby it has to overcome an inner and vascular resistance R, depending on the diameter and the length of the vessel. Analogous to Ohm's law the relation between the pressure difference ΔP and current I can be formulated as

$$I = \frac{\Delta P}{R} \tag{II.1}$$

with I describing the blood volume ΔV per time Δt, passing the cross-sectional vessel area:

$$I = \frac{\Delta V}{\Delta t}. \tag{II.2}$$

With the decreasing diameter of the vessels, the resistance increases. The Hagen-Poiseuille-Law describes a stationary and laminar current in a rigid cylinder and can serve as a rough approximation of the blood flow, depending on the vessel's inner radius r, its length l and the fluid viscosity (η):

$$I = \frac{r^4 \pi \Delta P}{8 \eta l} \tag{II.3}$$

Using Equation II.1, the resistance of a vessel can be expressed as

$$R = \frac{8\eta l}{r^4 \pi}. \tag{II.4}$$

The resistances of the systemic vascular system are cumulated in the Total Peripheral Resistance (TPR) which is calculated from the Mean Arterial Pressure (MAP) and the cardiac output (CO):

$$TPR = \frac{MAP}{CO}. \tag{II.5}$$

The MAP is the mean value of the arterial pressure waveform. The cardiac output is the Heart Rate (HR) times the stroke volume. Another important parameter in this context is the Central Venous Pressure (CVP). It is measured in the right atrium and reflects the ability of the right heart to pump blood [25]. During CPB it is an important measure to prevent the venous systemic vessels from collapsing.

The Hagen-Poiseuille-Law does not consider the elasticity of the vessels and the Non-Newtonian characteristics of blood (viscosity is not constant but depends on the flow characteristics). The flow resistance is usually higher than the calculated value.

A more accurate flow model can be derived when the elasticity of the arteries is considered. Flow of incompressible fluid through elastic tubes can be described by the Navier-Stokes equation, which, in its general form, reads

$$\frac{\partial \mathbf{v}}{\partial t} + (\mathbf{v}\nabla)\mathbf{v} = -\frac{1}{\rho}\nabla \mathbf{p} + \frac{\eta}{\rho} \triangle \mathbf{v} + \mathbf{f_f} \tag{II.6}$$

with $\mathbf{v}$ representing the flow velocity, ρ the fluid's density, $\mathbf{p}$ the pressure, η the dynamic viscosity and $\mathbf{f_f}$ the body force applied to a volume element. Based on several assumptions and simplifications, Misgeld [25] shows how to simplify the nonlinear Equation II.6 to a system of differential equations, yielding

$$p_n - p_{n+1} = L_n \cdot \frac{\partial q_n}{\partial t} + R_n q_n \tag{II.7}$$

$$q_n - q_{n+1} = C_n \cdot \frac{\partial p_n}{\partial t} \tag{II.8}$$

with the parameters

$$L_n = \frac{9\rho\Delta l_n}{4\pi r_n^2} \qquad R_n = \frac{81\mu\Delta l_n}{8\pi r_n^4} \qquad and \qquad C_n = \frac{3\pi r_n^3 l_n}{2E_n d_n}. \tag{II.9}$$

Equations (II.7) and (II.8) describe the relation between pressure and flow in the n-th vascular compartment, where E represents the elastic modulus, d the tube gauge and μ the kinematic viscosity. Rideout and Dick [34] have shown how to derive the parameters L, C and R. They also show how to construct electrical circuits, representing a vascular compartment. L describes the fluid inertance, C the vascular compliance and R the vascular resistance.

The presented relationships form the basis of computer models and hydraulic representations of the circulatory system as presented in chapters III and V. Using physical data (length, radius, blood viscosity, etc.), models of the circulatory system can be built with different complexity. Exemplarily, the famous Avolio-model of the arterial tree consists of 128 compartments [30].

3. The Heart-Lung Machine

The age of modern heart-surgery with HLMs starts on May 6, 1953, when John Heysham Gibbon Jr. successfully closed an atrial septal defect under surgical vision and CPB, after many years of research beginning in the 1930s [35]. The patient, an adult woman, recovered completely and the normal circulation was detached from the heart for 25 min. Already in 1812 Le Gallois thought about an artificial replacement of the heart: If one could substitute for the heart a kind of injection of arterial blood, either naturally or artificially made, one would succeed in maintaining alive indefinitely any part of the body whatsoever [36]. In 1885, Max von Frey and Max Gruber developed one of the first prototypes of a HLM, containing a film oxygenator and a syringe pump for closed-loop system perfusion. Half a century later, along with technical evolution and a deeper understanding of human physiology, Gibbon made a revolutionary breakthrough and presented a HLM with a roller pump and a film oxygenator [37]. His work was technically and financially supported by IBM. Further developments, including bubble and membrane oxygenators, fostered advances in heart surgery.

During cardiac surgery, HLMs take over the pumping function of the heart and the gas exchange function of the lungs. Although minimally invasive operation techniques have been established during the last years, a vast amount of interventions is conducted at the rested heart. With an ECCS a sufficient perfusion and, hereby, a sufficient oxygenation of the patient is ensured [38]. ECC has turned from first experimental perfusion of organs into a standard procedure of heart surgery. It will always be necessary when operations require a rested heart, or if circulation support of the beating heart is necessary [39].
Figure II-3 shows two state of the art HLMs, the S5 HLM from Sorin, a model used in operating theaters, and the Lifebridge HLM, a portable ECCS designed for short-term peripheral cardiopulmonary bypass in emergency circulatory resuscitations [40].

(a) (b)

Figure II-3.: State of the art HLMs. S5 HLM from Sorin (a) and portable HLM from Lifebridge (b). From [23, 41].

In a basic setup a HLM consists of the following main components:

- Venous Reservoir
- Blood Pump

- Oxygenator
- Heat Exchanger
- Filter
- Arterial and Venous Cannula

A HLM replaces the function of both the lungs (gas exchange) and the heart (provide energy to ensure circulation of blood). Typically, blood is drained by gravity through the cannulas in the Superior Vena Cava (SVC) and Inferior Vena Cava (IVC) or IVC and Right Atrium (RA) into the HLM, from where it is pumped (with a roller or centrifugal pump) through the artificial lung ("oxygenator") back into the systemic vasculature, through an arterial cannula placed in the ascending aorta [42]. The functional principle of the Lifebridge HLM is shown in Figure II-4 with the main components of the HLM connected to a patient via femoral cannulation.

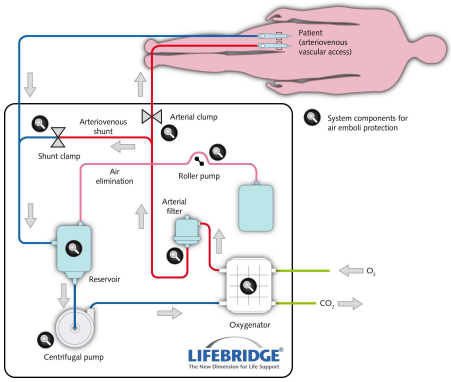

Figure II-4.: Functional principle of a HLM with main components and peripheral cannulation of the patient. From [23].

3.1. Venous Reservoir

The reservoir collects blood from the venous system of the patient. It serves as a buffer for fluctuations in venous drainage and is a source of fluid for rapid transfusion [42]. Usually the drainage is passive, since the reservoir level is lower than the patient level. Additionally, blood from the surgical field and vent suction devices can be collected in the reservoir. Reservoirs are either designed as hard shells or soft bags. The rigid design seems to be superior, since the hard shells are usually bigger and air elimination and volume measure are easier [43]. Hard shell reservoirs are typically used in open-loop systems with the advantage of a better air elimination. During ECC the filling level must be observed constantly, since an empty reservoir would lead to the delivery of air into the arterial line.

3.2. Blood Pumps

Two kind of blood pumps are used in today's HLMs: Displacement/roller pumps and centrifugal pumps. The pumps have to deliver sufficient volume, minimize damage to blood cells and operate reliably. In operating theaters roller pumps are commonly used. Their setup is simple, cheap and allows a pulsatile blood flow. Two rollers are placed opposite to each other and move the blood by occlusion of the surrounding tubing. However, blood traumatization in long-period ECC application is higher than for centrifugal pumps [44]. Centrifugal pumps are predominantly used in portable HLMs. The pump head is driven by an electro motor via magnetic coupling and, by the rotational speed, kinetic energy is transfered to the liquid [38]. Centrifugal pumps do not transport air bubbles, since the lower density of air compared to blood keep possible bubbles in the pump center. However, air bubbles in the pump significantly reduce the produced pump flow. Figure II-5 displays schematic drawings of a roller pump and a centrifugal pump to illustrate the functional principle of the two different types.

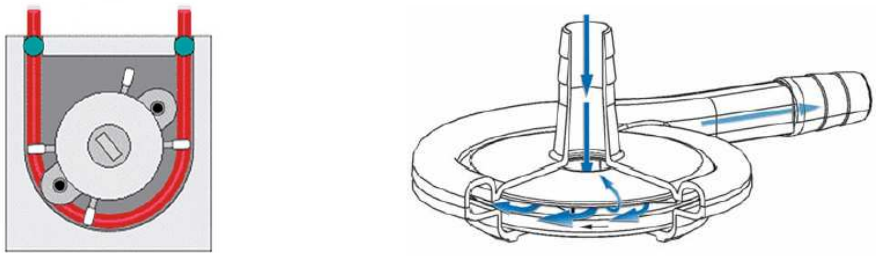

(a) (b)

Figure II-5.: Roller (a) and centrifugal (b) pump. From [43].

3.3. Oxygenators

Oxygenators take over the function of the lungs, i.e. to exchange vital gases [39]. Membrane oxygenators are routinely used to oxygenate the blood. They have a semi-permeable membrane, usually made of polypropylene, separating gas from blood. State of the art oxygenators allow operating times between 6 and 8 hours. Due to diffusion processes there is an exchange between O_2 and CO_2. The driving force of these processes is the partial pressure of O_2 and CO_2. Due to the pressure difference gas penetrates from one side of the membrane to the other (from high to low pressure regions). The diffusion rate is proportional to the pressure gradient [45]. After the oxygenator the oxygen-rich blood passes an arterial filter before entering the CVS of the patient again. The filter eliminates bubbles and micro particles from the ECC.

3.4. Cannulation

The interface between the ECCS and the human CVS are the cannulas. The arterial cannula transports the externally oxygenated blood back into the CVS of the patient, while

the venous cannula draines blood from the vascular system into the ECCS. Central arterial cannulation is usually done via the aorta ascendens. Venous cannulation takes place via the superior or inferior vena cava. Peripheral cannulation (via A. femoralis and V. femoralis) is favored in emergency situations due to the better accessibility. In contrary to the central cannulation a total circulation support is not possible. About 80% of the blood volume is drained, while 20% pass the lungs. This leads to a lower pump volume (3.5–4 lpm). During femoral perfusion this also means, that the arterial blood only reaches up to the aortic arch, where it collides with the residual cardiac output of the heart [43]. Cannula size depends on the patient's anatomy, as well as on the required cardiac output, which is usually between 3.5 and 6 lpm for adults.

3.5. Miniaturization and Application outside Operating Rooms

The HLM is the most frequently employed type of ECC [43]. Miniaturization and technical innovations have led to the development of numerous cardiovascular support systems (HLM, Extracorporeal Membrane Oxygenation (ECMO), Ventricular Assist Device (VAD), etc.), which are also used outside the cardiac operating room [20]. In comparison to standard HLMs, miniaturized versions need less tubing and therefore less priming volume. However, they need to be placed closer to the patient. Another functional difference is, that Mini-HLMs are closed loop systems. At the initiation phase of ECC air in the venous line has to be removed completely. Existing built-in bubble traps are only designed for small air volumes [43].
One of the most reduced form of an ECCS are ECMOs. They consist of a pump and a membrane oxygenator, the main components of a regular HLM. Being closed-loop systems without a venous reservoir, ECMOs are designed for continous long-term support in hospitals (ICU) or during transportation.

The major indications for mechanical circulatory assist devices outside the hospital are listed in Table II.1. The listed indications are critical and life-threatening situations and require the presence of trained staff for therapy and a secure operation of the ECCS. Up until now a cardiac surgeon with sufficient experience in percutaneous cannulation and a cardiac perfusionist operating the HLM are needed. The application in emergency situation offers new opportunities to treat patients with acute or severe cardiovascular insufficiency, but also faces regulatory and organizational problems [20]. This work focuses on the development of an automated pump speed regulation. Together with intelligent patient monitoring it can support the emergency staff, increase the patient safety and ease the complex application of ECCSs outside the hospital. However, animal experiments (see Chapter IV) have shown, that sometimes an adequate blood flow can not be maintained with percutaneous cannulation. Segesser et al. [46] state, that there is a conflict of interest in remote access perfusion, as the operator's preference goes to relatively small cannula diameters, whereas larger diameters are necessary to achieve high blood flows.

4. Perfusion during Extracorporeal Circulation

The primary objective of cardiac surgery is a healthy, productive long-term survivor, rather than simply hospital survival and absence of gross organ dysfunction. Optimal perfusion

Protracted cardiogenic shock
Refractory acute lung dysfunction
Intoxication with acute cardiovascular failure
Hypothermia with/without circulatory collapse
Pulmonary embolism with acute right-sided heart failure

Table II.1.: Indications for the application of HLMs outside the cardiac operating room. From [20].

can be defined as that, which is followed by the best long-term patient outcome in terms of survival and function of all organ systems [47]. Perfusion during ECC is complex and subject to several influences. The operation and monitoring of the HLM is the task of a perfusionist, who communicates with the surgeon and the anaesthesiologist. Especially in the beginning and at the end of ECC support and during all major activities, clear coordination between those three parties is essential. ECC support is a severe intervention to the human CVS. Moreover, patients are in an exceptional state, being narcotized, under the influence of medication and usually with some acute cardiac disease. Following [48] and [45], the major factors influencing the patient state under ECC support are displayed in Figure II-6. Since this work deals with the automatic control of an ECCS, specifically

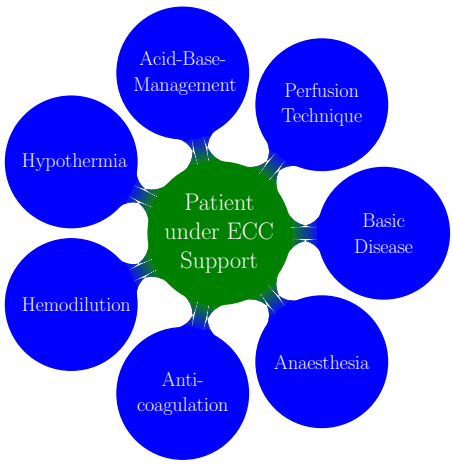

Figure II-6.: Multiple influences on a patient under ECC support.

controlling the pump speed, the hemodynamic aspects and variables during ECC support are described in more detail, while details on other perfusion related influences, such as acid-base management or anaesthesia, can be found in the related literature.

4.1. Pulsatile vs Constant Flow Perfusion

Most heart centers use a non-pulsatile perfusion technique [24], resulting in a constant blood flow. Proponents of pulsatile perfusion argue, that pulsatile flow patterns improve

major organ blood flow. Others have concluded, that pulsatile pumps increase the complexity of the CPB circuit and enhance the destruction of red blood cells and platelets [47]. More than 150 articles, comparing pulsatile and nonpulsatile perfusion, have been published [49]. However, the diversity of the devices used to generate pulsation [50], the lack of a clear definition of pulsatile flow [51], and the variety in the experimental design of related studies, hinder a quantitative analysis. So far, efforts to optimize pulsatile perfusion patterns during ECC, that resemble the physiological perfusion, do not seem to be justified [52].

4.2. Patient Monitoring during Extracorporeal Circulation

During ECC support the following parameters should be monitored at the patient (from [24]):

- invasive measurements of MAP and CVP
- body temperature
- oxygen delivery
- acid-base balance and electrolyte metabolism
- coagulation
- urine production
- Electrocardiogram (ECG)

On the machine side perfusionists should observe the following parameters (from [43]):

- pump flow
- pump inlet and outlet pressure
- bubble sensor
- gas monitor
- reservoir filling level

In the following, parameters relevant for this work are described in more detail.

4.3. Mean Arterial Pressure

One of the most important patient parameters to monitor during ECC is the Arterial Blood Pressure (ABP). Using a non-pulsatile perfusion technique, the blood pressure can be registered as a mean value only. The MAP depends on the produced pump flow of the HLM, mainly restricted by the cannula size and the TPR. To increase the MAP, the pump speed can be increased, or, if that's not sufficient, the peripheral resistance can be increased medicamentously. Since the MAP is influenced by a multitude of factors (flow, temperature, hematocrit, depth of anesthesia and others), and due to a large amount of

controversary studies, guidelines for optimal perfusion pressures are hard to give. Murphy [47] suggests, that the choice of perfusion pressures must be based on the assessment of the benefits and risks of higher and lower MAPs on a case-by-case basis (see Table II.2). Usually, pressures between 40 and 60 mmHg are recommended [45]. Some studies support

Potential advantages of higher MAPs	**Potential advantages of lower MAPs**
Enhanced tissue perfusion in high risk patients (hypertensive, diabetic, elderly)	Less trauma to blood elements
Improved collateral flow to tissues at risk of ischemia	Reduction of blood in the surgical field
Allows for higher pump flow rates on CPB	Less cardiotomy suction
	Permits the use of smaller venous and arterial cannulae
	Enhanced myocardial protection (reduced collateral coronary blood flow)
	Reduced embolic load to the central venous system (reduced pump flow)

Table II.2.: Arterial Pressure Management. From [47].

MAPs above 70 mmHg. Especially for certain patient populations as elderly [53], hypertensive [54], diabetes [55] patients or people with advanced atherosclerotic disease of the aorta [56], higher perfusion pressures seem to be appropriate.

4.4. Central Venous Pressure

The CVP, measured in the superior vena cava or in the right atrium, is a good indicator for the cardiac state and the volume status of the patient. Any deficit in cardiac function will elevate the CVP, if blood volume and vascular dynamics are stable. When cardiovascular function is stable, the central venous pressure will tend to vary directly with alterations in blood volume [57]. A low CVP is usually caused by hypovolemia, while several factors, such as increased blood volume, cardiac insufficiency or pulmonary embolism among others, can cause a high CVP [58]. Also the usage of too small or wrong positioned cannulas, as well as kinking of the venous line, can cause high CVPs during ECC [45]. Usually the CVP is between 0 and 15 mmHg, in the superior vena cava at around -3 mmHg and in the right atrium even lower [58].

4.5. Pump Flow

Following Lauterbach [45], the produced pump flow should be high enough to cover the oxygen demand of the patient and as low as possible in order to avoid blood traumatization. Again, the blood flow depends on multiple factors with the Body Surface Area (BSA), the degree of hypothermia and the oxygen consumption of the patient being the most important ones. There is no evidence from large-scale randomized trials supporting a minimal safe flow rate during normothermic or hypothermic CPB. Furthermore, the optimal

flow rate, that supports the most favorable organ perfusion and results in improved clinical outcomes, has not been determined [47]. Usually a flow rate of $2.4\,l/min/m^2$ is pursued for normothermic perfusion [43, 45]. This flow rate approximates the cardiac index of a normothermic anesthetized patient with a normal hematocrit [59]. Depending on the degree of hypothermia, the flow rate can be adapted (see Table II.3).

Degree of hypothermia	**Recommended flow rate**
Normothermia	$2.2 - 2.6\,l/min/m^2$
Light Hypothermia ($32 - 35\,°C$)	$2.0\,l/min/m^2$
Moderate Hypothermia ($26 - 31\,°C$)	$1.5\,l/min/m^2$

Table II.3.: Recommended flow rates per BSA based on the degree of hypothermia. From [43].

4.6. Hematocrit and Hemodilution

In the early beginnings of heart surgery HLMs were primed with whole blood. After studies have shown, that asanginous liquids (Ringer solution) for priming did not lead to worse outcomes, hemodilution became a standard practice. Hemodilution is due to the addition of volume for hemodynamic stabilization during anaesthesia, the priming volume of the HLM, and the application of cardioplegia [42, 45]. Overall, hemodilution leads to a reduction of the hematocrit value of about 50% and a decrease of blood viscosity [58]. This leads to an improved microcirculatory flow, a reduced risk of hypertension during higher bypass flow, and a decreased requirement for intraoperative transfusions. Excessive hemodilution, however, may compromise DO_2 at the tissue level and contribute to hypotension during CPB [47]. The decrease of blood viscosity comes along with a decrease of the TPR. Flow is increased and blood flow characteristics are improved, leading to a better organ perfusion [45]. An obvious disadvantage of hemodilution is the decrease of the carrying capacity of oxygen. Again, the maximum degree of hemodilution should be assessed individually for each patient, considering factors such as age, sex or previous diseases.

4.7. Oxygen Delivery

Sufficient oxygen supply of the patient during ECC is a major task for perfusionists in order to avoid hypoxia. The O_2-Supply can be calculated as the product of the flow Q and the arterial concentration of O_2:

$$O_2\text{-Supply} = Q \cdot CaO_2. \tag{II.10}$$

The oxygen consumption is calculated as the product of the flow and the arteriovenous oxygenation difference:

$$O_2\text{-Consumption} = Q \cdot avDO_2. \tag{II.11}$$

A high oxygen consumption of an organ is associated with a large $avDO_2$ and a low concentration of oxygen on the venous side. The Oxygen Saturation (SpO_2) is determined

by the partial pressure of oxygen, the pO_2, and expresses the percentage of O_2-saturated hemoglobin. The relation between pO_2 and SpO_2 is displayed in the oxyhemoglobin dissociation curve II-7. At a pO_2 healthy adults have a SpO_2 value of about 97%. On the

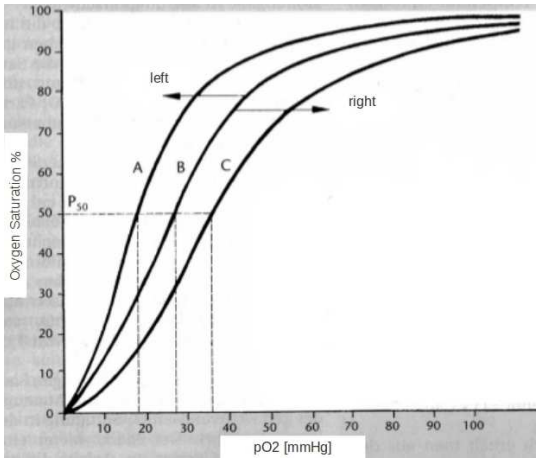

Figure II-7.: Oxyhemoglobin dissociation curve. Modified from [45].

venous side an average pO_2 of about 40 mmHg is measured, associated with a saturation of 73% [45]. Several factors can influence the dissociation curve. If, for any reasons, the pH-value increases, the pO_2 or the body temperature decreases, the dissociation curve is shifted to the left. Vice versa, if these parameters change in the opposite way, the dissociation curve is shifted to the right. Oxygen delivery to the tissue is eased, however, a larger pO_2 is needed to adsorb the same amount of oxygen. During ECC oxygen delivery can be improved by increasing pump flows, increasing hematocrit concentrations, or by increasing hemoglobin saturation and the amount of dissolved oxygen [47].

Chapter III

State of the Art

Contents

1	**Hydraulic Mock Circulation Systems**	23
2	**Mathematical Models and Circulatory System Simulations**	29
3	**Automatic Control of Heart-Lung Machines**	32

1. Hydraulic Mock Circulation Systems

CVS modelling has been subject to numerous studies for more than 50 years now. One of the first reported artificial circulatory setups was the Kolff model in 1959 [60]. Especially in the 1970ies much effort was put into building artificial hearts and circulatory mock models [61–66]. This development was also driven by the contributions of Guyton et al. [67], who turned physiology from a speculative into an engineering science, by providing a complete system analysis of circulatory regulation. Guyton's simulation model consisted of 18 modules, containing about 600 physiological parameters and variables [68].

One of the most popular artificial models from that time is the three-element windkessel or Westerhof model [26]. For the first time Westerhof et al. give an in-depth description of the design, construction and testing of an artificial circulatory model. Starting from an electrical model of the systemic arterial tree [69] (Figure III.1(a)), their work deals with the hydrodynamic equivalent. The setup consists of two resistances, replicating peripheral resistance and characteristic impedance of the vessels. Furthermore, a compliance, representing the total compliance of the arterial tree. The model was validated in two ways: First, a pump, producing sinusoidal flows in a range of 0.4-30 Hz was used to measure input impedances. This data was then compared to reported in vivo values of a dog's and cat's input impedances. As a second verification, the model was used as a load for an isolated heart of a cat and pressure and flow curves were compared. Both tests agreed well with in vivo data and the realistic pressure and flow wave shapes have been confirmed by other authors as well [70, 71]. In conclusion, the Westerhof model imitates the normal cardiac load very well and shows, that it is possible to arrive at an easily adjustable hydraulic load for a heart with an input impedance close to the arterial tree.

A few years later Donovan [72] developed a hydraulic analog of the circulatory system for evaluating artificial hearts. The setup comprised four chambers, simulating systemic and pulmonary arterial and venous vasculature. A good comparison between the mock circulatory system response and the system response of a calf was reported. Another famous mock model is the Pennsylvania State circulation model, described by Rosenberg et al. [73]. In addition to the Donovan Setup a parallel plate resistor, downstream of the aortic compliance, simulates the systemic resistance of the circulation [74]. The Penn State model showed adequate results when compared to human data and was mainly used for in vitro testing of blood pumps. However both the Donovan and the Penn State model lack thorough system analysis and evaluation.
Also the test circulation system of Arabia and Akutsu [75] lack a thorough evaluation. Their mock model included several RLC lumped parameter elements to mimic aorta, pulmonary artery, systemic and pulmonary veins. With the objective to study artificial hearts, the contribution of their work is the derivation of a complete mathematical description of their model, which many other authors omit. Arabia and Akutsu examined blood-volume and pressure distributions, as well as flowrates in steady conditions. However, some deviations between measured parameters and physiological data were reported.

The circulation loop of Vermette et al. [76] was built in order to test cardiovascular devices with a focus on the evaluation of different materials, used for cardiovascular applications. It consisted of a feed tank, a centrifugal pump, three valves, a regulating flow tank and a pulsatile mechanism. Pulsatile flow was produced by axial displacement of a cylinder, that periodically compressed the conduit. This setup allowed to study both pulsatile and constant flow patterns. However, the cylinder produced an additional flow resistance and, for high flow rates, the range of achievable mural pressures was significantly reduced. Still, the setup allowed to create flow and pressure waveforms in a broad range, similar to the wave propagation in peripheral circulation.

Stergiopulos et al. [77] describe the three-element windkessel model of Westerhof as an almost perfect load for isolated heart studies, but criticise that it does not lead to accurate estimates of the total arterial compliance. They argue, that for low frequencies the whole blood mass is accelerated simultaneously and hypothesize, that an initial term is missing from the three-element model. They showed, that when a three-element windkessel is used to fit aortic pressure with aortic flow as input, the estimates of the compliance and the characteristic impedance of the aorta deviate significantly from their values obtained with standard methods used in the literature. Particularly, the arterial compliance is overestimated, while the characteristic impedance is underestimated. In conclusion, the three-element windkessel can produce realistic aortic pressures and flows, but only with parameter values that quantitatively differ from the vascular properties [70].
To overcome this deficiancy they introduce a fourth element, an inertial term in parallel to the characteristic impedance (Figure III.1(b)) and show, that their model is superior to the three-element version in terms of Root-Mean-Square Errors (RMSEs). Four-element windkessels have been studied before and the better accuracy to in vivo data was known. However, there was no physical interpretation of the inertial element and was therefore only considered as a further degree of freedom [78]. Stergiopulos et al. now interpret the fourth element as the summation of all local inertances of the arterial system. For mean pressure and flow (0 Hz), wave transmission is of no importance and only the peripheral resistance contributes [77]. The examined ECCS (Lifebridge) in this work produces constant flow

and, therefore, a fourth element, adding more complexity, seems to be unnecessary for the hydraulic mock model.

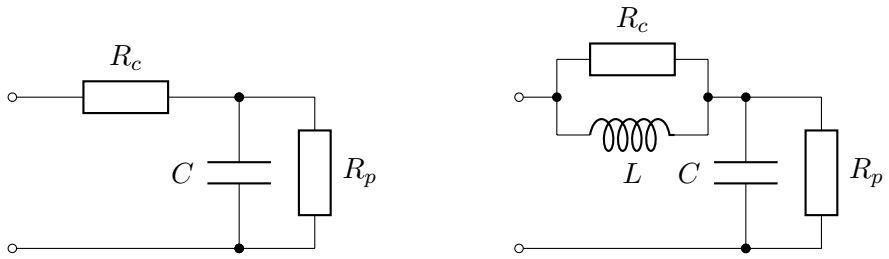

(a) Three-element windkessel model (b) Four-element windkessel model

Figure III-1.: Electric representation of three- and four-element Windkessel models with characteristic resistance R_c, peripheral resistance R_p, arterial compliance C and inertia L.

Kind et al. [79] questioned the use of a four-element model, due to low identifiability of the inductivity. In their study they estimated three- and four-element windkessel parameters using a subspace model identification algorithm. Systematic errors in the parameter estimation were investigated using simulation data. From a simulated aortic flow curve, the corresponding aortic pressure curve was calculated using the two windkessel models. The models were compared to the real pressure curve in terms of the RMSE. They found a systematic error in the identification of the four-element model, while all parameters for the three-element windkessel were estimated with an error of less than 1%. A limitation in the study of Kind et al. is, that no in vivo data had been used, so modeling errors cannot be excluded. Although the four-element model seems more suitable from a physiological point of view and achieves a better RMSE, the parameter estimation turns out to be more problematic. Also Lambermont [80] states, that the four-element windkessel model increases the statistical fit, but the differences to parameter predictions in three-element windkessel models are small and do not warrant the additional complexity.

Sharp and Dharmalingam again find the three-element model among others to exhibit the best tradeoff between simplicity and accuracy [81]. They first used computer studies to identify the configuration of lumped parameter elements in a model of the systemic circulation. They simulated RC, RCR, RLRC and RCLRC combinations to find the best match of impedance to human data. The models were compared to data from 5 normal subjects [82]. The accuracy increased with the number of elements in the system, but the three-element model already showed a good match with a minimum number of elements and was chosen for the construction of a physical replicate as a compromise between accuracy, size, weight and complexity. The hydraulic mock model was designed and constructed analogous to simulations. Sliding plates were used as adjustable resistors to vary the flow area and a variable-volume air chamber as an adjustable compliance (Figure III.2(a)). Their results show a close match with data from humans and the setup was compared to the Donovan [72] and the Penn State [73] mock models, with superior results in the low, fundamental heartbeat frequency range. Water was used as a blood substitute, because the non-Newtonian properties of blood do not substantially impact bulk pressure and flow

response in large vessels under normal conditions [83].

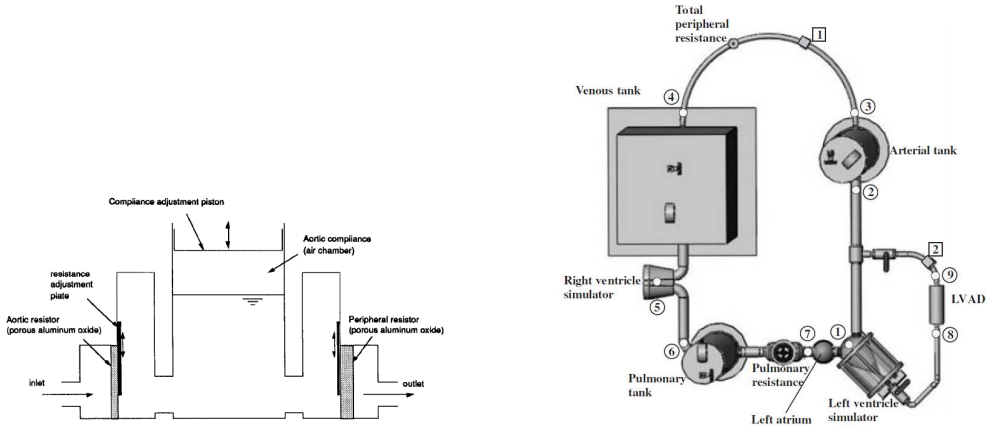

(a) (b)

Figure III-2.: Schematics of the hydraulic mock circulation loops of (a) Sharp and Dharmalingam [81] and (b) Liu et al. [84].

Verdonck et al. [85] constructed a computer-controlled mock model to test mitral valves. It consists of a model of the human heart, connected to a windkessel model of the systemic circulation. The fluid enters the system from a preload reservoir, travels through two rigid pulmonary veins and a replaceable mitral valve to a left ventricle component. From there, it passes the aortic valve and enters the windkessel model, consisting of a compliance chamber and a hydraulic resistance. This model was also used by Vandenberghe et al. [86] to assess the hydrodynamic performance of an intra-arterial Left Ventricular Assist Device (LVAD).

Another mock model for the testing of LVADs was designed by Liu et al. [84]. The mock loop consisted of pulsatile left and right cardiac simulators, air/water tanks to model the arterial and venous compliances, tygon tubes to connect the elements and to model venous, arterial and other system flow resistances, and a tuning clamp to vary system resistance characteristics under different pressure/flow conditions (Figure III.2(b)). Several conditions, including healthy resting, healthy sleeping, healthy exercise and congestive heart failure, were tested. Parameters for several conditions were presented, but not validated. The mock model was said to be sufficient for testing continuous flow LVADs under various heart rates and contractility, however it does not provide accurate prediction of LVAD performance in the transition of activity levels, due to its inability to model the Frank-Starling response.

Pantalos et al. [87] presented a mock circulation model for testing cardiac devices in normal and pathologic states. Well-aware of already existing models, their focus was to show the ability of the model to mimic the Frank-Starling response of normal, heart failure and cardiac recovery conditions. The mock circulation consisted of atrium, ventricle, systemic and coronary vasculature components. It was validated by comparison of hemodynamic parameter values and ventricular pressure-volume relationships with published physiologic data [82]. Mechanical properties were estimated using the four-element wind-

kessel model. Lumped parameter elements (resistance, compliance, inertance and characteristic impedance) were adjusted, until the error between the experimentally measured impedance and the model derived impedance had been minimized. Pantalos et al. reported physiologically equivalent hemodynamic waveform magnitudes and morphology. Also the characteristic cardiovascular parameters were comparable with physiologic values. They concluded, that mock circulations are not intended to replace in vivo models, but can be a valuable research tool for assessing the performance of cardiac devices, developing experimental protocols in a controlled environment and training personnel on the operation and maintenance of cardiac devices. Koenig et al. [88] used this model to investigate hemodynamic and pressure-volume responses to continuous and pulsatile LVADs. And Glower et al. [89] evaluated an artificial vascular device with this model while Litwak et al. [90] focused on aorta outflow graft location.

Ferrari et al. [91] attest, that hydraulic circulation models are always a compromise between mechanical complexity and accuracy. When compared to numerical models, they are rather expensive and often not sufficiently flexible or accurate. However, those models are needed, e.g. when testing new cardiac devices. Therefore, Ferrari et al. proposed a hybrid mock circulatory system. From a closed loop model [92] left artrial and systemic arterial pressures were measured. Based on those values the left ventricular output flow was calculated on a computer, which controlled a gear pump, producing the designated flow. Results showed, that the model is coherent with the physiopathology of the circulatory system in relation to the pressure-volume distribution and arterioventricular interaction. The approach of merging numerical and physical models was also followed by Kozarski [93].

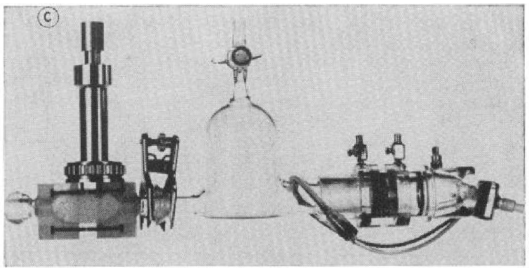

(a) Westerhof et al. (1971) [26]

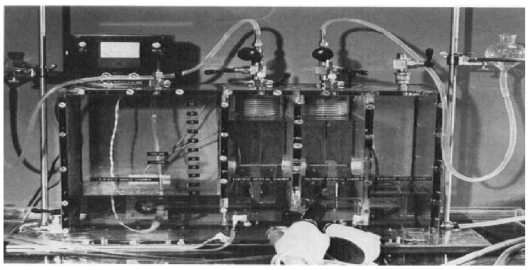

(b) Donovan (1975) [72]

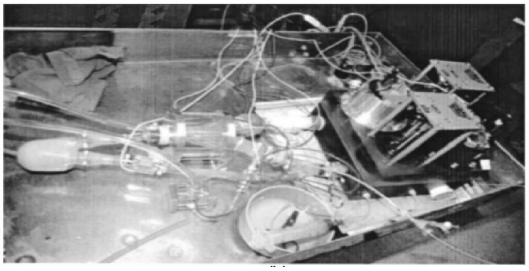

(c) Koenig et al. (2004) [88]

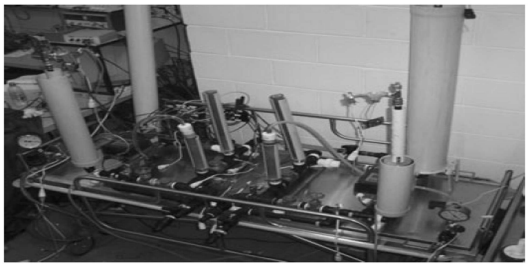

(d) Timms et al. (2005) [94]

Figure III-3.: Hydraulic mock circulation loops.

With continuous improvements Timms and colleagues established an advanced mock circulation loop [94–96]. The authors diagnose, that current circulation loops often lack the auto-regulatory feedback mechanisms of the natural cardiovascular system, such as the Frank-Starling mechanism, baroreceptor-reflex and shifts to volume, due to skeletal muscle pump and postural changes. Also, many mock models are designed for a specific use case and do not combine many circulatory features. The model of Timms et al. consists of a detailed replicate of the heart using multiple tubes as chambers and several mechanical valves even including left and right coronary circulations. It is completed with a five-element windkessel model, representing systemic and pulmonary vasculatures. A mathematical simulation was used to determine the physical properties, such as pipe dimensions and input pressures [97]. The mock loop was validated by replication of arterial pressure and flow rates of a patient progressing through therapy. The model is the basis for several studies and cardiovascular devices have successfully been tested with it [98, 99].

Author	**Year**	**3-el. WK**	**4-el. WK**	**>4-el. WK**	**Simulation**	**Validation**
Westerhof et al. [26]	1971	x				cat, dog
Donovan [72]	1975		x			calf
Rosenberg [73]	1981			x		human
Arabia and Akutsu [75]	1984			x	x	human
Sharp and Dharmalingam [81]	1999	x	x	x	x	human
Ferrari et al. [91]	2002			x	x	human
Pantalos et al. [87]	2004		x			human
Timms et al. [96]	2011			x	x	human

Table III.1.: Comparison of selected hydraulic mock circulation loops.

In summary, hydraulic mock circulation loops are a valuable tool to study cardiovascular dynamics in an in vitro setting. Since the 1970ies, those models became more and more advanced and accurate. The mock setups are predominantly used to test new cardiovascular devices, but also training of medical staff is an option. By several authors the 3-element windkessel was found to exhibit the best trade-off between simplicity and accuracy. Accuracy did not improve significantly with the addition of a fourth element. Improvements were only noticeable with a fifth element. Since many mock models were developed for specific applications, comparison is difficult. Table III.1 summarizes the key features of well-known hydraulic circulatory replicates. Indicated are the number of windkessel elements, the validation method (predominantly models were validated by comparison with human data) and whether a simulation or analytical analysis was done. Milestones are the contributions of Westerhof et al. [26] for the first in-depth analysis and design guidelines, of Sharp and Dharmalingam [81] for an extensive comparison between several windkessel models and the contributions of Timms et al. [96] for establishing a sophisticated and flexible mock circulation loop. With consideration of the requirements for this thesis, the 3-element windkessel model appears to be sufficient. The examined HLM produces constant flow, i.e. there is no need for considering frequency characteristics of the model. The

3-element model provides a simple analytical description, easing the process of control design. And the patient can be regarded as a black-box model, i.e. there is no need for flow or pressure analysis in specific compartments of the model, so that a lumped parameter approach is legitimate.

2. Mathematical Models and Circulatory System Simulations

Mock circulation loops are key elements during the development and testing of cardiac devices, but of course have limitations as described above. On the other hand, mathematical circulatory models permit the study of features and behaviors that would be impractical to investigate using physical mock circulation systems. For example, model components can be added or removed, and their parameters varied with relative ease [100]. Also, for the design of regulation and control systems, such as in this work, a simulation model is indispensable.

One of the first complete circulatory models was published by Avolio [30]. The arterial vasculature was segmented into 128 elements, arranged according to the anatomical architecture of the human arterial tree and considered vessels with a diameter of 2 mm or more. Each segment is considered as a thin-walled, uniform cylindrical tube with viscous, elastic and inertial properties. All terminations to peripheral segments consist of a resistance, determined by the nominal characteristic impedance of the segment and a specified reflection coefficient. The model was originally designed to examine the wave propagation in the arterial system and to study dynamics under pathologic conditions. Written in Fortran, it was later implemented in the Matlab/Simulink environment by Riesenberg [101] and served as the basis for the work of Meyrowitz [24] and Bauernschmitt et al. [102]. Along with technical advances and increasing computing power, simulations of the CVS became particularly popular from the 1990ies on.

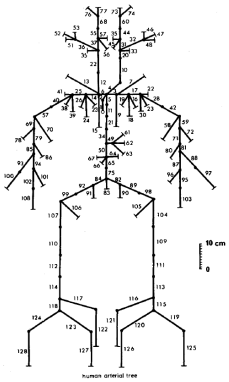

Figure III-4.: Structured representation of the arterial circulatory system from Avolio [30]. This model was the basis for the work of Bauernschmitt [102] and Meyrowitz [24] among others.

The pulsatile model of Ding and Frank [103] included several reflex control systems, such as baroreceptor feedback loops and non-linearities of vessel compliance. Again, the

circulatory system is represented by RLC networks. A major achievement of Ding and Frank was the implementation of an artificial heart. The rhythmical contractions of the right and left sides of the heart were simulated by time-variant compliances. A PFM controller was designed to control the volume and blood pressure of the circulatory system, with the measured pulmonary and systemic venous pressures being the inputs.

Vollkron et al. [104] developed a Matlab/Simulink model to study LVADs. Their circulatory system consisted of 6 segments: left and right ventricle, left and right atrium and pulmonary and systemic vascular segments. They studied the interaction of the model with a continuous-flow pump, the effects of changing pre- and afterloads and the possibilities for indirect estimation of hemodynamic parameters and pump control. The model was validated in 3 steps. First, different segments were validated by comparison with data from the literature and previously collected in vitro and in vivo data. In a second step, the entire closed loop circulation with parameter variations, was again compared to available data, while an assist device model was only included in the third step. Shape and value of the calculated arterial, pulmonary and central venous pressure patterns corresponded very well with findings in patients. Also the hysteresis behavior of the pressure-flow relation in the computer model showed excellent correlation with in vitro experiments.

With focus on developing a physiological controller for a LVAD, Wu et al. [105] presented yet another Matlab model of the arterial CVS. Ventricles were modeled as nonlinear capacitors and the TPR as a variable resistance. Different parameter settings were used to display different cardiovascular conditions. The authors did not give details about the validation process, but stated, that some hemodynamic parameter values may seem too high, compared with clinical data. However, this did not affect the validity of the model to test the LVAD control performance.

Korakianitis and Shi [106] presented a model to simulate human circulation dynamics. The heart was modeled as a four-chamber pump with variable elasticity, following a model of Suga et al. [107]. The systemic and pulmonary circulation was again modeled by RCL elements, representing segments of aortic and pulmonary artery sinus, artery, arteriole, capillary and vein. In addition to other models, atrioventricular interaction models and heart valve dynamics are presented. Results showed, that these advances greatly improved the simulation accuracy and it was possible to realistically simulate important physiological characteristics in the cardiac response, such as dicrotic notch or regurgitant flow. The model was implemented in the C programming language. Shi et al. [108] later used this model to compare the hemodynamic response in the CVS, when three types of VADs were applied to assist a diseased left ventricle.

A functional model, representing the CVS, was also presented by Hassan et al. [109]. Their 14-compartment model was implemented in Matlab and, in comparison to many other models, also included a baroreflex-feedback regulatory mechanism. In addition to represent a normal state, the model was used to simulate hypertension and acute congestive heart failure. The magnitudes and shapes of all resulting variables were reported to agree well with the medical references and literature. Shi et al. [110] also included a baroreceptor model. Along with simulation, they built up an electrical circuit and reported good agreement with medical data.

Sheffer et al. [111] presented a Matlab model of the CVS in order to study various flow models and pathological conditions. They focused on a modular setup with the intention to easily replace building blocks, depending on the application. Their toolbox was made

available online and consisted of Simulink models of the heart, vessels, oxygen transportation and others. However, no validation data was provided.

Hassani et al. [112] tried to improve existing models by adding more segments and parameters and, thereby, create a more detailed model. Their circuit representation included 42 segments, each again modeled by resistance, compliance and impedance elements. Left and right ventricles were modeled by AC power supplies and ideal diodes, generating a pulsatile 1 Hz signal, which is equivalent to a HR of 60 bpm. The authors report good agreement with medical data extracted from articles and textbooks. The model was later used to simulate aorta artery aneurysms and renal artery stenosis [113].

Bauernschmitt and colleagues presented a mathematical circulation model under cardiopulmonary bypass [102, 114]. Following the model of Avolio [30], the arterial circulation was segmented into 128 branches. Each branch was characterized by physical properties (length, diameter, wall thickness, module of elasticity). Patient specific properties, such as height, weight or total blood volume could be simulated by changing the corresponding model parameters. With the future goal of an automated HLM, their model was able to simulate the effects of different perfusion regimens on arterial hemodynamics and whole body oxygen consumption. Implemented in Matlab/Simulink, the model proved to simulate hemodynamic responses during bypass in accordance with data from the literature and similar to the clinical situations in the operating theatre. A modified sinusoidal wave was used as an input signal and hypothermia, acid-base management, hemodilution and oxygen consumption were studied. A baroreflex control was added later [115]. For future models, the authors expressed the need for a useful reduction of variables, which does not alter the circulatory behavior.

Pennati et al. [116] developed a lumped-parameter mathematical model of the hydraulic behavoir of the arterial side of an extracorporeal circuit under pulsatile flow conditions. In contrast to other studies they focus on the description of the extracorporeal circuit. A membrane oxygenator, an arterial filter and an arterial cannula were modeled as lumped RLC elements. The simulation model was compared to a hydraulic setup under static conditions and with increasing forward and backward flow rates. A fairly satisfactory matching between the simulated and experimentally measured tracings was reported.

Also Mayrowitz [24] further developed a preexisting circulation model on the basis of the Avolio model [30]. Realized in Matlab/Simulink, the model considers the circulatory system under ECC and contains several subsystems which model organs and physiological processes, such as the blood, blood gases or acid-base-management. As input parameters, individual patient parameters can be given, including age, sex, height and weight. Like in the work of Bauernschmitt et al., several perfusion regimes can be tested. Perfusion rate, pump flow characteristics, acid-base-management, blood temperature and Fraction of inspired Oxygen (FiO_2) can be set independently. Again an electrical analogon is derived with RLC elements, described by differential equations. Small vessels were modeled as terminating resistors. For the CVS under ECCS, a 128-element model was used, following the Avolio model [30]. Employing the Navier-Stokes-Equations, blood pressure and flow were calculated in each segment. Hypothermic conditions were modeled by adjusting the resistance elements. Terminating resistances of the periphery were increased to have more blood volume in the central parts of the body. Several perfusion regimes, including low- and high-flow perfusion were evaluated. A good accordance with clinical data was reported.

3. Automatic Control of Heart-Lung Machines

Until today there are only few studies dealing with the automation of HLMs. Some of the first considerations towards computer-controlled ECC were published by Prilutskii et al. [117]. As one of three major design principles, the authors suggest to monitor physiologic and technical parameters in hierarchic sequence, i.e. a preference series should be formulated in selecting control and optimization criteria for the machine and the body. As the major control goal, the maintenance of a given perfusion rate is identified. If a deviation in one of the parameters occurs, an examination and possibly a correction of the parameter must be made (design principle 2). The third principle considers the individual physiological deviations of the patients and demands, that control criteria for adequate perfusion are based on the current state of the body and possible pathogenetic disturbances.

Beppu et al. [118] described a computerized control system for CPB in 1995. A PIC with a control interval of 1 s regulated the CVP based on a total fluid balance of a patient. A blood level sensor for the venous reservoir was used as the input parameter. The PIC controlled both a pulsatile infusion and a withdrawal pump. The setpoint of the reservoir could be adjusted and, depending on the current filling level, either the infusion or withdrawal pump was activated. An additional screening algorithm was able to detect measurement artefacts and artifical noise by monitoring the intensity of the CVP frequency spectrum. If any disturbances were detected, the current flow rates were maintained. Several additional safety mechanisms were implemented. During all applications the total fluid balance was maintained satisfactorily. The system was tested in 15 patients with similar constitution during cardiac operations. Compared to a reference group with manually controlled CPB no significant difference was noted.
The concept of rule-based reservoir level control had already been applied by Fukui et al. [119] for use in infants and later by Momose et al., with the intention to stabilize the preload of the heart during the initiation and weaning stages of ECC [120].

As an all-embracing approach towards automated ECC, Boschetti et al. implemented a computer simulation of a patient connected to a ECCS [21]. The virtual patient consisted of five models: (i) hemodynamic, (ii) thermal, (iii) biochemical, (iv) volume and (v) drug model, while the ECC circuit comprised a heat exchanger, a gas transfer and a hemodynamic model. Several parameters, such as the patient's age, height or weight could be adjusted. A model validation or evaluation was not reported. The system was intended for education and training purposes.

An advanced study on ECC control was done by Misgeld et al. [25, 121]. In comparison to other authors [118, 119, 122], only arterial pressure and flow were controlled, since in a HLM with a buffered venous bag, the control of venous conditions plays a secondary role. They compared three different aortic flow controllers, a PIC, a HINFC and a General Predictive Controller (GPC). Starting from a five-compartment model of the CVS, the PIC and the HINFC were robustly tuned and then compared to the self-tuning GPC. For the controller design a worst-case approach was chosen, depending on non-linearities, time-variant parameter disturbances and additive/multiplicative model parameter uncertainty. The controllers were tested in a closed-loop control simulation and showed stable behavior. Later, the controllers were tested in a hydrodynamic mock model (2-element Windkessel) [123, 124]. To test the robustness of the controllers, the model parameters (resistance and compliance) were changed. In terms of the Integral of Absolute Error (IAE) the

HINFC was superior to the other controllers, but showed only a slight advantage over the PIC. It was found, that the GPC adapted very slowly to parameter changes, due to the linear parameter estimator that was used. Since the PIC generally showed a good performance and is easier to implement, it was then used for both pressure and flow control.

Apart from the work of Misgeld, the study of Meyrowitz [24] also deals with a comprehensive approach towards the automation of a HLM. Starting from a 128-element virtual model of the circulatory system under ECC (see 2), Meyrowitz implemented a PID-Controller, a State Space Controller and a Model Predictive Controller for the control of hemodynamics (pressure and flow), temperature and acid-base-equilibrium. Again, the PIC is recommended, due to its simplicity and robustness. The controller was tested in simulations and in animal experiments (pig).

Chapter IV

Animal Experiments

Contents

1 **Overview** 35
2 **Anaesthesia, Preparation and Sensor Placement** 36
3 **Experimental Procedure and Results** 37
4 **Prototype Controller Test** 42
5 **Summary** 44

1. Overview

During this project several animal experiments have been carried out. The experiments had been approved by the Bavarian authorities and the animals received human care in compliance with the Guide for the Care and Use of Laboratory Animals (NIH publication 85-23). The experiments served several purposes:

- **Hardware/Sensor Performance Test:** Sensors and data acquisition hardware can be tested and verified in a real-world setup. Hardware from different manufacturers can be compared and evaluated.
- **Software Test:** The developed software for recording, processing and visualization of sensor and machine data can be verified in an in-vivo setting.
- **Reference Data for System Models:** Recorded data from both the HLM and the patient undergoing ECC serves as reference data for the hydraulic and the virtual system model.
- **Prototype Controller Test:** A prototype fuzzy controller for the HLM was tested during one of the experiments.

During the experiments domestic pigs were given anaesthesia and connected to the Lifebridge HLM via femoral cannulation. The subsequent tests followed a protocol as far as

the current state of the subject under ECC allowed. This included recording a steady state with and without ECC, application of vasoactive drugs and variations of the HLM pump speed among others. The general procedure for the experiments is shown in Figure IV-1.

The sections 2 and 3 of this chapter follow a publication in the Journal of Medical Engineering & Physics [15] and the dissertation of Alejandro Mendoza [27].

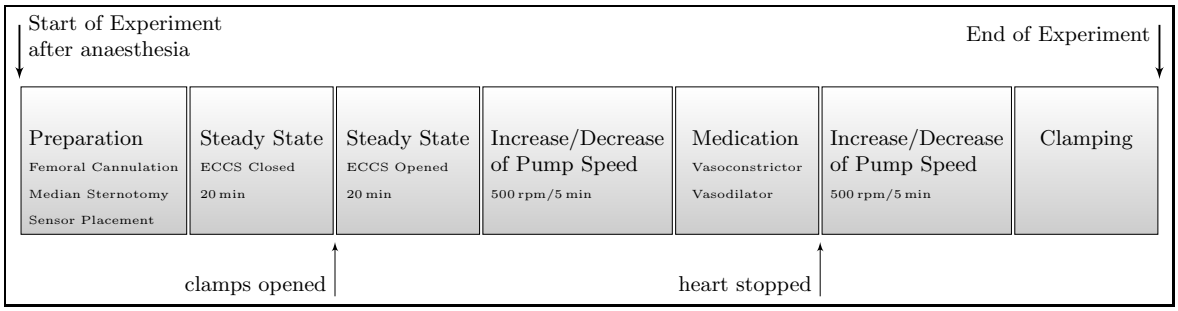

Figure IV-1.: Experimental protocol

2. Anaesthesia, Preparation and Sensor Placement

Four domestic pigs weighing 50 ± 0.7 kg were pre-medicated with an intramuscular injection of ketamine (15 , Ketanest®, Parke Davis, Munich Germany) and an atropine sulphate injection (0.5 , Braun, Melsungen, Germany). General anaesthesia was induced by intravenous injection of propofol ($60 - 100$ mg, Propofol, Lipuro, B. Braun AG, Melsungen, Germany). Anaesthesia was maintained by continuous intravenous application of propofol (10 mg/kg/h Propofol 2%) and Fentanyl (30 ug/kg/h, Fentanyl, Jannsen Cilag, Neuss, Germany) through a syringe pump.
After endotracheal intubation, the pigs were placed on a respirator and ventilated with a mixture of oxygen and air. The FiO_2 was set to 0.5. A catheter was inserted into the jugular vein (ArrowHowes ™Quad-Lumen central venous catheter, Arrow International Inc., USA) for monitoring the CVP. Through the right femoral artery, a catheter tip manometer (Millar MIKRO-TIP ®SPC350, Houston, TX, USA) was placed in the descending aorta for monitoring the aortic pressure.
Median sternotomy was done and the pericardium was opened. To measure the aortic flow, a perivascular ultrasonic flow probe (A-Serie, Transonic Systems Inc., Ithaca, NY, USA) was placed at the descending aorta above the crossing of the pulmonary veins. Another flow probe (C-Serie, Transonic Systems Inc., Ithaca, NY USA) was placed in the ascending aorta.

The pig was connected to the ECCS through femoral cannulation. From the arterial side a 20F arterial cannula (Medtronic, Inc. Minneapolis, Minnesota, USA) was introduced into the femoral artery and a 22F cannula (Edwards Lifesciences, CA, USA) was placed in the femoral vein.
For online blood gas analysis the CDI 500 gas analyzer (Terumo Medical Corp, Tokio, Japan) was used with the sensors placed between the arterial and venous cannulas and

the ECSS. This device works with a sampling rate of 1 sample every 6 seconds and measured hematocrit and hemoglobin values, partial pressures of arterial and venous carbon dioxide, as well as arterial and venous SpO_2 values.
For heart beat and ECG readings a 4 lead ECG reader (EMI12, Corscience, Erlangen, Germany) was used with 4 gel electrodes. ECG was captured at a 200 Hz sampling rate. An oxymeter (ChipOx, Corscience, Erlangen, Germany) was placed at the ear to measure oxygen saturation and an additional reading of heart rate at 1 Hz.
From the ECSS readings of pump flow, input and output pressure and pre-oxygenator pressures were obtained via a CAN-Bus reader.
All sensor data was recorded using the tailor-made software *AutoMedic* [2] and a 16-bit data acquisition board with a set sampling frequency of 200 Hz (NI PCMCIA 6036E, National Instruments, TX,USA). Figure IV-2 shows the experimental setup with the pig connected to the ECCS and sensor positions and illustrates impressions of the real-world experiments.

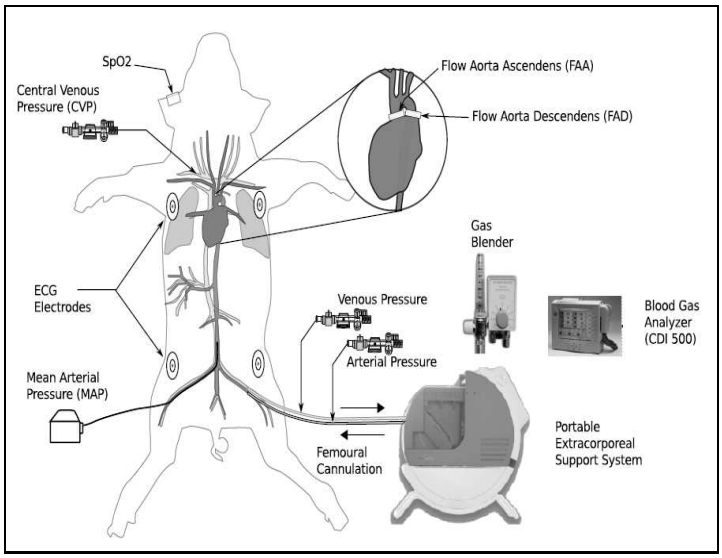

(a)

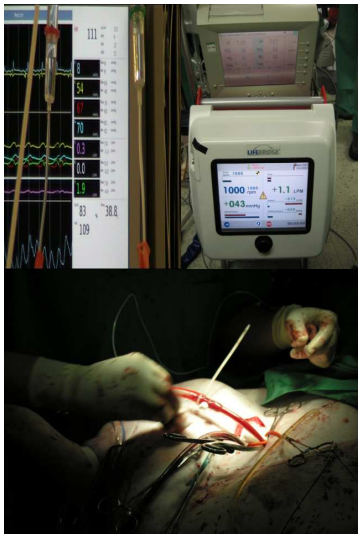

(b)

Figure IV-2.: Experimental setup with pig, Lifebridge ECCS and sensor positions (a) as well as pictures from one experiment (b) showing the tailor-made patient monitor, the Lifebridge HLM together with the CDI 500 blood gas analyzer and the femoral cannulation process.

3. Experimental Procedure and Results

3.1. Steady State with and without ECCS

After administration of anaesthesia, placement of the sensors, and cannulation (with both venous and arterial lines clamped) 20 minutes of steady state were recorded. After this, clamps were opened and the ECC was initiated. The pump speed was increased, until an

Extracorporeal Flow Rate (EFR) of about 4.5 lpm was reached. Online gas analysis was started and again 20 minutes of steady state were recorded. Appropriate adjustments to the gas blender were made by changing the FiO_2 and gas flow in order to keep the arterial oxygen partial pressure at 150 mmHg and oxygen saturation at approx. 75% of the venous return. The CO2 partial pressures were kept around 45 mmHg.

Figure IV-3 shows the average results of the HR, MAP and flows obtained from the different experiments, as well as a screenshot from the recording software *AutoMedic*. A comparison is shown before ECC (A) and during ECC with beating (B) and rested heart (C). The heart rate had a slight increase, when ECC was started, however, there was no significant difference. The MAP slowly decreased from 75 ± 23 mmHg to 61 ± 17 mmHg during the experiment, even after setting the ECCS blood pump to full speed. The arterial flow measure in the aorta ascendens started at 5.18 ± 1.2 lpm and reduced to 2.1 ± 0.9 lpm. From the aorta descendens an initial flow of 2.4 ± 1.4 lpm was registered, decreasing to -0.3 ± 0.3 lpm on ECC. When the heart was at a complete stop, the average MAP decreased to 50 ± 10 mmHg. The flow at the aorta ascendens showed a small negative flow of -0.3 ± 0.3 lpm, which could be a possible indication of backflow to the heart. The aorta descendens showed a negative flow of -1 ± 0.5 lpm, indicating a flow going towards the upper body.

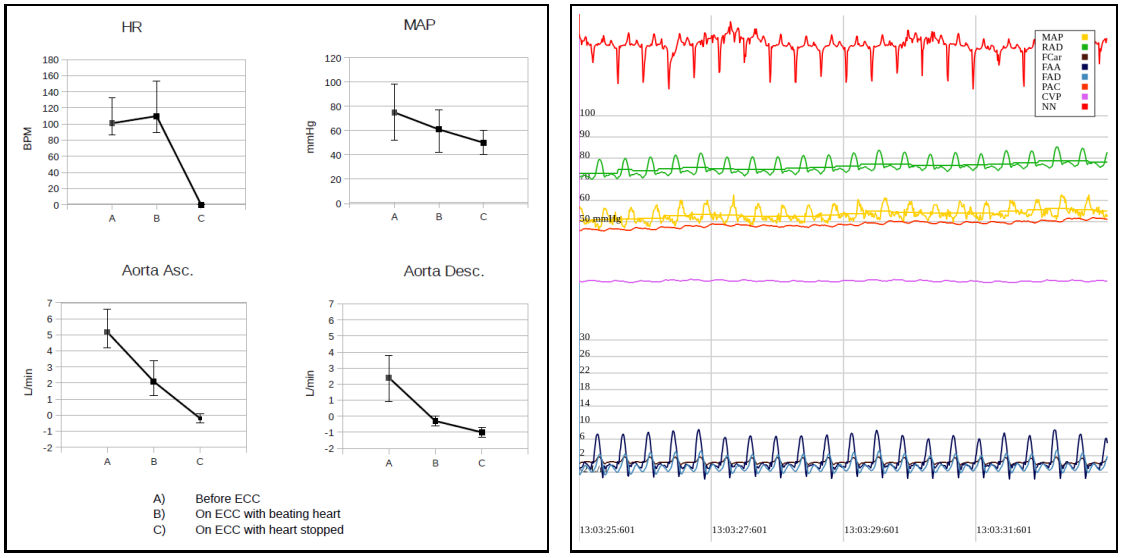

(a) Steady State Analysis (b) Screenshot from *AutoMedic*

Figure IV-3.: Steady state measurements. Shown are overall analysis (a) as well as a screenshot from the recording software during one of the experiments (b)

3.2. Medication: Vasoconstriction and Vasodilation

Medication was administered in order to examine the behavior of the ECCS and to collect valuable reference data for the system models. The medication experiment was later implemented in the virtual system model, as well as in the hydraulic mock model, where

it corresponds to changes of the peripheral resistance, simulating various patient parameters. In one experiment medication was used to test a prototype controller (see section 4).

As a vasoconstrictor 0.1 mg of Norepinephrine (NEP) were given. In all test cases the HR was increased above 200 bpm and then slowly decreased again. Also the MAP was increased by 30 ± 20 mmHg, while the CVP remained relatively constant (see Figure IV.4(b)). As a vasodilator drug Sodium Nitroprusside (SNP) was used. Exemplarily Figure IV.4(a) shows the HR, MAP and CVP for the vasodilation case during one experiment. The HR and the CVP did not show any significant change. The MAP decreased from 65 ± 4 mmHg to 55 ± 4 mmHg. Due to the already low HR the pump speed of the HLM had to be increased after about 2 min, counteracting the drug effect.

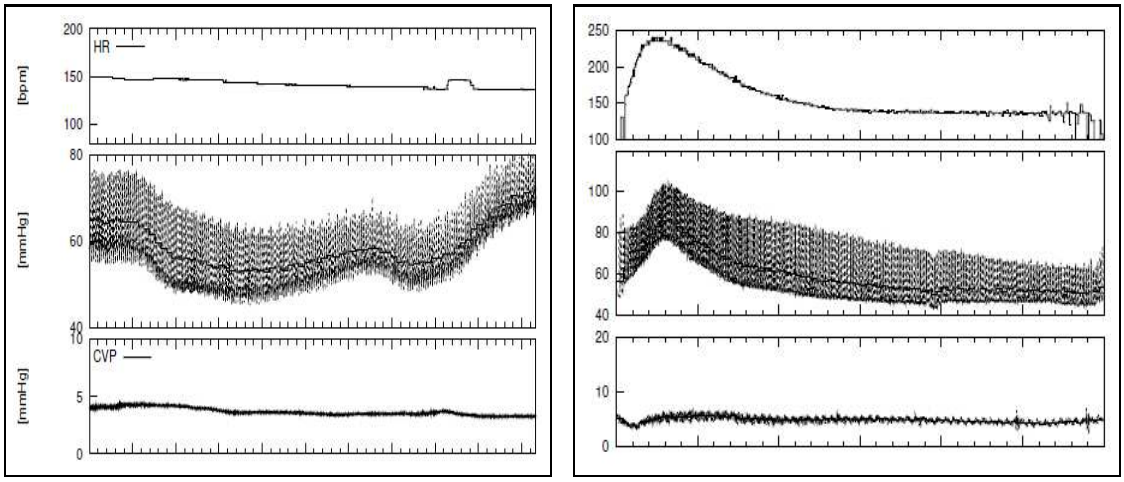

(a) Vasodilation (b) Vasoconstriction

Figure IV-4.: From top to bottom the HR, the MAP and the CVP are shown during the administration of a vasodilator (a) and a vasoconstrictor (b) in one of the experiments.

3.3. Pump Speed Variation

Variations of the pump speed during the animal experiments are a good opportunity for in vivo system identification. The measurements provide approximations of the system dynamics and the relations between the major parameters pump speed, pressures and flows. During the experiment the pump speed was gradually decreased and increased again in steps of 500 rpm. Recordings of the produced pump flow and the different pressure sensors in the HLM were made during each step. The experiment was aborted, if the current state of the pig did not allow a further reduction of the pump speed. Exemplarily, Figure 3.3 shows results from two experiments, in which the pump speed was gradually increased from 1500 rpm to 3500 rpm. From top to bottom, readings from different pressure sensors, the MAP and flow values measured at the HLM (EFR), the aorta ascendens (FAA) and descendens (FAD) are shown. The recordings of pressure values include outlet and

inlet of the HLM, as well as the internal sensor placed before the oxygenator (Pre-Oxy). Additionally, pressure sensors were placed at the cannulas (Art Can, Ven Can).

The highest pressure values were observed before the oxygenator. The change in pump speed leads to a pressure increase on the arterial side and a decrease on the venous side. Regarding the MAP, the two experiments were different. In the first a slight increase of the MAP was observed, while it stayed relatively constant during the second test, where the initial value was already high. Both experiments showed an approximately linear correlation between the pump speed and flow measurements. The EFR started from 1 ± 0.2 lpm and increased up to 4 ± 0.5 lpm at full speed.

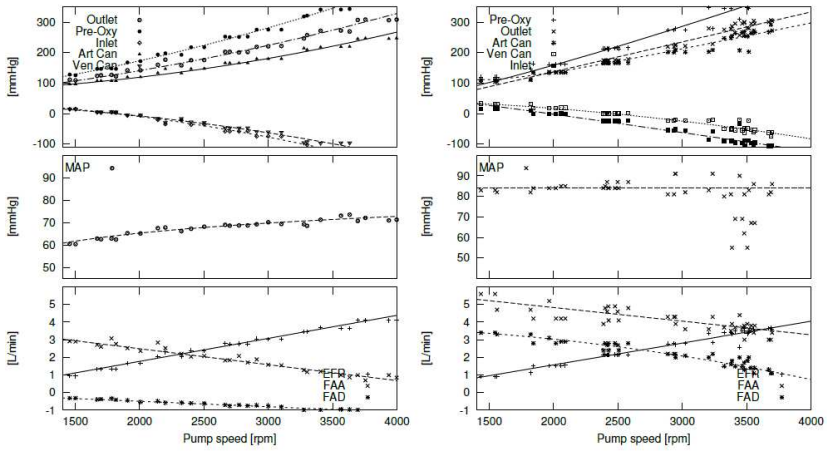

Figure IV-5.: Pump speed variation in two experiments. Shown from top to bottom are readings from pressure sensors, the MAP and flow values.

3.4. Cannula Obstruction

During the experiments the effect of kinking either the arterial or the venous line of the HLM was studied. Since the portable HLMs will be moved together with the patient, obstructions and kinking of the tubings are a possible real world scenario. Kinking events have to be registered immediately, since they put the patient at high risk and can cause severe damage to HLM components.

In this experiment, both the arterial and venous tubings were subsequently clamped and opened again. Figure IV.6(a) shows the closing (left) and opening (right) of the clamp at the arterial line. Obstructing the line led to an immediate decrease of the EFR down to 0 lpm and an increase of the output pressure of the HLM (POut) above 600 mmHg. The intervention is also noticed in the MAP now with a rapid decrease. After about 2 s a pressure increase at the inlet of the HLM can be observed (Pin). Saturation of the pressure transducer before the oxygenator (POxy) was noticed with the arterial line closed, showing 0 mmHg. The countereffects are shown on the right hand side of Figure IV.6(a), when the clamp is opened again and the parameters go back to a normal range again.

In the second part of the experiment the venous line was kinked (see Figure IV.6(b)). Again, the tubing was clamped and opened again. In the MAP and the inlet pressure

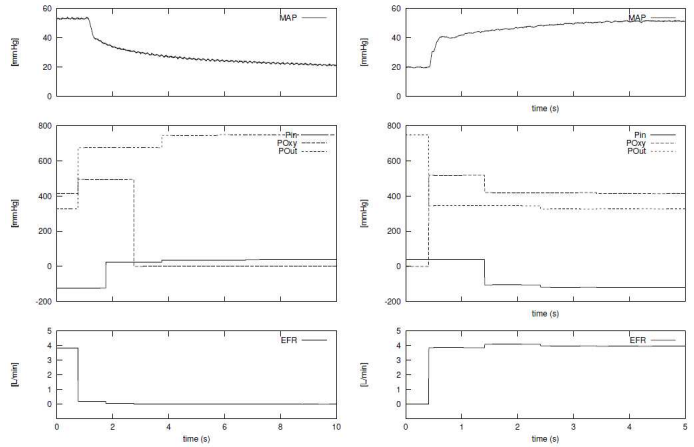

(a) Arterial kinking

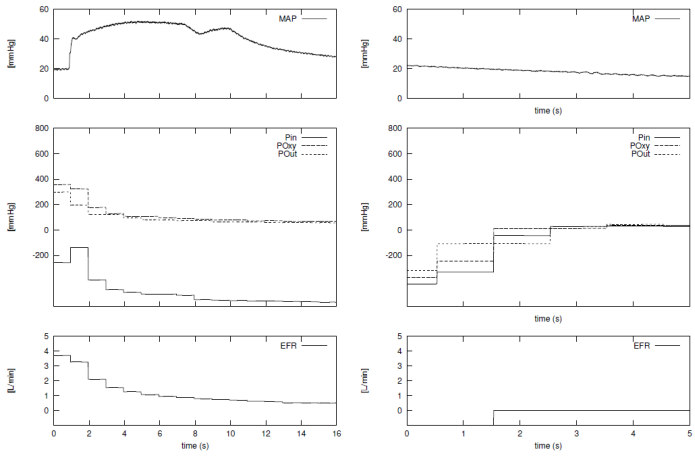

(b) Venous kinking

Figure IV-6.: Cannula obstruction. Closing (left) and opening (right) of the arterial and venous lines.

of the HLM the closing can be observed as a rapid increase. After 2 s a drop in the EFR is visible and also all pressure sensors record decreasing values. Since there is no blood drained into the HLM anymore, the reservoir runs empty after a while. When opening the clamp again, a recovery of the EFR was not possible in the displayed experiment anymore, because the machine was filled with air already. Obviously, the clamping of the venous line is more dangerous for both the patient and the machine.

4. Prototype Controller Test

During one of the experiments there was the opportunity to test a FUZZYC in an in-vivo setting. Although this happened during an early stage of the project, results showed the general applicability of such controllers in the given system setup.

The results of this section have also been published in the Conference Proceedings of the 5th Russian-Bavarian Congress on Biomedical Engineering [1].

A standard fuzzy system with Mamdani inference to control the pump speed of the HLM was implemented. The input parameter of the control loop is the MAP, since it is a major variable in perfusion. For the input variable 3 fuzzy sets are defined, labled as *low*, *medium* and *high*. The controller output is a correction factor of the current pump speed (Delta_RPM). The pump speed is increased if the MAP drops below 50 mmHg (*low*). It is decreased, when the MAP is above 80 mmHg (*high*). For a pressure value in between these limits, the pump speed remains constant (*medium*). The fuzzy sets for both input and output variables are displayed in Figure IV-7. The controller is operating at 1 Hz, i.e. every second the current MAP is obtained and a new pump speed is set accordingly.

In terms of software the MATLAB Fuzzy Toolbox was used to design the controller in the first place. A C++ wrapper for the controller was then developed, which can be used as a stand-alone application and integrates into the *AutoMedic* software framework.

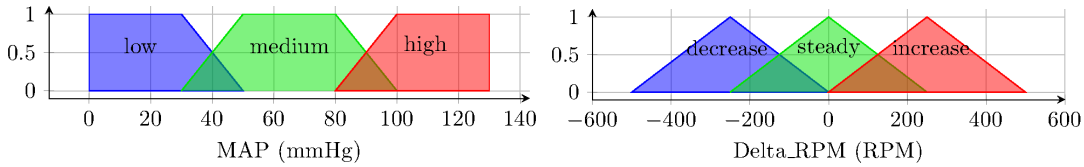

Figure IV-7.: Fuzzy sets for the controller's input variable, the MAP (a), and its output variable Delta_RPM (b).

In order to test the automatic pump speed control, vasoactive drugs were administered successively during the animal experiment. Vasoactive drugs increase or decrease the blood pressure and the heart rate. The taks of the controller was to counteract this effect. First, 0.1 mg of a vasoconstrictor was given, increasing the MAP. After the controller had regulated the MAP back to a normal range, 2 mg of a vasodilator were administered. As an effect the MAP decreased.

In the experiments the FUZZYC displayed expected behavior. Both experiments are illustrated in Figure IV-8. From top to bottom, the MAP, the controller's output (Delta_RPM),

as well as the nominal (RPM_nom) and currently measured (RPM_act) pump speed are displayed. The nominal pump speed is set by the controller, depending on the current pump speed and Delta_RPM. E.g. a current pump speed of 1200 rpm and a Delta_RPM value of -50 rpm result in a nominal speed of 1150 rpm. The actual pump speed is measured by a built-in tachometer of the HLM and can be accessed via the device's CAN Bus.

During vasoconstriction (Figure IV.8(a)), the controller reacts with a decrease of the current pump speed, until the MAP is in a convenient pressure range again. During vasodilation (Figure IV.8(b)) the pump speed is increased to counteract the drop of the MAP value. Both experiments exhibited smooth control characteristics without overshoots or oscillations.
It took about 25 s to regulate the effect of vasoconstriction. Looking at the vasodilation case, the MAP first dropped below 50 mmHg, resulting in an increase of the pump speed. After about 70 s, the MAP had reached the value of 50 mmHg again, which made the controller keep the current pump speed for a while, before pressure dropped again, yielding a further increase of the pump speed. Compared to the experiments without automatic pump speed control during medication, the effect of the administered drugs is alleviated, which encourages automated pump speed control for handling patient-specific variations of the CVS.

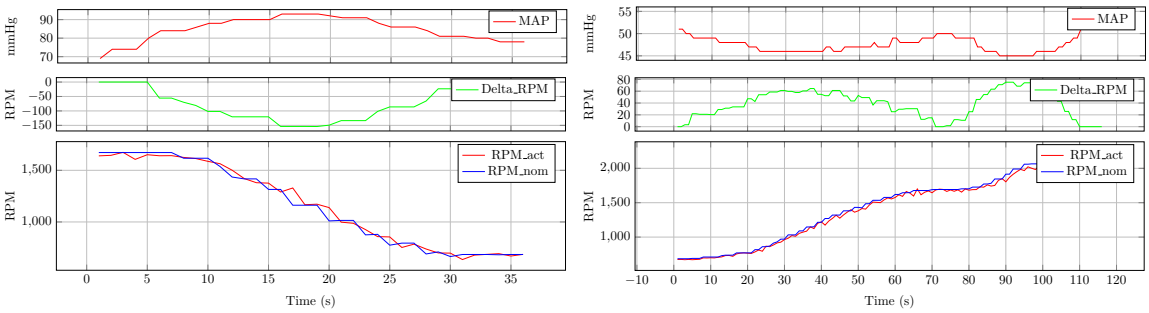

(a) Vasoconstriction

(b) Vasodilation

Figure IV-8.: Control during application of vasoactive drugs. From top to bottom the MAP, the controllers output, Delta_RPM, as well as the nominal (RPM_nom) and currently measured (RPM_act) pump speed are displayed.

In comparison to other control methodologies, the fuzzy approach has several advantages: expert knowledge can be implemented ad hoc and no experimental or mathematical system analysis is needed. Also system maintenance is simple. This allowed the application of the controller in an early stage of the project. However, the controller's simplicity holds some pitfalls: since the controller only monitors the MAP, the pump of the HLM might even be stopped, if the pump speed is decreased due to a high MAP. But also if the MAP is within the given boundaries the pump speed might be set too low to generate sufficient blood flow. Thus, favorable organ perfusion can not be guaranteed. A possible solution to this problem is to integrate more variables into the control loop, such as the arterial and venous oxygen saturation and the blood flow. A second control loop with the blood flow as an input variable has been implemented in successive stages of this project

(see V). Meyrowitz [24] implemented control methods for both parameters with the possibility to manually switch between the controllers. Although it is relatively easy in fuzzy logic to integrate more input parameters, this comes along with an increase of the rulebase (there are m^n rules for a system with n inputs and m fuzzy sets). Automated rulebase generation is also discussed in [27]. A hierarchical fuzzy approach, as introduced by Wang [125], is not applicable, since the pump flow and the MAP are not independent variables. Methods for monitoring and automatically assessing the current state of a patient and using this meta-information for an extended control loop are desirable.

5. Summary

Animal experiments allowed the analysis of different patient and HLM parameters obtained during ECC. The experiments provided the reference data necessary to create the mathematical and hydraulic model of the CVS together with an ECCS. The experiment results show, that a linear relation between EFR and pump speed may be considered, however, the response in pressure may be different. The amount of EFR, that the machine produces will change from one patient to another, also depending on whether the heart is still beating or not, the heart strength and the vascular resistance. In the case of a beating heart, it was noticed, that the load of the heart was effectively reduced during ECC. The negative flow at the aorta ascendens indicates, that the ECCS can produce a small back flow. Most of the cardiac output is used to perfuse the head and upper extremities, while the centrifugal pump flow perfuses the organs in the lower systemic circulation. At different experiments it was not possible to achieve an EFR greater than 5 lpm and a MAP greater than 80 mmHg, even when running the HLM at full speed. Further analysis indicated, that the resistance caused by the cannulas causes a considerable pressure drop. Several studies are already focusing on reducing cannula resistance [46].

Apart from the steady state measurements, system dynamics were identified by a controlled reduction and increase of the centrifugal pump speed. These measurements are approximate only, since they can change from one patient to another. However, they are a good reference for the hydraulic system setup, described in the following part of this work. Additionally, real-world scenarios were simulated during animal experiments, including the administration of vasoactive drugs and kinking of the venous and arterial lines. Clamping the inlet or outlet of the HLM endangers the patient and can do severe damage to the ECCS. Therefore, these events should be detected immediately. Vasoactive medication was also done to test a prototype controller. In all experiments, this controller showed good results and was able to regulate the MAP accurately.

Chapter V

Development and Automation of a Hydraulic Circulatory Mock Model

Contents

1	**Hydraulic Circulatory Model**	45
2	**Proportional-Integral-Controller**	57
3	**H_∞-Controller**	60
4	**Model Reference Adaptive Controller**	63
5	**Fuzzy–Controller**	66
6	**Results**	68
7	**Summary**	77

1. Hydraulic Circulatory Model

Hydraulic models of the circulatory system allow to simulate hemodynamics in a standardized setting. Such models are used for testing and evaluating new devices and their performance prior to clinical implementation. In this work an in-vitro mock model is developed, that mimics hemodynamics under ECC. The model replicates pressure-flow relationships, as observed in animal experiments, and plays an important role in the development of an automated HLM, since it links animal experiments with the mathematical system description. Moreover, the setup allows parameter variations in order to represent natural differences in the human CVS dynamics. Thereby the variability from one patient to another is imitated. For the first time, an objective and comprehensive comparison of different HLM control strategies in an in-vitro setting is made. The purpose of the mock loop in this work is manifold:

- **Hardware/Sensor Test:** The circulation loop can be used to test HLM performance and sensors before animal experiments.

- **Software Test:** The developed software for recording, processing and visualizing sensor and machine data can be examined prior to in-vivo experiments.
- **Mathematical System Description:** Since the component parameters of the mock model can be identified, a mathematical system description can be derived, relating flow, pressure and pump speed variables.
- **Controller Design:** Based on the mathematical system description, robust pump speed controllers for the HLM can be designed.
- **Controller Evaluation:** The setup allows objective and reproducible comparisons between different control strategies due to the standardized setting.

In the following the model setup is described in detail and a mathematical system description is derived and validated. Flow and pressure measurements of the model are compared to data from animal experiments in order to verify the mock loop setup. Based on the analytical description, four state-of-the-art controllers are implemented: a PIC, a HINFC, a FUZZYC and a MRAC. Controllers for both pressure and flow control are designed, in which the control task is to keep the produced pump flow or the pressure difference at the pump at a predefined target value. In the results section of this chapter, the controllers are evaluated in three different scenarios:

1. **Changes of Target Value:** Flow and pressure targets are changed during test runs in order to examine accuracy and response time of the controllers.
2. **External Perturbations:** Sensor data is disturbed by a random noise signal, while the controllers have to follow a given target value.
3. **System Parameter Variation:** System parameters are changed during test runs, revealing the applicability of the different control strategies to a system with uncertain or changing parameters.

1.1. Layout and Components

The design goals for a physical representation of the HLM and the CVS were accuracy, simplicity and usability. Since the Westerhof model, also known as three-element windkessel model, is widely accepted in the community and has been examined thoroughly (see Chapter III), the mock circulatory system used in this work is based on the model described by Sharp and Dharmalingam [81].
The three-element model consists of two resistances (R) and one compliance element (C) in a RCR configuration. This setup was found to be both simple and accurate by multiple studies. The HLM is represented by a motor-driven centrifugal pump connected to a venous and arterial cannula at its in- and outlet. In the most basic configuration other components of the HLM, such as the oxygenator or arterial filters, are replicated by a static resistance at the pump outlet, since their influence on pressure-flow-dynamics is linear with the pump speed. Resistances can be driven via two step motors varying the aperture area of the connected tubings. The compliance is represented by an air chamber. Its dimension can be changed by increasing or decreasing the filling level. Figure V.1(a) shows

a schematic overview of the used components and Figure V.1(b) a photograph of the physical setup.
The following sensors are used to measure the model's parameters: Two pressure sensors (P) measure the in- and outlet pressure of the pump. A flow sensor (F) and a tachometer (W) complement the setup with measures of the pump speed and produced pump flow. An AD/DA-Converter (National Instruments DAQ 6036E) together with a control unit (laptop) is used to receive and process sensor signals, as well as to control the motor speed and the variable resistances of the patient module via electric motors (M).

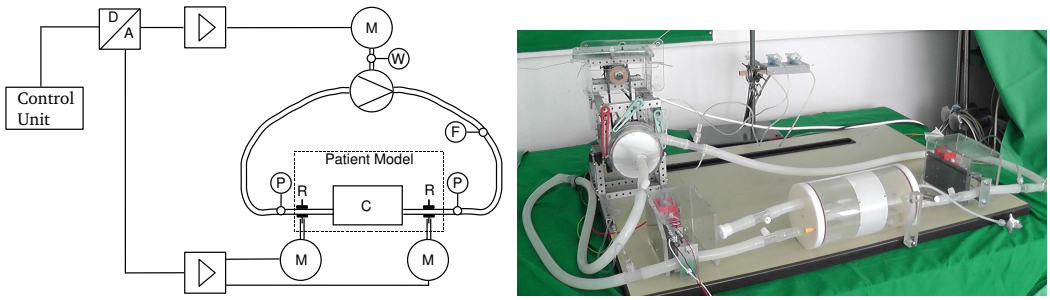

(a) (b)

Figure V-1.: Schematic (a) and physical (b) layout of the hydraulic mock model with connected sensors and control unit.

In order to design controllers for the plant, an analytical description of the components is needed. In the following, the various elements are described in detail and their mathematical representation is derived in parallel. First, motor parameters are identified, followed by the pump and the CVS component. After that, all components are aggregated and the system is validated by comparison of the mathematical system description with measurements from the mock circulation loop. Finally, the model is justified by comparison with data from animal experiments.

1.1.a. Motor

To drive the centrifugal pump a direct current motor (Faulhaber Company) is used. The motor is controlled via a direct current power controller that can be actuated by the analog output of the AD/DA-Converter. The motor speed is measured by a tachometer.
A mathematical representation follows the state space model of a direct current motor [126]:

$$\begin{bmatrix} \dot{I}_A(t) \\ \dot{\omega}(t) \end{bmatrix} = \begin{bmatrix} -\frac{R_A}{L_A} & -\frac{K_T}{L_A} \\ \frac{K_T}{J} & -\frac{T_{Fl}}{J} \end{bmatrix} \cdot \begin{bmatrix} I_A(t) \\ \omega(t) \end{bmatrix} + \begin{bmatrix} \frac{1}{L_A} & 0 \\ 0 & -\frac{1}{J} \end{bmatrix} \cdot \begin{bmatrix} V_A(t) \\ T_L(t) \end{bmatrix} \tag{V.1}$$

The armature current I_A and the motor's rotation speed ω are the states of the differential equation system. Inputs are the armature voltage V_A and the load torque T_L. R_A, L_A and K_T describe the armature resistance, the phase inductivity and the engine torque constant. These constants are given in the motor's data sheet. The load torque T_L can be derived from characteristics of the centrifugal pump (see 1.1.b). The friction torque T_{Fl} and the

motor's inertia J are identified experimentally.
Since the time constant of I_A is much lower than of ω, a state reduction of the equation system can be performed. I_A is considered as steady state, which yields $\dot{I}_A(t) = 0$. Now the first part of the equation system reads

$$0 = -\frac{R_A}{L_A} I_A(t) - \frac{K_T}{L_A}\omega(t) + \frac{1}{L_A} V_A(t). \tag{V.2}$$

If Equation (V.2) is solved for $I_A(t)$ and applied to the second state in Equation (V.1), $\dot{\omega}(t)$ is given as

$$\dot{\omega}(t) = \frac{K_T}{J}\left(-\frac{K_T}{R_A}\omega(t) + \frac{1}{R_A} V_A(t)\right) - \frac{T_{Fl}}{J}\omega(t) - \frac{1}{J} T_L(t). \tag{V.3}$$

For the sake of simplicity Equation (V.3) can be written as

$$\dot{\omega}(t) = k_1 V_A(t) - k_2\omega(t) - k_3 T_L(t), \tag{V.4}$$

with

$$\begin{aligned} k_1 &= \frac{K_T}{J R_A} \\ k_2 &= \frac{K_T^2}{J R_A} + \frac{T_{Fl}}{J} \\ k_3 &= \frac{1}{J}. \end{aligned}$$

The motor's response to changes in the actuating variable V_A can be recorded now and T_{Fl} and J can be identified using Equation (V.4). Figure V-2 shows the experimentally measured rotation speed in comparison to the calculated speed and with respect to step changes in the armature voltage. For motor speeds below 1000 rpm a rather large difference between the model and the real setup can be observed. However, the identified parameters give a good approximation for motor speeds above 1000 rpm, which are mainly used in this application.

1.1.b. Pump

By magnetic coupling the motor drives a centrifugal pump (FloPump by IBC). Following [126], the pump can be modeled as

$$\Delta p(t) = h_{NN}\omega(t)^2 - h_{NV}\omega(t)q(t) - h_{VV}q(t)^2. \tag{V.5}$$

$\Delta p(t)$ represents the pressure difference between pump inlet and pump outlet. $q(t)$ stands for the produced pump flow. h_{NN}, h_{NV} and h_{VV} are pump constants, that can be identified experimentally: to identify h_{NN}, the inlet is connected to a water tank, while the outlet is branched off, thus the pump does not produce any flow. If the pressure difference $\Delta p(t)$ at different pump speeds is measured with all flow-related terms equal 0, then h_{NN} reads

$$h_{NN} = \frac{\Delta p(t)}{\omega(t)^2}. \tag{V.6}$$

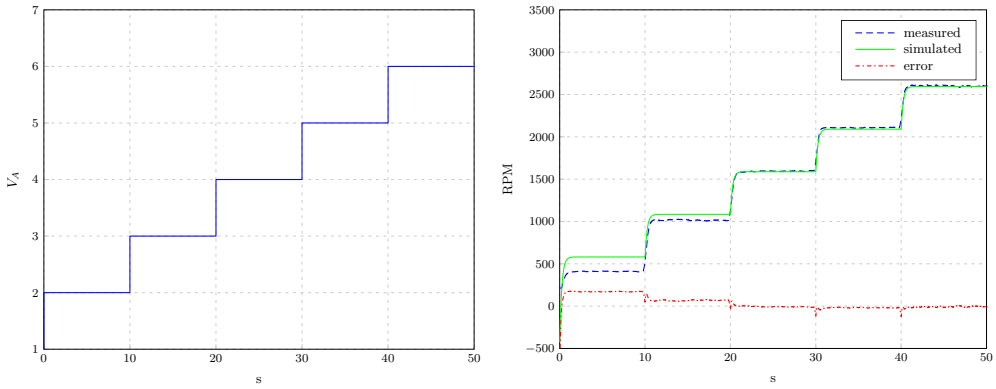

(a) Armature voltage (b) Rotation speed

Figure V-2.: Comparison of measured and simulated rotation speed of the dc-motor (b) as a response to step changes in the armature voltage (a).

To determine h_{NV} and h_{VV}, the pump is connected to a water circulation that consists of an open water tank and connecting tubings. The tubing is elastic, so its resistance is variable. The pump runs at constant speed. While increasing the tube resistance, changes in pressure and flow are measured. This procedure can be repeated for different pump speeds. Using the standard least square method, the pump constants can be identified from the experimental data. In all tests ordinary tap water, mixed with copper sulfate (0.5 g/l), was used as a circulating medium. The different viscosity compared to blood is not significant for the identification of the model components and the control design. Tests have shown, that air bubbles in the system significantly change the produced pump flow. Therefore, it had to be assured that the system was air-free before experiments.

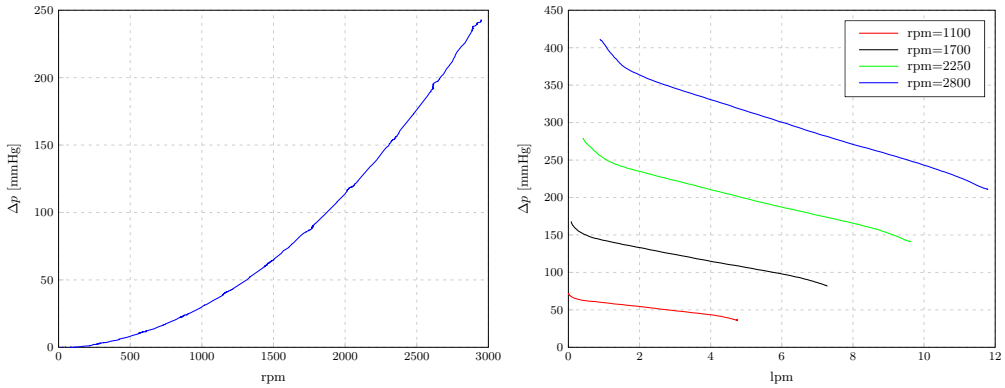

(a) (b)

Figure V-3.: Collected data for pump identification. Pressure difference Δp during increase of ω with a branched off pump outlet (a) and resistance-dependant pressure-flow-relation at constant speeds (b).

Figure V-3 shows the experimental data that was collected during the identification process. V.3(a) shows the pressure difference that was measured at the pump with a final resistance (no flow) and constantly increasing pump speed. V.3(b) displays the pressure-flow relation at constant motor speeds and variable tube resistances. To verify the pump model, the measured pressure difference and flow at various rotation speeds are compared with their predicted values. Figure V-4 shows the comparisons for the produced pressure difference Δp (a) and pump flow (b). There was a good prediction for Δp with a mean

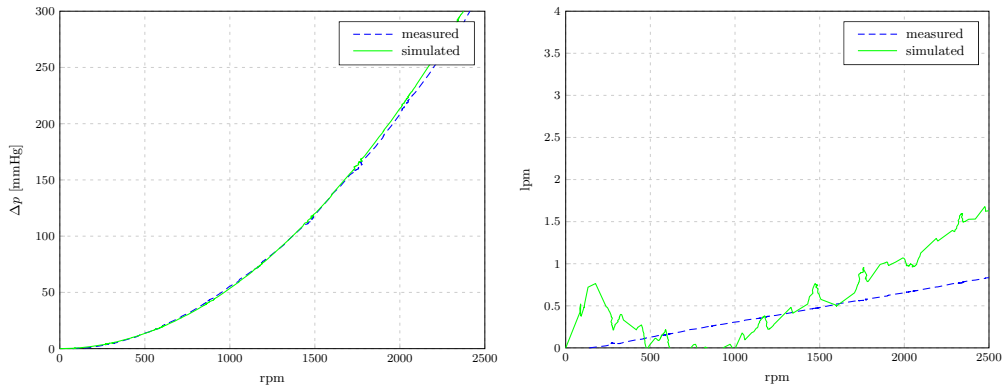

(a) (b)

Figure V-4.: Comparison of predicted (green) and measured (blue) pressure difference (a) and flow (b).

error of 5.68 mmHg but a rather large mean error of 0.48 lpm for flow prediction. Those variations are considered as parameter uncertainties in the control design.

Measurements for pump identification are also used to derive the motor's load torque T_L. The required power for the pump is

$$P = q(t)\Delta p(t). \tag{V.7}$$

Furthermore it holds, that

$$P = T_L \omega(t). \tag{V.8}$$

Hence, the required torque is

$$T_L = \frac{q(t)\Delta p(t)}{\omega(t)}. \tag{V.9}$$

1.1.c. Cardiovascular Components

The setup for the cardiovascular component follows the three-element Windkessel model [81]. Arteries are modeled as elastic chambers, veins and capillaries as linear resistances. In the RCR-configuration used, the two resistances replicate the aortic and peripheral resistance. The air chamber represents the total compliance of the aortic tree.

The analytical description is derived from the electrical analogon, a parallel circuit of a capacitor and a resistance (see Figure V.5(a)). The pressure-flow relationship in the cardio-

vascular component can be described by the following equation:

$$\left(1 + \frac{R_a}{R_p}\right) q(t) + C R_a \frac{dq(t)}{dt} = \frac{p(t)}{R_p} + C\frac{dp(t)}{dt} \tag{V.10}$$

R_a and C describe the aortic resistance and capacity, while R_p models the peripheral resistance. Equation (V.10) can be derived by simple considerations from circuit theory. First, the circuit is redrawn with common labels from network theory (Figure V.5(b)).

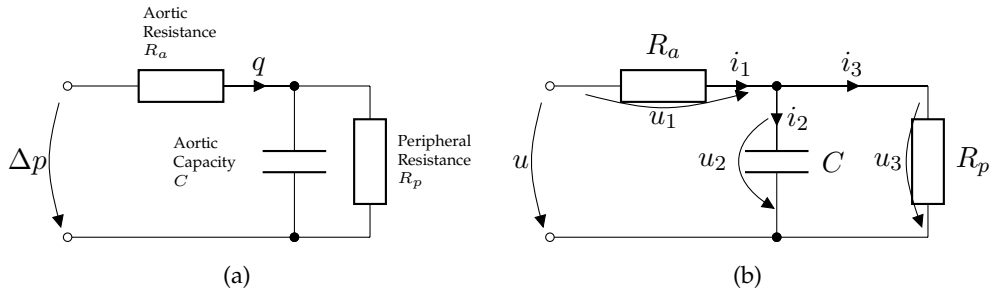

Figure V-5.: Network representation of the three-element Windkessel model (a) with standard labels from circuit theory (b).

Applying Kirchhoff's and Ohm's laws the following relationships hold:

$$\begin{aligned}
i_1(t) &= i_2(t) + i_3(t) && \text{(V.11)}\\
i_2(t) &= C\frac{du_2(t)}{dt} && \text{(V.12)}\\
i_3(t) &= \frac{u_3(t)}{R_p} && \text{(V.13)}\\
u(t) &= u_1(t) + u_2(t) && \text{(V.14)}\\
u_1(t) &= i_1(t)R_a && \text{(V.15)}\\
u_2(t) &= u_3(t) && \text{(V.16)}
\end{aligned}$$

With (V.12) and (V.13) in (V.11) $i_1(t)$ reads

$$i_1(t) = C\frac{du_2(t)}{dt} + \frac{u_2(t)}{R_p}. \tag{V.17}$$

Replacing $u_2(t)$ in (V.17) with (V.14) yields

$$i_1(t) = C\frac{d(u(t) - u_1(t))}{dt} + \frac{u(t) - u_1(t)}{R_p}. \tag{V.18}$$

With (V.15) $i_1(t)$ can be written as

$$i_1(t) = C\frac{d(u(t) - i_1(t)R_a)}{dt} + \frac{u(t) - i_1(t)R_a}{R_p}. \tag{V.19}$$

Rearranging the equation yields

$$\left(1 + \frac{R_a}{R_p}\right) i_1(t) + CR_a \frac{di_1(t)}{dt} = \frac{u(t)}{R_p} + C\frac{du(t)}{dt}. \tag{V.20}$$

Since $i_1(t)$ corresponds to the flow $q(t)$ and $u(t)$ represents the pressure difference $\Delta p(t)$, Equation (V.20) is equivalent to Equation (V.10).

In the physical setup a change of resistances is realized by a change of the tube diameter. Resistances can be changed via two step motors, which are actuated via the analog output of the AD/DA-Converter.

A closed air chamber represents the aortic capacity. Changes in the capacity are related to changes in the gas volume within the chamber. They can be realized by changing the filling level of the fluid. To identify the capacity, changes in pressure at different filling levels were measured (see Table V.1). The dimensions of the chamber allow capacity values in the range of 0.46 to $0.9\frac{ml}{mmHg}$.

Filling level (ml)	Pressure change ($mmHg$)	Capacity ($\frac{ml}{mmHg}$)
500	166	0.9
550	180	0.83
600	197	0.76
650	225	0.67
700	256	0.58
750	290	0.52
800	324	0.46

Table V.1.: Capacity measurements of the closed chamber.

1.2. Model Aggregation

In the last section the components of the hydraulic model of the human circulatory system, together with a simplified model of a HLM (motor, pump), were introduced. Each individual component was identified and described mathematically. As an overview, the descriptive equations for the motor (V.21), the load torque (V.22), the pump (V.23) and the cardiovascular component (V.24) are listed again:

$$\dot{\omega}(t) = k_1 V_A(t) - k_2\omega(t) - k_3 T_L(t) \tag{V.21}$$

$$T_L = \frac{q(t)\Delta p(t)}{\omega(t)} \tag{V.22}$$

$$\Delta p(t) = h_{NN}\omega(t)^2 - h_{NV}\omega(t)q(t) - h_{VV}q(t)^2 \tag{V.23}$$

$$\left(1 + \frac{R_a}{R_p}\right) q(t) + CR_a\frac{dq(t)}{dt} = \frac{\Delta p(t)}{R_p} + C\frac{d\Delta p(t)}{dt} \tag{V.24}$$

In the following. those Equations are transformed into a nonlinear state space representation of the complete system. A linearized form of this representation will be the basis for the design of the controllers.

1.2.a. State Space Representation

In the state space representation nonlinear, time-variant systems with one input and one output variable can be written as

$$\dot{\mathbf{x}}(t) = \mathbf{f}(\mathbf{x}(t), u(t)) \tag{V.25}$$

$$y(t) = g(\mathbf{x}(t), u(t)). \tag{V.26}$$

$\dot{\mathbf{x}}(t)$ is a vector with the time-dependent terms of the system, the system states. In this particular case $\dot{\mathbf{x}}(t)$ is two-dimensional with $\mathbf{x}(t) = [\omega(t) \quad q(t)]^T$ for flow and $\mathbf{x}(t) = [\omega(t) \quad \Delta p(t)]^T$ for pressure control representation. In the given system there is only one input variable, the armature voltage, $u(t) = V_A(t)$, which controls the motor speed. The control (output) equation reduces to $y(t) = q(t)$ for flow and $y(t) = \Delta p(t)$ for pressure control.

Exemplarily, the state space representation with the pump flow as a control variable is derived. The state space model for pressure control can be calculated in an analogous manner. For reasons of clarity, time-dependancy of the variables is not indicated in the following considerations.

First, the load torque equation (V.22) and the motor's equation (V.21) are combined:

$$\dot{\omega} = k_1 V_A - k_2 \omega - k_3 \frac{q \Delta p}{\omega} \tag{V.27}$$

Δp is replaced by the pump transfer equation (V.23):

$$\dot{\omega} = k_1 V_A - k_2 \omega - k_3 \left(h_{NN} q \omega - h_{NV} q^2 - h_{VV} \frac{q^3}{\omega} \right) = f_1(\omega, q, V_A) \tag{V.28}$$

Equation (V.28) is the first equation of the state space representation.

Since the system is a closed-loop system, the pressure difference at the pump is equal to the pressure difference at the CVS. Therefore, Δp in (V.24) is replaced by (V.23). With the derivative of Δp

$$\frac{d\Delta p}{dt} = 2h_{NN}\dot{\omega}\omega - h_{NV}\dot{\omega}q - h_{NV}\omega\dot{q} - 2h_{VV}\dot{q}q \tag{V.29}$$

(V.24) can be written as

$$\begin{aligned} \left(1 + \frac{R_a}{R_p}\right) q + C R_a \dot{q} &= \frac{h_{NN}\omega^2 - h_{NV}\omega q - h_{VV} q^2}{R_p} \\ &+ C(2h_{NN}\dot{\omega}\omega - h_{NV}\dot{\omega}q - h_{NV}\omega\dot{q} - 2h_{VV}\dot{q}q) \end{aligned} \tag{V.30}$$

and solved for $\dot{q}$:

$$\dot{q} = \frac{\frac{1}{Rp}\left(h_{NN}\omega^2 - h_{NV}\omega q - h_{VV} q^2\right) + C\left(2h_{NN}\dot{\omega}\omega - h_{NV}\dot{\omega}q\right) - \frac{1}{Rp}\left(Rc + Rp\right) q}{C\left(Rc + h_{NV}\omega + 2h_{VV} q\right)}. \tag{V.31}$$

Replacing $\dot{\omega}$ in (V.31) by (V.28) finally yields the second equation of the state space model:

$$\begin{aligned}\dot{q} &= \frac{\frac{1}{Rp}\left(h_{NN}\omega^2 - h_{NV}\omega q - h_{VV}q^2\right)}{C\left(Rc + h_{NV}\omega + 2h_{VV}q\right)} \\ &+ \frac{C\left(2h_{NN}\omega - h_{NV}q\right)\left(k_1 V_A - k_2\omega - k_3\left(h_{NN}q\omega - h_{NV}q^2 - h_{VV}\frac{q^3}{\omega}\right)\right)}{C\left(Rc + h_{NV}\omega + 2h_{VV}q\right)} \\ &- \frac{\frac{1}{Rp}\left(Rc + Rp\right)q}{C\left(Rc + h_{NV}\omega + 2h_{VV}q\right)} \\ &= f_2(\omega, q, V_A)\end{aligned} \tag{V.32}$$

By the equations (V.28) and (V.32) the state space representation of the second-order model with $\mathbf{x}(t) = [\omega(t) \quad q(t)]^T$ is fully characterized:

$$\begin{bmatrix} \dot{\omega} \\ \dot{q} \end{bmatrix} = \begin{bmatrix} f_1(\omega, q, V_A) \\ f_2(\omega, q, V_A) \end{bmatrix} \tag{V.33}$$

$$y = q \tag{V.34}$$

1.2.b. Linearized State Space Representation

In control theory linear models are often used, even if the given system has nonlinear characteristics. If the control has to keep a system at a certain working point, despite external perturbations, then the system may be linearized around that working point. If the control is successfull, the system will always stay close to the working point and it is sufficient to characterize the system around that setpoint. This is a common procedure to ease the design of controllers and can also be deployed in this work, since the control task is to keep pressure or flow at predefined setpoints. In the following, the derived system description is linearized and then compared to its nonlinear version.

A linearized version of a general state space representation with one input variable reads

$$\Delta\dot{\mathbf{x}} = \mathbf{A}\Delta\mathbf{x} + \mathbf{B}\Delta u \tag{V.35}$$

$$\Delta y = \mathbf{C}\Delta\mathbf{x} + \mathbf{D}\Delta u \tag{V.36}$$

with

$$\mathbf{A} = \left[\frac{\partial f_i}{\partial x_j}\right]_{(x^*,u^*)}, \mathbf{B} = \left[\frac{\partial f_i}{\partial u_j}\right]_{(x^*,u^*)}, \mathbf{C} = \left[\frac{\partial g_i}{\partial x_j}\right]_{(x^*,u^*)}, \mathbf{D} = \left[\frac{\partial g_i}{\partial u_j}\right]_{(x^*,u^*)}. \tag{V.37}$$

$\mathbf{A}$ denotes the system matrix, $\mathbf{B}$ the input matrix, $\mathbf{C}$ denotes the output matrix and $\mathbf{D}$ the direct matrix. The operating point is described by x^* and u^*. For the given setup the linearized system representation can be written as

$$\begin{bmatrix} \Delta\dot{\omega} \\ \Delta\dot{q} \end{bmatrix} = \mathbf{A}\begin{bmatrix} \Delta\omega \\ \Delta q \end{bmatrix} + \mathbf{B}\,\Delta V_A \tag{V.38}$$

$$\Delta y = \mathbf{C}\begin{bmatrix} \Delta\omega \\ \Delta q \end{bmatrix} + \mathbf{D}\,\Delta V_A \tag{V.39}$$

with

$$\mathbf{A} = \left[\begin{array}{cc} \frac{\partial f_1}{\partial \omega} & \frac{\partial f_1}{\partial q} \\ \frac{\partial f_2}{\partial \omega} & \frac{\partial f_2}{\partial q} \end{array} \right]_{(\omega^*, q^*, V_A^*)} \tag{V.40}$$

$$\mathbf{B} = \left[\begin{array}{c} \frac{\partial f_1}{\partial V_A} \\ \frac{\partial f_2}{\partial V_A} \end{array} \right]_{(\omega^*, q^*, V_A^*)} \tag{V.41}$$

$$\mathbf{C} = \left[\begin{array}{cc} \frac{\partial g}{\partial \omega} & \frac{\partial g}{\partial q} \end{array} \right]_{(\omega^*, q^*, V_A^*)} = [0 \quad 1] \tag{V.42}$$

$$\mathbf{D} = \left[\begin{array}{c} \frac{\partial g}{\partial V_A} \end{array} \right]_{(\omega^*, q^*, V_A^*)} = [0]\,. \tag{V.43}$$

The linearized state space model can be equivalently represented by a second-order transfer function in the frequency domain:

$$G(s) = \frac{b_1 s + b_0}{s^2 + a_1 s + a_0}. \tag{V.44}$$

The transformation from the state space representation to the transfer function using an element-wise Laplace Transformation is described in [127], volume 1, p.246ff, for example.

1.2.c. Comparison of Linear and Nonlinear System Representation

In order to justify the linearization, the linarized state space representation is compared with the nonlinear system representation. The working point is set at $V_A^* = 6\,\mathrm{V}$, yielding a pump flow of $q^* = 2.54\,\mathrm{lpm}$, a pressure difference of $\Delta p^* = 235.32\,\mathrm{mmHg}$ and a rotational motor speed of $\omega^* = 302.06\,\mathrm{rad/s}$. To identify differences between the two representations, the system is excited with a sinusoidal input voltage, varying V_A between 4 and 8 V at a frequency of 0.16 Hz. Figure V-6 shows the pressure and flow dynamics of the nonlinear model and its linearized state space representation. The mean absolute error between the two representations was 10.68 mmHg for the pressure difference between the pump inlet and pump outlet, and 0.07 lpm for the pump flow. Both values are considered as acceptable for the control design. Please note that the linear representation is only used for the design of the controllers and not for their evaluation.

1.3. Model Validation

1.3.a. Validation of analytical system description

To validate the mathematical system description, the motor speed, flow and pressure values under step changes of the input variable V_A are measured and compared to their predicted values. Figure V-7 shows the dynamics of the variables in comparison. Generally a good congruency between the experimentally measured values and the mathematically predicted values can be observed. Absolute mean errors were 41.66 rpm for the motor speed, 0.11 lpm for the pump flow and 6.92 mmHg for the pump's pressure difference. Detailed analysis revealed a time delay of $T_t = 200\,\mathrm{ms}$ between the simulated and physical model. To account for this delay in the controller design, the model's transfer function can be written as

$$G(s) = \frac{b_1 s + b_0}{s^2 + a_1 s + a_0} \exp\left(-s T_t\right). \tag{V.45}$$

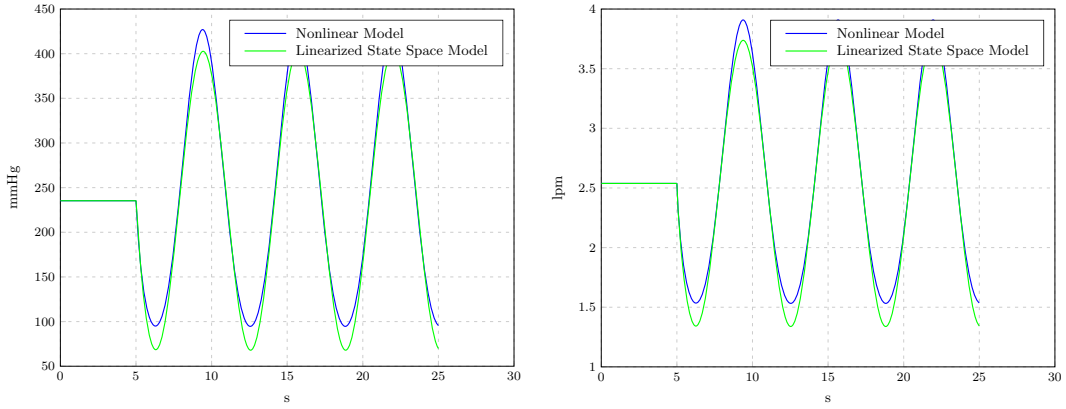

(a) (b)

Figure V-6.: Pressure (a) and flow (b) dynamics of the nonlinear system model and its linearized state space representation during sinusoidal changes of the pump speed around a predefined working point.

1.3.b. Comparison with animal experiments

The hydraulic model is compared with data from animal experiments. During two experiments the motor speed of the HLM was decreased from 3500 rpm to 1500 rpm in steps of 500 rpm, and increased again to the initial value (see Chapter IV). Pump parameters (flow and pressure difference) were recorded. Figure V-8 shows the animal data in comparison with the hydraulic setup. The hydraulic model data is compared with respect to the mean values of the animal experiments. There was a rather large difference for pressure values (Fig.V.8(a)) with a mean error of 44.45 mmHg and a standard deviation of 33.63 mmHg. For the pump flow (Fig.V.8(b)) results were better with a mean error of 0.33 lpm and a deviation of 0.05 lpm. However, many factors influence the acquired data of the animal experiments such as the animal's weight, height or current physiological condition. Also different cannula size influences the results. The difference in pump flow between the two displayed experiments of around 0.5 lpm at a pump speed of 2000 rpm examplarily shows how big the deviations from one subject to another can be. Therefore, the primary goal of the hydraulic setup was not to exactly match one experiment, but to display the same pressure and flow dynamics within a reasonable range of values. Considering these factors, the constructed model replicates the in-vivo data sufficiently.

In the following, four control strategies are designed based on the mathematical system description. Each control method is shortly introduced and the design steps needed for this model are described.

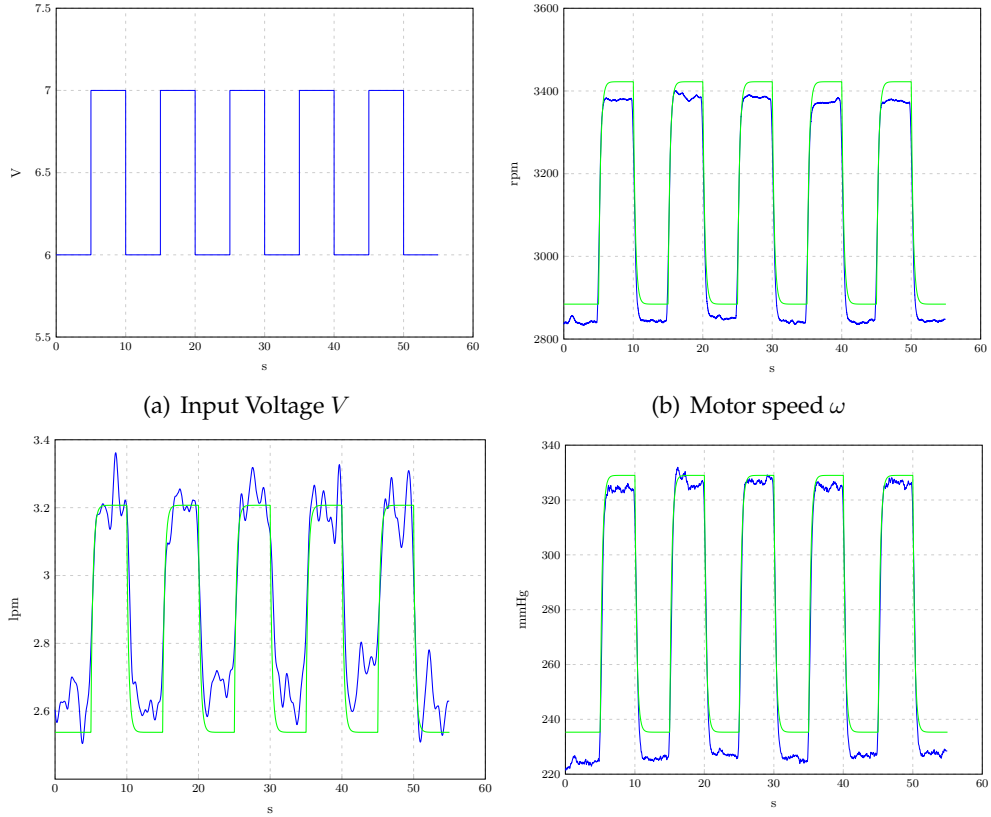

(a) Input Voltage V

(b) Motor speed ω

(c) Flow q

(d) Pressure difference Δp

Figure V-7.: Comparison of simulation model (green) and the hydraulic model (blue). Shown are the input voltage for speed control (a) and the resulting motor speed (b), flow (c) and pressure (d) curves.

2. Proportional-Integral-Controller

The PIC is one of the most established methodologies in control theory. Its mechanism is rather simple. The P-Contribution accounts for the present error, while the I-Contribution accounts for accumulated errors in the past. I.e., as long as there is a deviation from the setpoint, the manipulating variable should be changed. Given the control loop in Figure V-9, the control output $u(t)$ in the time domain is given as

$$u(t) = K_P\, e(t) + K_I \int_0^t e(\tau)\, \mathrm{d}\tau. \tag{V.46}$$

The parameter K_P proportionally weighs the offset $e(t)$, while K_I amplifies the integrated control deviation.

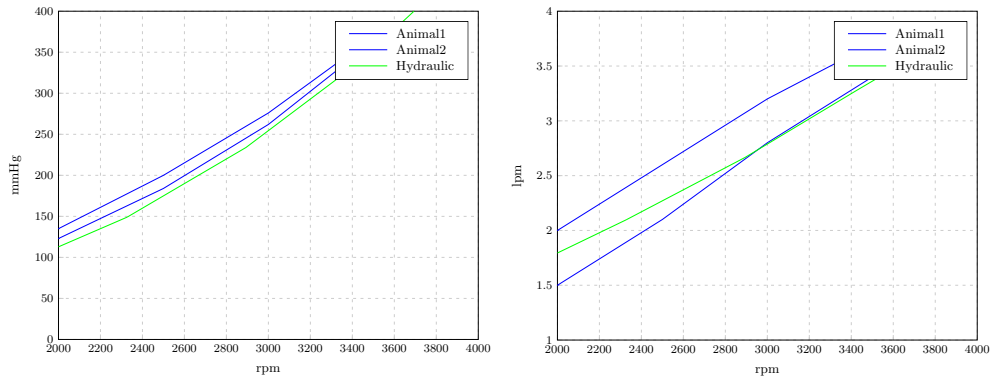

(a) (b)

Figure V-8.: Comparison of hydraulic model and data from two animal experiments. Shown are pump flow (b) and pressure (a) characteristics.

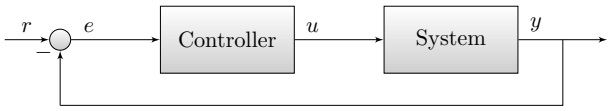

Figure V-9.: PI-Controller structure diagram.

2.1. Control Design

The parameters K_P and K_I are to be identified, such that the control system is stable. Generally spoken, control systems are stable, if bounded excitations lead to bounded system reactions. A common approach to verify system stability is to analyze the transfer function $G(s)$. Considering Figure V-9 again, the transfer function of the closed loop system reads

$$G(s) = \frac{G_C(s, K_P, K_I)G_S(s)}{1 + G_C(s)G_S(s)}. \tag{V.47}$$

G_C specifies the transfer function of the controller and G_S the transfer funtion of the plant (system). The control system is stable, if every pole of $G(s)$ has a negative real part (see [127]):

$$\Re\{s_i\} < 0 \quad (i = 1, 2, \ldots, n) \tag{V.48}$$

Replacing G_C and G_S by numerator and denominator polynomials ($G_C = \frac{N_C}{D_C}$, $G_S = \frac{N_S}{D_S}$), Equation (V.47) can be written as

$$G(s) = \frac{D_C(s, K_P, K_I)D_S(s)}{N_C(s, K_P, K_I)N_S + D_C(s, K_P, K_I)D_S(s)}. \tag{V.49}$$

The denominator polynomial of Equation (V.49) is the characteristic polynomial $P(s)$ of the control loop, which is used to analyze the stability criterion. An elegant method to verify system stability is the Paramter Space Approach introduced by Ackermann [128]. In the

Parameter Space Approach the Laplace variable s is replaced by the complex frequency $j\omega$, which is restricted to real non-negative values [128].

The boundaries between stable and instable candidates for the control parameters are given by

$$Re\{P(j\omega, K_P, K_I)\} = 0 \tag{V.50}$$
$$Im\{P(j\omega, K_P, K_I)\} = 0. \tag{V.51}$$

Equations (V.50) and (V.51) determine an equation system with 2 unknown parameters (K_P, K_I) and a control variable ω. K_P and K_I can be expressed in dependency of ω:

$$K_P = f_1(\omega) \tag{V.52}$$
$$K_I = f_2(\omega) \tag{V.53}$$

The stability boundaries for K_P and K_I can be found by sweeping over ω.

To robustly design the PIC for the mock system, the motor's inertia J, the friction torque T_{Fl}, the pump constants h_{NN}, h_{NV}, h_{VV} and parameters of the CVS R_a, R_p and C are varied by 10%. For each parameter constellation the stability boundaries are plotted in the K_P-K_I-plane (Fig. V-10), for both flow and pressure control. Each curve is the envelope function for stable K_P-K_I-pairs at certain model parameters. The green area marks stable K_P-K_I-pairs for the plant, considering the 10% variations of the plant parameters.

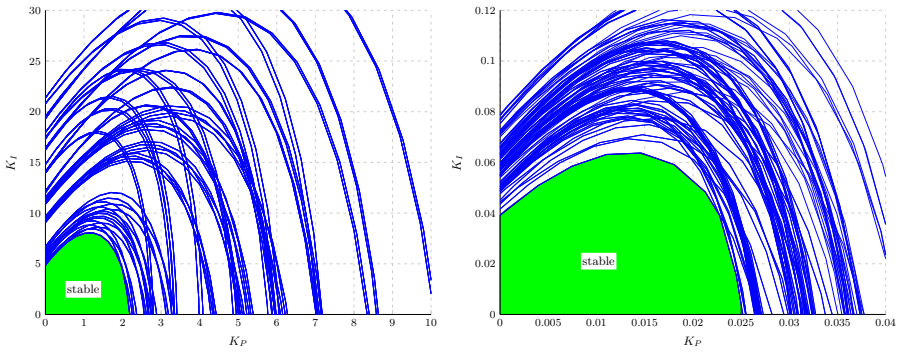

(a) Stability boundaries for flow control. (b) Stability boundaries for pressure control.

Figure V-10.: Stability boundaries for various model parameters. K_P-K_I-pairs within the green area lead to stable control of the plant, considering parameter uncertainties of 10%.

Given the pairs of candidates for a stable control, specific parameters can be selected based on a quality criterion which calculates the accumulated control error:

$$J = \int_0^T |r(\tau) - y(\tau)| \, \mathrm{d}\tau, \tag{V.54}$$

with the target value $r(\tau)$ and the system's output $y(\tau)$. A specific K_P-K_I-pair can be chosen, that reveals a small J value and minimal overshoots in the system's step response.

Figure V-11 shows the system response to a unit step of the input variable for three parameter pairs that exhibited the smallest values of J. The step response is displayed for both flow and pressure control again.

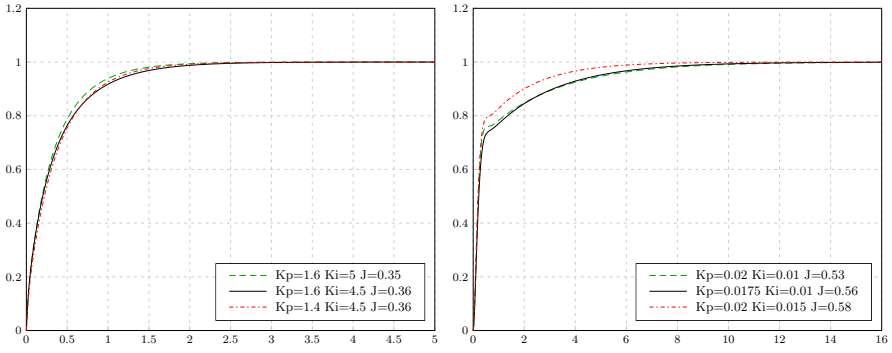

(a) Step response for flow control. (b) Step response for pressure control.

Figure V-11.: System's step response for different K_P-K_I-pairs.

3. H_∞-Controller

H_∞-Control is a popular strategy for robust control. It is based on frequency response characteristics, resulting in a controller, that accounts for particular specifications, such as bandwidth limitations or robustness against parameter uncertainties [129].

In H_∞-Control the control problem is formulated as an optimization problem and the controller is considered as a solution of that problem. The simple control loop (Figure V.12(a)) is extended with the additional input w and output z, which are used for the performance rating of the controller (Figure V.12(b)). Following [127], the control path in Figure V.12(b) is described by

$$\begin{pmatrix} Z(s) \\ Y(s) \end{pmatrix} = \begin{pmatrix} G_{zw}(s) & G_{zu}(s) \\ G_{yw}(s) & G_{yu}(s) \end{pmatrix} \begin{pmatrix} W(s) \\ U(s) \end{pmatrix} \tag{V.55}$$

with

$$U(s) = -K(s)Y(s) \tag{V.56}$$

and

$$Z(s) = G(s)W(s). \tag{V.57}$$

The design task is to identify a controller $K(s)$, that minimizes the norm of $G(s)$:

$$\min_{K(s)} ||G(s)||_\infty \tag{V.58}$$

For single-input-single-output systems the H_∞-norm is defined as

$$||G(s)||_\infty := \sup_\omega |G(j\omega)| \tag{V.59}$$

and describes the maximal amplitude gain of a harmonic input signal with frequency ω [130]. H represents the Hardy-Space, which defines bounded and analytical functions in the right upper half complex plane.

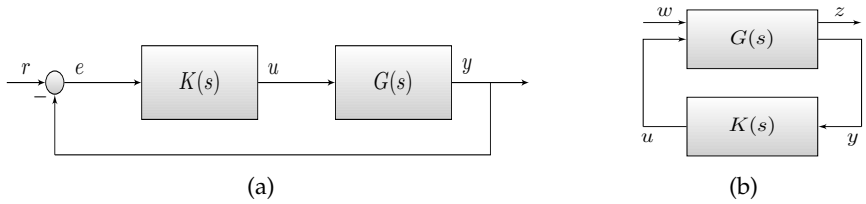

Figure V-12.: Simple control loop (a) and H_∞-standard-problem (b).

A very popular specification of the H_∞ problem is the $S/KS/T$ scheme, depicted in Figure V-13. In this layout the specifications for the robust controller are expressed as requirements to the gain response of the sensitivity $S(s)$ and the complementary sensitivity $T(s)$:

$$S(s) = \frac{1}{1 + G(s)K(s)} \tag{V.60}$$

$$T(s) = \frac{G(s)K(s)}{1 + G(s)K(s)} \tag{V.61}$$

The weighting functions W_S, W_{KS} and W_T can be used to influence the control characteristics.

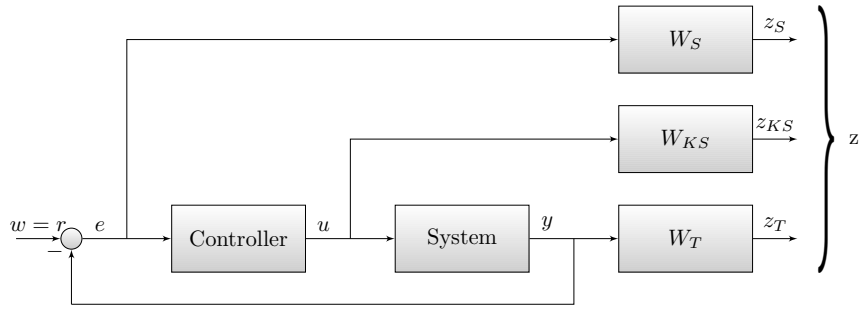

Figure V-13.: Standard H-∞ weighting scheme.

The transfer matrix $T_{zw}(s)$ for the $S/KS/T$ scheme reads

$$T_{zw}(s) = \begin{bmatrix} W_S(s)S(s) \\ W_{KS}(s)KS(s) \\ W_T(s)T(s) \end{bmatrix}. \tag{V.62}$$

The H_∞-Algorithm tries to find a solution for the following optimization problem:

$$||T_{zw}(s)||_\infty \leq \gamma, \tag{V.63}$$

with the arbitrary positive value γ. This yields an inequality for each component of $T_{zw}(s)$:

$$|W_S(j\omega)S(j\omega)| \leq \gamma \tag{V.64}$$
$$|W_{KS}(j\omega)K(j\omega)S(j\omega)| \leq \gamma \tag{V.65}$$
$$|W_T(j\omega)S(j\omega)| \leq \gamma. \tag{V.66}$$

W_S is used to express specifications, regarding the system's sensitivity (control error). Exemplarily, choosing $W_S(0) = 100$ implies, that the static control error should be lower than 1%. Additionally, W_T is used to design robustness against multiplicative model uncertainties [127]. For example, $W_T(0) = 0.1$ refers to robustness for a model uncertainty of 10% in the stationary case. W_{KS} weights the actuating variable and should be chosen low in order to suppress extensive control activities. Algorithmically, the H_∞ method reduces to solving 2 Riccati equations (see [129] for further details).

3.1. Control Design

In the control design parameter uncertainties are introduced analogously to the PIC (see Section 2.1). In Figure V-14 the frequency characteristics of the nominal system (green) and the system under parameter variations (blue) are shown. Since W_T is used to account for parameter uncertainties, it is chosen, such that the system, weighted with W_T, covers all system variations (Figure V-14, red).

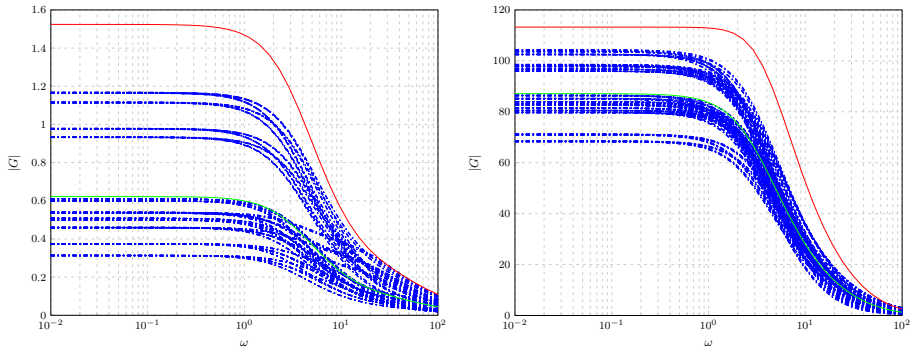

(a) Flow (b) Pressure

Figure V-14.: Amplitude response of the nominal system (green), under parameter variations (blue), and the W_T-weighted nominal system (red) for flow (a) and pressure (b) control model

The transfer function of $W_S(j\omega)$ was modeled as a PT1 element with a stationary error of 0.01 and a gain crossover frequency of 0.2 . To avoid extensive control activities W_{KS} was chosen small and constant ($W_{KS} = 1e^{-4}$). Figure V-15 shows the amplitude response of W_S and W_T.

Due to the system extension (w, z), possible solutions for $K(s)$ have a higher order than the original system. Furthermore, solutions include modi that are hardly relevant for the input-output-characteristics of the controller [129]. Therefore, a system order reduction is desirable and can be achieved using Moore's algorithm [131]. The system order can be

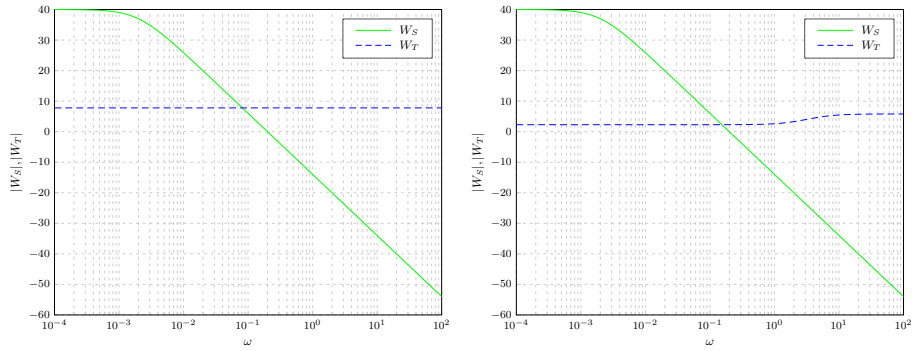

(a) Flow (b) Pressure

Figure V-15.: Amplitude response of W_S and W_T for flow (a) and pressure (b) control.

reduced step-wise as long as there is no performance degradation. With Moore's algorithm the order of the HINFC for the mock model was reduced from 12 to 3. Finally, Figure V-16 shows the step response for the designed controller.

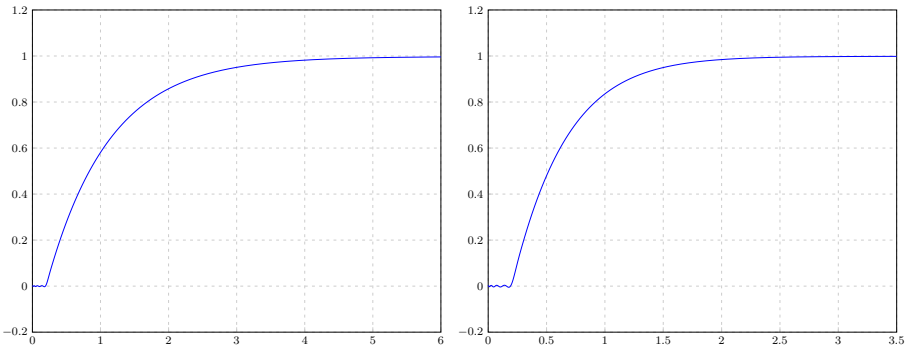

(a) Flow Control (b) Pressure Control

Figure V-16.: HINFC step response for flow and pressure control.

4. Model Reference Adaptive Controller

In Adaptive Control the controller is redesigned online by looking at its performance and automatically changing its dynamics. The core elements of Adaptive Control are

- an online parameter estimator, based on current measurements and control actions and
- a control law, that recalculates the controller based on those parameters [132].

Obviously, the control performance strongly depends on a successful parameter estimation. Usually, a differentiation is made between direct and indirect adaptive control. In the

indirect case the estimated parameters refer to the plant, while they refer to the controller in the direct case. A feedback loop for the direct case is shown in Figure V-17. The parameter estimator directly modifies the controller's parameters, based on the controller's and the system's output. A MRAC is one of the main approaches to Adaptive Control. A

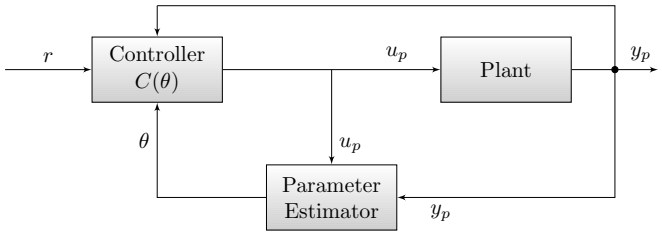

Figure V-17.: Direct Adaptive Control loop.

reference model is chosen to generate a desired trajectory y_m that the plant output y_p has to follow. The tracking error $e_1 = y_p - y_m$ represents the deviation of the plant output from the desired trajectory [133]. By the definition of the reference model, control characteristics can be implemented. The Adaptive Control feedback loop can be extended by the reference model and redrawn as shown in Figure V-18.

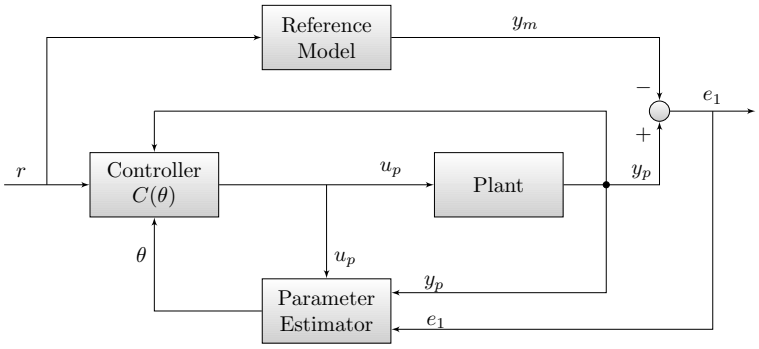

Figure V-18.: Direct MRAC loop.

4.1. Control Design

The design task is to specify the parameter adjustment mechanism, such that all signals in the closed-loop plant are bounded and the error e_1 is kept small.
In [133] a control law and an adaptation mechanism for second-order SISO-LTI Systems with a relative degree of $n^* = 1$ is derived. Table (V.2) displays the results. The parameters that need to be identified are summarized in the vector $\theta = [\theta_1\, \theta_2\, \theta_3\, c_0]^T$ and are identified using a gradient operation with step size γ_i.

For both flow and pressure control the reference model

$$W_m(s) = \frac{3}{s+3} \tag{V.67}$$

Plant	$y_p = k_p \frac{Z_p(s)}{R_p(s)} u_p, \quad n^* = 1$
Control law	$\dot{\omega}_1 = -2\omega_1 + u_P, \quad \omega_1(0) = 0$ $\dot{\omega}_2 = -2\omega_2 + y_P, \quad \omega_2(0) = 0$ $u_p = \theta_1\omega_1 + \theta_2\omega_2 + \theta_3 y_P + c_0 r$
Reference model	$y_m = W_m(s)r, \quad W_m(s) = k_m \frac{Z_m}{R_m}$
Adaptive law	$\dot{\theta}_i = -\gamma_i \, e_1 \, \omega_i \, \text{sgn}(k_p/k_m), \quad i = 1, ..., 4$ $\theta = [\theta_1 \, \theta_2 \, \theta_3 \, c_0]^T$ $e_1 = y_p - y_m$

Table V.2.: Direct MRAC scheme for second-order SISO plants with relative degree $n^* = 1$.

was chosen with its step response depicted in Figure V-19. For a successful parameter identification sufficient excitation of the input signal r is important. As suggested by [133], a superposition of two sinusoidal signals with different frequency and amplitude was used as an iput signal. The identification process for both pressure and flow control is shown in Figure V-20. The identified parameters were then chosen as the initial values of the controller.

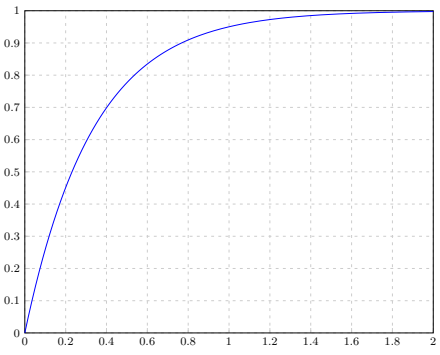

Figure V-19.: Step response of the reference model $W_m(s) = \frac{3}{s+3}$

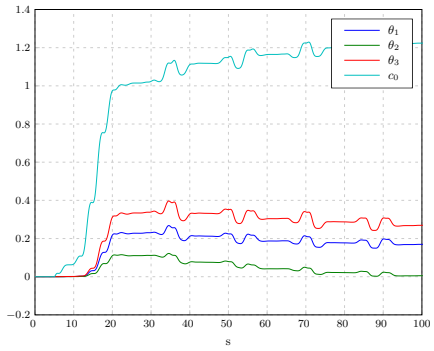

(a) Parameter identification flow control

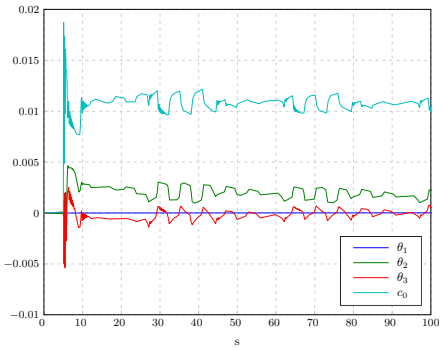

(b) Parameter identification pressure control

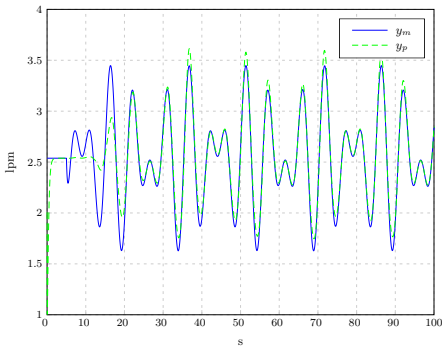

(c) Plant and reference model output flow control

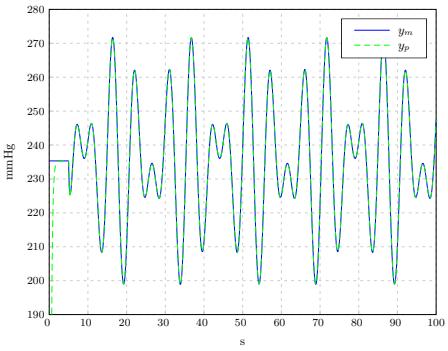

(d) Plant and reference model output pressure control

Figure V-20.: MRAC identification process. Shown are the identified parameters for flow (a) and pressure control (b), as well as the corresponding plant and system output (c)-(d) for an input signal with sufficient excitation.

5. Fuzzy–Controller

Fuzzy control is a well-established method in control engineering and has been applied to a wide range of problems in diverse disciplines. It is especially useful, if a direct analytical description of the control process seems unsuitable. Since fuzzy logic is able to interpret vague and subjective knowledge, and allows qualitative system descriptions, it is well qualified for medical decision making. Fuzzy logic was introduced by Zadeh in the 1960s [134]. In fuzzy logic, complex systems are described on a verbal or symbolic level. The use of IF-THEN rules facilitates the design process of the controller and expert knowledge can be implemented ad hoc. Compared to the other control mechanisms described in this chapter, no mathematical system description is needed. Also the maintenance and adaptivity of the controller is simple. Rules can be added or deleted easily. Fuzzy Logic permits simultaneous membership in more than one set, and thus is able to model systems with roughly known response characteristics.
In fuzzy control, input and output variables are described by fuzzy sets. Each set consists of membership functions, mapping symbolic to numerical values. For example, the fuzzy

set for the control variable flow can be described by the linguistic terms *low*, *medium* and *high*. Now membership functions can be defined for each term. E.g. a flow of $q = 3\,\text{lpm}$ is considered medium (cmp. Figure V.22(a)), while a flow below 2 lpm is low. Membership function values are limited to the interval $[0, 1]$. Membership functions can overlap, e.g. a flow of $3.5\,\text{lpm}$ partly belongs to the two sets of *medium* and *high*. Like this, fuzzy sets for each variable can be defined. Together with a rulebase, control characteristics can be implemented.
Fuzzy controllers consist of 4 stages (cmp. Figure 5):

1. **Fuzzification:** The fuzzification step determines the degree of membership by which the inputs belong to the corresponding fuzzy sets. The input of fuzzification is a crisp numerical value, while the output is a fuzzy degree of membership in the interval of $[0, 1]$.

2. **Rulebase:** The rulebase defines the control characteristics by linguistic rules and is usually given by experts.

3. **Inference Mechanism:** Based on the fuzzified inputs and the rulebase, an output fuzzy set is calculated.

4. **Defuzzification:** The defuzzification calculates a crisp number from the output fuzzy set. The most popular method for defuzzification is the centroid calculation, which returns the center of the output fuzzy set.

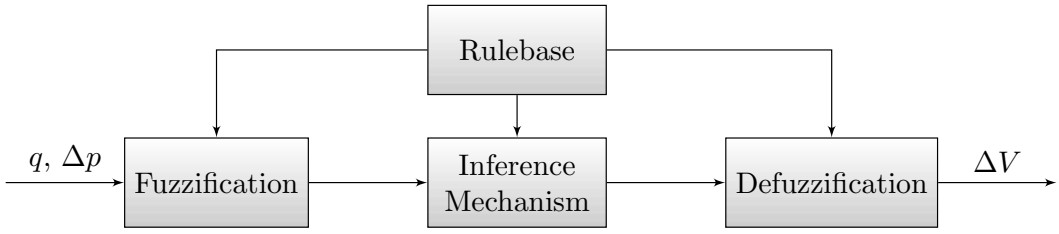

Figure V-21.: General structure of a Fuzzy-Controller.

5.1. Control Design

For pressure and flow control of the hydraulic circulatory model, fuzzy sets for the flow V.22(a) and the pressure V.22(b) are defined. Since the fuzzy controller can not react to changes in the target values, several controllers (for each target value) are implemented. Now, depending on the target values, different controllers can be activated. The control output is an incremental change of the input voltage V of the motor, with corresponding sets illustrated in Figure V.22(c). The rulebase is intuitive:

1. IF $\{q, \Delta p\}$ is *low* THEN ΔV is *increase*.

2. IF $\{q, \Delta p\}$ is *medium* THEN ΔV is *steady*.

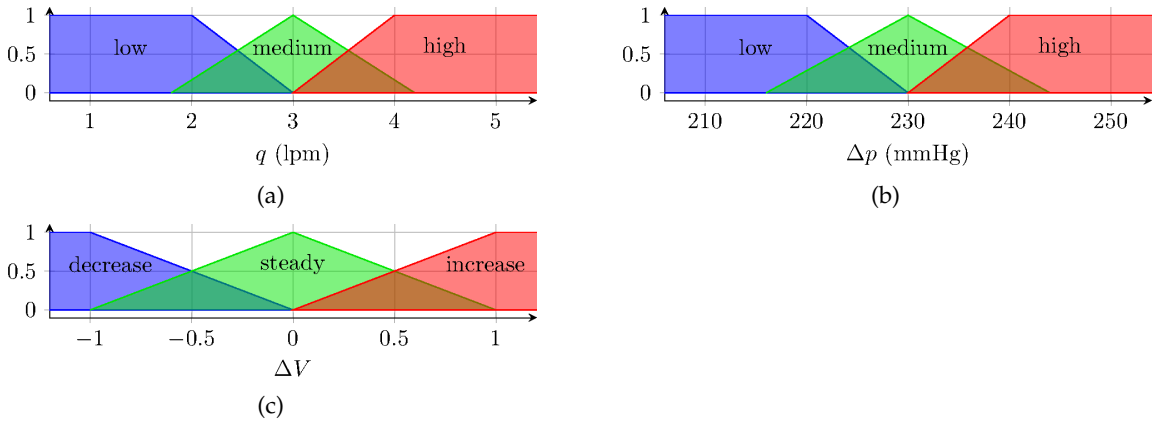

Figure V-22.: Fuzzy sets for the controller's input variables pump flow q and pressure difference Δp and for the controller's output V.

3. IF $\{q, \Delta p\}$ is *high* THEN ΔV is *decrease*.

For evaluation purposes controllers for a medium flow of 2, 3 and 4 lpm were defined and pressure controllers for a medium pressure difference of 210, 230 and 250 mmHg.

6. Results

The controllers designed in the last sections are evaluated in three different scenarios. First, the controllers have to follow target values, that are changed during the test run. In the second scenario the control input is perturbed with noise, while in the last setting the peripheral resistance of the mock model is changed. The controllers are compared quantitatively, using the normalized IAE:

$$IAE = \frac{1}{T} \int_{t=0}^{T} |r - y| dt \tag{V.68}$$

In the discussion, the different methodologies are also compared qualitatively.

6.1. Changes of Target Value

In this setting the control targets are changed step-wise. For pressure control the targets were set at 210, 230 and 250 mmHg. For flow control targets were 2, 3 and 4 lpm. Using a step function, targets were changed after 10 s and the controllers had to follow those changes. Figure V-23 shows the step changes in the target values and the variables under control (flow or pressure). The IAEs for the different control methods are shown in Table V.3.

Proportional-Integral Controller: The PIC revealed the lowest IAE for both pressure and flow control and reached the target values quickly. During flow control overshoots with a maximal offset of 0.24 lpm and small oscillations were observed.

H_∞-Controller: The HINFC reached the control targets without overshoots or oscillations, but was inert during flow control, reaching the target value only about 5 s after the change was triggered. For pressure control the delay was smaller.

Fuzzy Controller: The FUZZYC was also able to reach the control targets, but similar to the HINFC showed inert behavior during flow control. In pressure control small overshoots were observed. However, the overshoot was below 1% and fading quickly without oscillation.

Model Reference Adaptive Controller: The MRAC showed a fast response without overshoots for pressure control. During flow control an overshoot of 1% was observed when increasing the target value from 3 lpm to 4 lpm and the control was slow when the reference variable was decreased to 2 lpm, reaching the target value after about 4 s.

IAE	PIC	HINFC	FUZZYC	MRAC
Pressure	0.53	0.91	1.39	0.67
Flow	0.02	0.08	0.10	0.05

Table V.3.: IAE during changes in the target value.

6.2. External Perturbations

In the second scenario the control variable is perturbed externally. The measured flow and pressure values are biased with a gaussian random noise signal, before fed to the controller's input. Such noisy signals were observed during animal experiments and can be due to vibrations or movements of the patient or the HLM as well as to malfunctioning sensors. The additional noise implies, that the control error is unlikely to become 0 and the controllers constantly have to react to small changes. For flow control the noise signal was zero mean with a variance of 1 lpm, while the variance was 10 mmHg for pressure control. Again, the step function of the first setting is used as a reference input and shown together with the control variables in Figure V-24. The IAEs are shown in Table V.4.

Proportional-Integral Controller: The PIC showed high-frequency oscillations in the control variables for both pressure and flow control, but it was able to follow the reference variable with a low IAE. Maximal overshoots were around 1% for both pressure and flow control.

H_∞-Controller: The HINFC also displayed high-frequency noise and followed the characteristics of the reference curve without significant overshoots, but the target value was not reached well during flow control. As in the first setting, control was slightly inert.

Fuzzy Controller: The FUZZYC showed smooth behavior without high-frequency oscillations. There were constant but little deviations from the target. Again little overshoots in pressure control and a slowed reaction for flow control were observed.

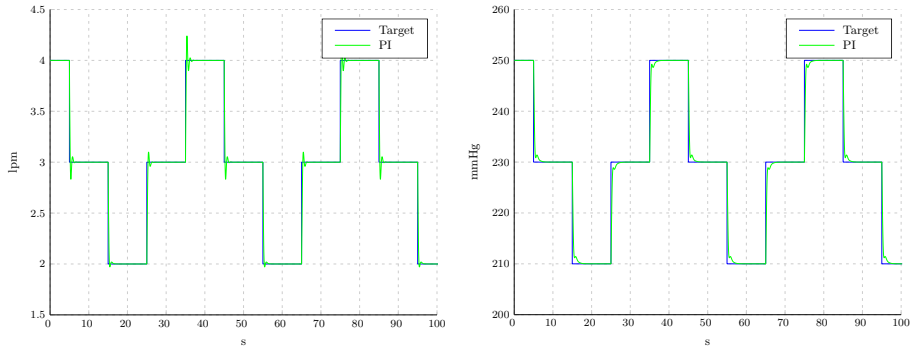

(a) PI Flow Control (b) PI Pressure Control

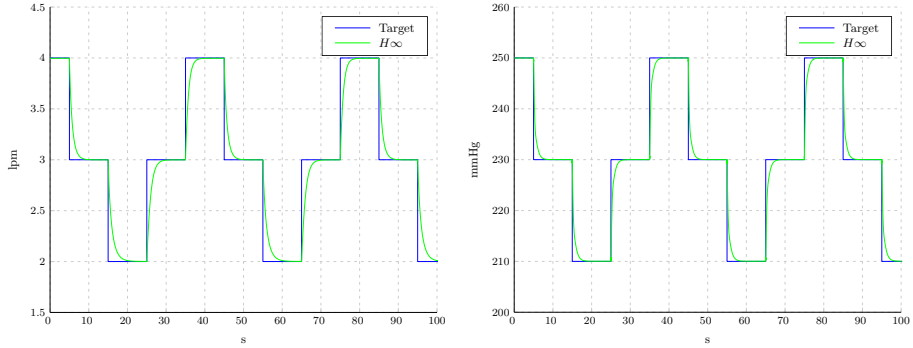

(c) H∞ Flow Control (d) H∞ Pressure Control

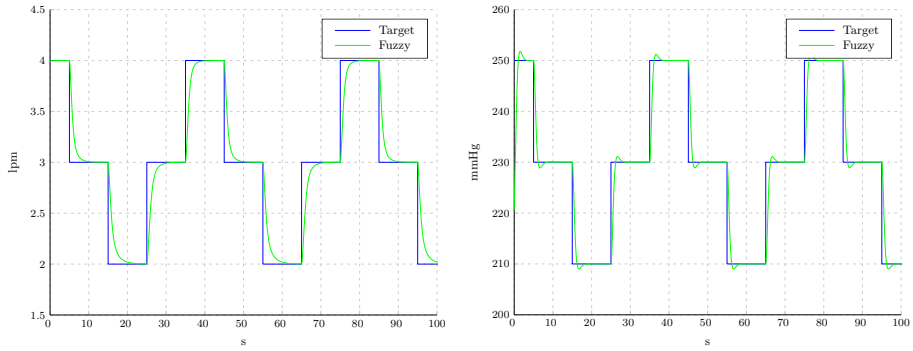

(e) Fuzzy Flow Control (f) Fuzzy Pressure Control

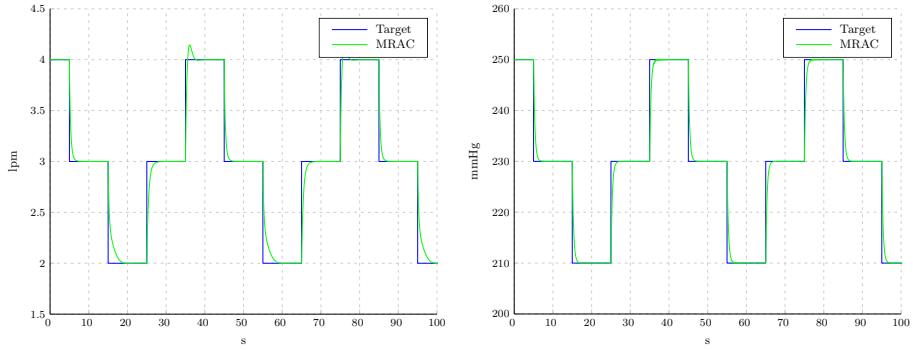

(g) MRAC Flow Control (h) MRAC Pressure Control

Figure V-23.: Control during changes of target value (scenario 1).

Model Reference Adaptive Controller: The MRAC displayed smooth characteristics with the lowest IAE for this setting. Again, a small overshoot of 1% was observed when the target flow was increased to 4 lpm. For pressure control the target was followed accurately and fast without noticeable deviations.

IAE	PIC	HINFC	FUZZYC	MRAC
Pressure	0.82	1.59	1.69	0.69
Flow	0.07	0.09	0.11	0.05

Table V.4.: IAE during external perturbations.

6.3. System Parameter Variation

In the final evaluation setting, the peripheral resistance R_p is changed. This is equivalent to increasing or decreasing the tube diameter in the hydraulic setup. Starting from its initial, medium value, the diameter is altered by 25%. We distinguish again between flow and pressure control. In contrast to the preceeding scenarios, the target value is kept constant now. For pressure control this target is 230 mmHg and 3 lpm for flow control. Figure V-25 shows the characteristics of the uncontrolled plant during the change of R_p for both cases. If the resistance is decreased, flow rises while the pressure difference drops. After 10 s the resistance is changed back to its initial value. Afterwards it is increased, making the pressure increase and the flow decrease. The challenge for the controllers is to keep the target value, despite the change of the plant parameter. The results are displayed in Figure V-26 and the IAE is shown in Table V.5.

Proportional-Integral Controller: The PIC dealt well with the parameter variations. Deviations from the target value were observed, while the tube diameter was changed, but they were small (0.03 – 0.06 lpm for flow and 0.5 – 1.8 mmHg for pressure control) and control was back to target, when the resistance parameter reached its setpoints. Concerning the IAE, the PIC is ranked first for flow and second for pressure control.

H_∞-Controller: The HINFC was also able to compensate for the parameter changes, but again control was slow compared to the PIC. The IAE was worst for flow control with 0.44 and a maximal deviation of 2.4 mmHg.

Fuzzy Controller: The FUZZYC also compensated for the R_p variations and had the lowest IAE for pressure control. Maximal deviations of 0.21 lpm during the change of R_p were observed in flow control but were smaller for pressure control (1.3 mmHg).

Model Reference Adaptive Controller: Noticeable results were observed for the MRAC, since it was not able to compensate for the R_p variation during the given time. This lead to maximal deviations of 0.65 lpm during flow control. The deviations were smaller when R_p was increased.

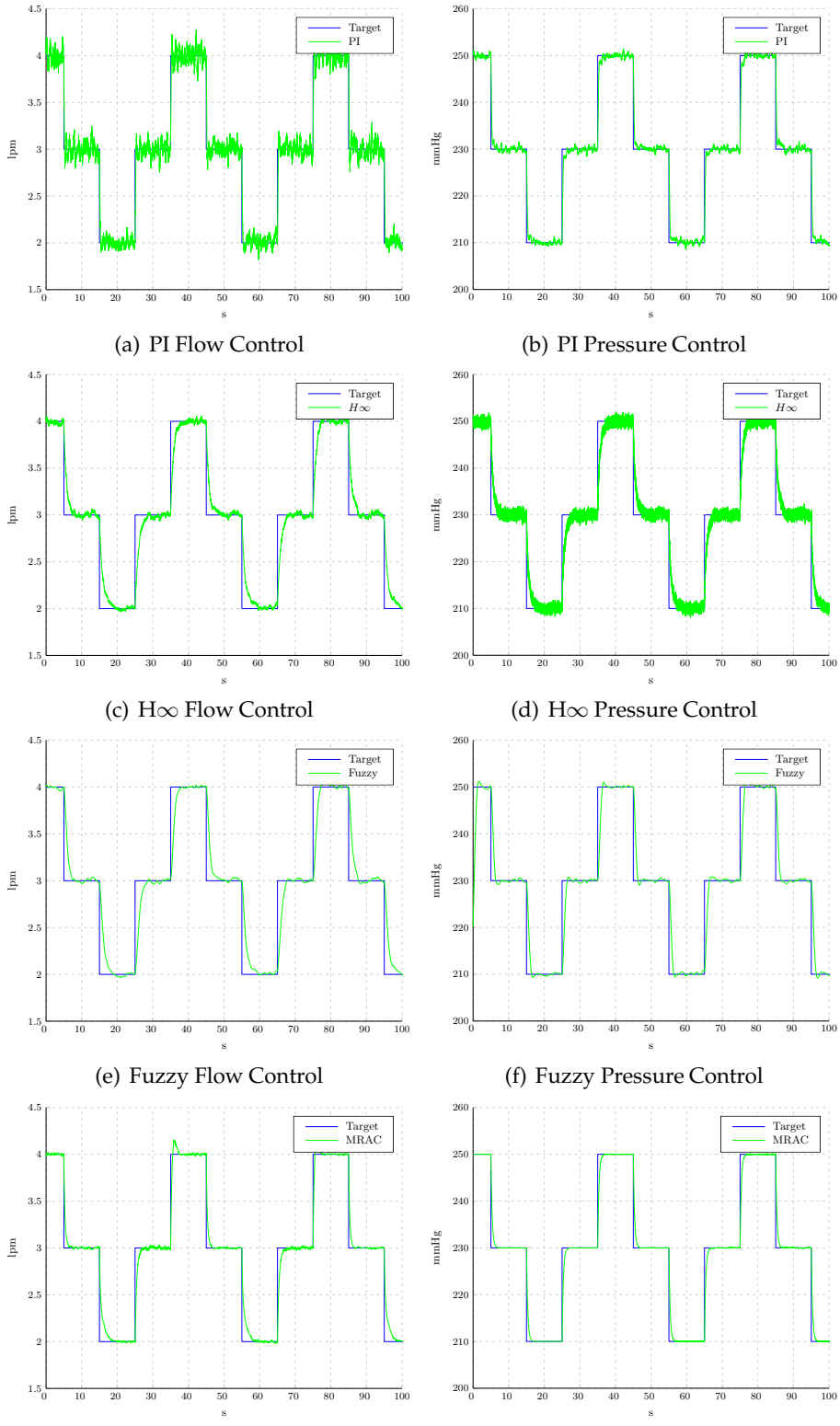

(a) PI Flow Control

(b) PI Pressure Control

(c) H∞ Flow Control

(d) H∞ Pressure Control

(e) Fuzzy Flow Control

(f) Fuzzy Pressure Control

(g) MRAC Flow Control

(h) MRAC Pressure Control

Figure V-24.: Control during external perturbation (scenario 2).

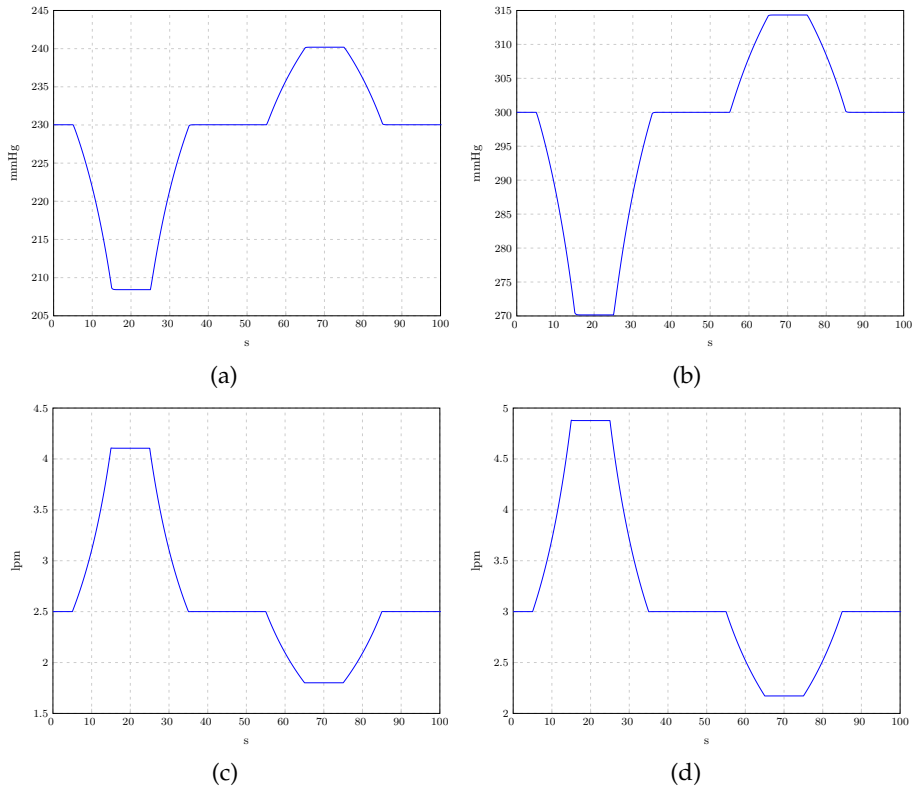

Figure V-25.: Plant characteristics during variation of R_p. Shown are pressure difference and flow, starting from the fixed setpoint of 230 mmHg for pressure control ((a), (c)) and 3 lpm for flow control ((b), (d)).

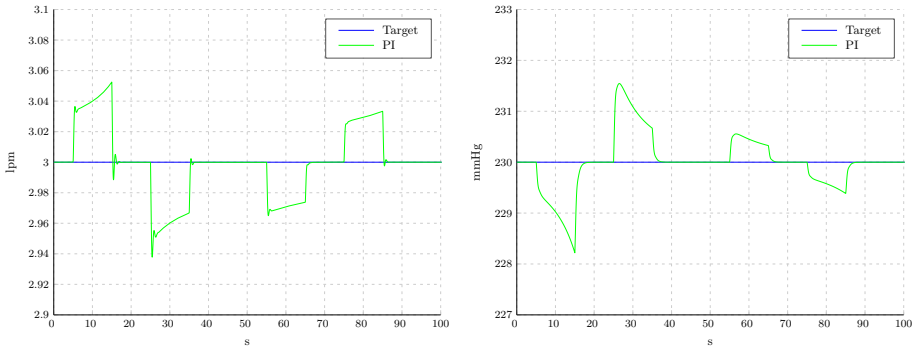

(a) PI Flow Control

(b) PI Pressure Control

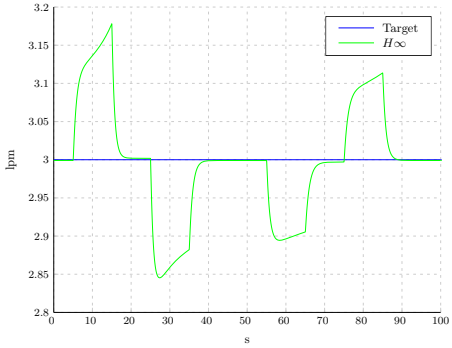

(c) H∞ Flow Control

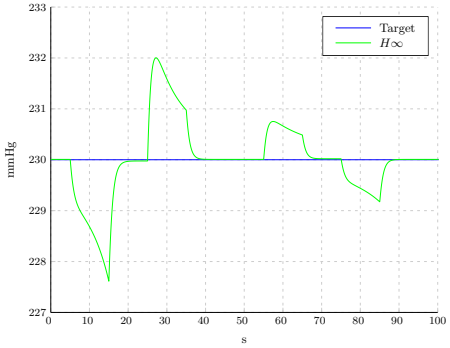

(d) H∞ Pressure Control

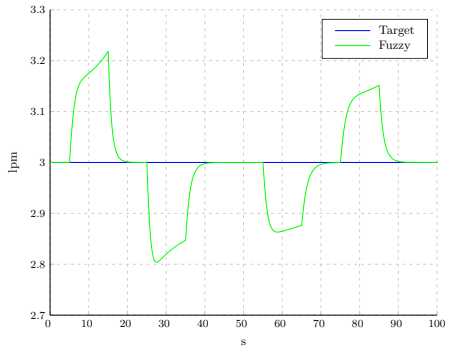

(e) Fuzzy Flow Control

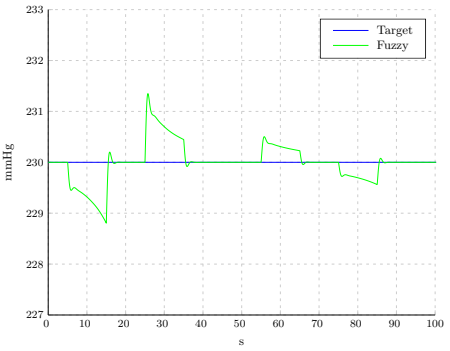

(f) Fuzzy Pressure Control

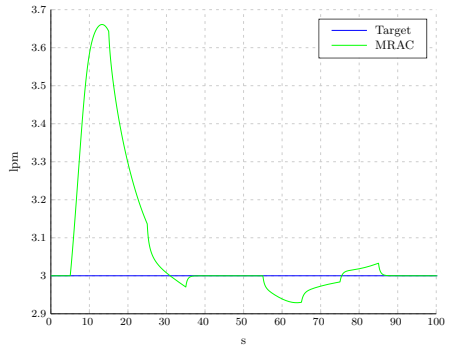

(g) MRAC Flow Control

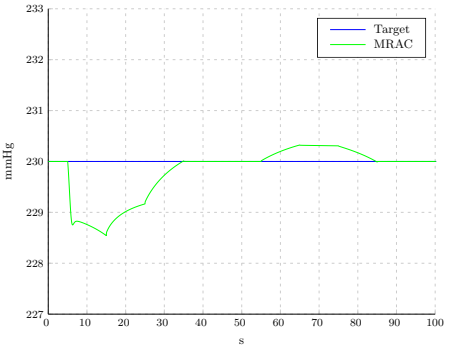

(h) MRAC Pressure Control

Figure V-26.: Control during variation of peripheral resistance (scenario 3).

IAE	PIC	HINFC	FUZZYC	MRAC
Pressure	0.31	0.44	0.22	0.32
Flow	0.01	0.05	0.06	0.09

Table V.5.: IAE under system parameter variation.

6.4. Discussion

The PIC was ranked first or second in all three scenarios. It was able to follow target values, despite external perturbations and handled parameter variations of the system well. The small overshoots observed during flow control can be eliminated by a fine-grained grid search in the K_p-K_I-plane. The good results are due to the fact, that the controller was designed based on an accurate system model. In the design process parameter uncertainties and time delays of the output variables were already considered. Its structure is rather simple, but parameters need to be well-tuned.

The HINFC showed smooth behavior in most cases. It reached the given target values without big overshoots. Noticeable was the high-frequent noise during pressure control in the second scenario. Also the control was rather slow compared to its competitors. A system model is indispensable during the design process of the HINFC. Similar to the PIC, parameter uncertainties and time delays can be accounted for in the design. However, the design process is rather complex and control behavior is hard to follow for people without a background in control engineering. The observed inertia for most of the scenarios can be impaired by a better choice of the gain crossover frequency of the weighting functions. But target values were still reached within an acceptable period and a rather slow change of the pump speed might even be beneficial for the patient compared to large and fast variations.

The MRAC showed very smooth behavior during external perturbations, with the top rank concerning the IAE, but did not cope well with the parameter variation in the third scenario. However, additional tests showed that, if the parameter variations were repeated, the control error was lower than shown in V.26(g) or V.26(h). The reason is, that control parameters are changed online and the controller can react more adequately on upcoming parameter changes. Since the methodology is based on an identification process a complete system model is not needed but the system order is sufficient for the design. To guarantee a successful identification of the control parameters, the input signal should have enough excitation. This is not the case for a constant target value as in the third scenario and explain the big deviations from the target. As for the PIC and HINFC the design is rather intransparent.

Concerning the IAE, the FUZZYC performed bad and was ranked fourth in scenario one and two. However, it showed the lowest IAE for pressure control during the variation of R_p. Although there were deviations from the target value it did not exhibit the high-frequency noise during external perturbation such as the HINFC and PIC. Since the FUZZYC is a knowledge-based method, no analytical system model is needed. Using a reasonable rulebase and membership functions, the control problem can be well characterized. Also limits for the control variables can be set easily, while some low-level control would be needed for the other controllers to prevent the generation of unphysiological

values. Due to its independence from a system model, the FUZZYC deals well with the third scenario. A big advantage is its transparency, enabling even the untrained to quickly design a controller for a given task. The natural language rules ease discussions with experts from the medical domain and the control behavior is comprehensible, as long as the rulebase is kept small.

In summary, all evaluated controllers led to a stable control and showed good performance in the given control tasks. In terms of the IAE the results were close together with slight advantages for the robustly tuned PIC. In the first scenario with step changes of the target value, fine-tuning could even improve the good results and diminish the IAEs, making it hard to favor a specific control method. In the second scenario the MRAC outperformed the other methods, but also the FUZZYC led to smooth control without high-frequency noise. In the third scenario the IAEs were close together again. As stated before, the bad performance of the MRAC is due to the initial choice of the control parameters and the control error decreases in longer test runs. This adaptivity to unknown or only roughly known plants is an advantage, compared to its competitors. Although the PIC and the HINFC are robustly tuned, they rely on an accurate analytical system description and would need to be retuned for large changes or disturbances of the system. For example, if a different blood pump was used in the setup, the pump parameters would change and the plant description would need to be recalculated. As a consequence, the controllers would also need to be redesigned. However, the adaptive MRAC and the knowledge-based FUZZYC are indifferent to such changes and would cope well with the new system setup.

In the work of Misgeld et al. [121] three controllers were designed for robust blood flow control under ECC. They designed a robust PIC and HINFC. From adaptive control they used a self-tuning GPC and tested the performance in a two-element mock model under variation of resistance and compliance. Results showed the best performance with the HINFC, closely followed by the PIC. For the GPC nearly instable behavior was reported in regions of strongly varying non-linear system gain. External perturbation was not considered by Misgeld et al. and there was no knowledge-based control method evaluated. However, the results presented in this work verify the results of Misgeld et al., that robust PIC and HINFC perform well for the given control task. Still, in vivo tests might require a redesign of those controllers. Considering the negligible differences in the IAEs for all of the four control methods evaluated, soft factors need to be considered if a recommendation for a favorable strategy should be given. It was shown, that the PIC and HINFC revealed similar behavior, but the design process for the robust PIC is easier. The FUZZYC and the MRAC are convenient, since they can adapt to unknown system parameters. However, the MRAC is not the method of choice for quickly varying system parameters or for constant target value control, since the input signal usually has hardly any excitation and the parameter identification process might fail. Although the FUZZYC was ranked fourth in two scenarios, concerning the IAE, qualitative comparison shows, that it is well-suited for the given control task. It can be designed easily, using natural language rules. Changes or later adaptations are possible without complex calculations or grid searches. And control behavior is transparent and comprehensible. From a medical point of view all four evaluated control strategies are convenient, since they all reach the target values fast and precisely - better than a human operator could do. The differences in terms of the IAE are insignificant from that viewpoint. But again, the FUZZYC has the advantage, that it is

based on natural language rules and its behavior can be easily influenced or changed by physicians.

7. Summary

In this chapter a hydraulic circulatory model and a simplified representation of a HLM is introduced. The complete setup replicates flow and pressure dynamics under ECC. The model is used to design and evaluate control methods for the regulation of the HLM pump speed in a predefined setup. Moreover, the setup can be used to test hard- and software components prior to animal experiments.

The layout for the CVS representation follows the well-known Westerhof model, consisting of two resistances and a closed air chamber, representing the aortic compliance. The Westerhof model is predominant in literature and its layout is simple, but it accurately replicates a hydraulic load for a real pumping heart [26]. A centrifugal pump, driven by a direct current motor, together with a static resistance represent the HLM. Water was used instead of blood as a circulating medium. Although there are obvious differences such as viscosity or density between the two liquids, their influences are marginal and negligible for control design. Mathematical descriptions of the motor, the pump and the CVS are presented and combined for a complete analytical model of the setup. This description of the closed-loop circulation is then compared to experimentally measured data and a very good congruency is found. The model is also compared to data from two representative animal experiments. It was found, that the produced pump flow is close to the animal data while the pressure difference at the pump is lower, but still in an acceptable range.

For control design the state space representation of the system is derived and linearized in a working point. The linearization is justified by comparison to the nonlinear model representation. The control task is to adjust the pump speed in order to observe given target values for pump flow and pressure. Several control methodologies are designed and evaluated. Since the human circulatory system is a plant with uncertain and time-invariant parameters, controllers are tuned robustly. As a classical feedback controller the robust PIC was chosen. The HINFC represents the state of the art method of robust control. From the area of adaptive control a MRAC was designed and a FUZZYC from the family of intelligent control. The controllers are evaluated in three different scenarios. First, step changes of the target values are applied in order to examine the general control performance. In the second test the control signal is charged with an additive random noise signal. Noisy signals have been observed during animal experiments and can, for example, be due to vibrations or sensor malfunction. In the third scenario the periperal resistance of the CVS is varied during control in order to evaluate the adaptivity and robustness to system uncertainties and changes of patient parameters.

The different methods are quantitatively evaluated using the IAE. All controllers lead to a stable control with top rankings for the PIC in terms of the IAE. During external perturbations (scenario 2) the MRAC performs best. Again the PIC is ranked first during flow control under parameter variations (scenario 3), but is outperformed by the FUZZYC in pressure control. Since the IAEs are all close together, other factors, such as transparency and design complexity should be considered. Advantages can be found for the robustly tuned PIC and the FUZZYC, since they are rather simple to design and their behavior

is transparent. The FUZZYC has the additional advantage, that it is independent of an analytical system description, while the PIC would need to be redesigned if components of the system were changed.

It has to be mentioned, that the presented hydraulic model is not able to consider the observation and regulation of patient parameters, such as temperature or SpO_2, for example. However, pressure and flow relations under ECC and their control can be examined well using this model. Even more, the patient, represented by the Westerhof model, is considered as a black box system. The control manages parameters which are exclusively measured at the HLM, namely the pump speed, the produced pump flow and the pressure difference between the pump inlet and outlet. Animal experiments, observations in the OR and consultations with experienced physicians have shown, that a sufficient perfusion of the patient can be assumed, if those parameters are observed. As long as there are no unforeseen events, such as volume loss, kinking or technical problems, it is sufficient to observe the HLM parameters. The good results show, that those variables can be well controlled. In order to guarantee patient safety and to broadly examine ECC Control, a virtual simulation model is indispensable [27].

Chapter VI

Medical Data Mining for Intelligent Patient Monitoring

Contents

1	**Motivation and General Approach**	**79**
2	**Data Mining and Knowledge Discovery**	**81**
3	**Related Work**	**93**

1. Motivation and General Approach

The contributions of Misgeld et al. [121], Meyrowitz [24] and the previous chapters in this work have shown, that an automatic pump speed control of a HLM is feasible from a technical point of view. So far only well defined application settings have been described. Automated HLMs have been tested in hemodynamic simulators [9, 121] and in laboratory enviroments [1, 24].
The intention of this project, however, is to deploy HLMs in preclinical emergency situations. Using ECCSs outside the clinical environment is beneficial for patients suffering a cardiogenic shock or other cardiac insufficiencies [135]. They can be stabilized and transported to a cardiac surgery center for in-depth treatment. The early application of ECCSs implies several requirements and consequences. Ideally the HLM controller would have knowledge about the current constitution of the patient and would be able to recognize and cope with contextual events such as sensor failure or intervention of the staff. Therefore, medical DM methods for the assessment of monitoring signals shall be examined.
In the following, the requirements for ECCSs in non-clinical environments are reviewed (section 1.1) and the concepts of CDSSs (section 1.2) are introduced and reformulated for automated ECC control. The feasibility of intelligent monitoring and control for an automated ECCS is then shown in a benchmark test. DM methods are reviewed (section 2) and evaluated for the assessment of a patient's health status. Due to the lack of large-scale, publicly available databases for ECC applications a well-known database from ICU mon-

itoring is used, and the problem of high false alarm rates in patient monitoring is tackled (chapter VII).

1.1. Requirements for Automated Extracorporeal Circulation Systems in Non-Clinical Environments

In non-clinical environments ECC requirements are different compared to a standard application of HLMs in operating theaters. Human operators are presumably stressed during emergency duties and simultaneous supervision of both the patient and the HLM is hardly manageable, also because of the general lack of personnel in such situations. Both financial considerations and the limited space in ambulances or helicopters do not allow sufficient, specially trained personnel. Feindt et al. [20] identified requirements for the application of ECC devices outside the hospital. Regarding the staff, they call for at least a cardiac surgeon with sufficient experience in percutaneous and conventional cannulation under emergency conditions, as well as for a cardiac perfusionist with sufficient clinical experience. Concerning the equipment, arterial and venous cannulas in various sizes, a set of sterile surgical instruments and a coagulation and blood gas analyzer complement the standard emergency equipment.

An automated HLM reduces the workload of the staff and the patient can profit from being continuously perfused in accordance to his personal needs. The shift from clinical to pre-clinical applications of ECCSs involves some challenges regarding system safety and reliability. There is no surgical team as in a regular operating room, there is no standard system and monitoring setup. Additionally, medical records of the patient are often unknown [5]. Unpredictable context-driven events, such as kinking of arterial or venous tubings, vibrations during transportation, sensor failure or alike can change the system dynamics and require immediate attention. Such events not only increase system complexity but also influence the control behavior of an automated device and can set the patient at risk if the control is only based on pure numerical sensor data, unaware of the situational context. Therefore, a Supervising Unit (SU), validating sensor data and assessing the patient's condition, would be desirable in control applications, since it could give valuable feedback to both the controller and the human operator. Such systems, aggregating information about the patient and giving guidelines to the practitioners, are known as CDSSs but have neither been applied to online monitoring data nor to control applications.

1.2. The Clinical Decision Support Approach

Safe, effective and patient-centered delivery of care are main pillars of today's medicine [136]. Along this path automated diagnosis and decision support systems have been introduced to improve the quality of care. Most of them are designed for specific applications and operate on databases of medical records. These tools are used to define and follow evidence-based therapy guidelines. Usually, they generate care suggestions and became well-known as CDSS. Although their acceptance is still low and patient outcome is understudied, several CDSSs improved practitioner performance [137]. The requirements and specifications for such systems are manifold and strongly depend on the application. Several studies examined CDSSs in the context of cardiovascular diseases [138–141]. The main

objectives are to increase system safety, patient safety and thereby quality of care. Greenes [142] identifies 5 features of Clinical Decision Support (CDS):

1. The general aim of CDS can be to make data about a patient easier to assess by, or more apparent to a human; to foster optimal problem-solving, decision-making, and action by the human.
2. The decision support is provided to a user, who may also be a computer program.
3. A primary task of the computer is to select knowledge that is pertinent, and/or to process data to create the pertinent knowledge.
4. The selection of knowledge and processing of data involve carrying out some sort of inferencing process, algorithm, rule, or association method.
5. The result of CDS is to perform some action, usually to make a recommendation.

The concepts of CDS can also be applied in the context of this work. Particularly, three purposes of CDSSs can be followed (cmp. [143]) and reformulated as goals for a CDSS, supervising automated ECC:

- **Diagnosis**: Use statistical or DM/pattern recognition methods to assess the patient and/or the machine status.
- **Monitoring Actions**: Detect events such as user intervention or sensor failures in real-time and trigger alarms or influence the
- **Choice of Treatment**: Change the control behavior or give recommendations, e.g. for adequate medication, to the medical practitioners.

Literature does not reveal any approaches towards CDSSs for control application, and although there are many researches about ECG classification, studies on assessing the health condition, considering multiple data sources, are sparse (see section 3). Therefore, this work can only show the general feasibility of a CDSS in medical control and will focus on the first formulated goal, the use of DM methods for the assessment of the patient state. In the following, DM methods are reviewed and later applied to the application area of alarm management on ICUs (see chapter VII).

2. Data Mining and Knowledge Discovery

The sections 2.2, 2.3 and 2.4 summarize state of the art procedures in DM and, with minor changes, have been adopted from the master's thesis of Kolja Rödel [144].

Yoo et al. [145] introduce DM as a relatively new concept, that emerged in the middle of 1990's as a new approach to data analysis and KD. (...) While data mining mainly originated from work done in the field of statistics and machine learning as an interdisciplinary field, data mining has advanced from these beginnings to include pattern recognition, database design, artificial intelligence, visualization, etc. DM is the discovery of interesting, unexpected or valuable structures in large datasets [146] with the goal to gain new insights, which can then be used to support decision making [145].

There is a strong correlation with the term KD and the nomenclature has been used interchangeably. However, many researchers regard DM to be a partial task in the process of KD [147, 148]. Fayyad et al. [147] introduced the term "knowledge discovery in databases" as identifying valid, novel, potentially useful, and ultimately understandable patterns in data. The different steps of KD are shown in picture VI-1.
First, appropriate data has to be selected. This step often includes the consultation of domain experts. The given data mining task should be solvable, given the selected data. Exemplarily, patient monitoring data is used in the case study described in chapter VII to classify monitor alarms. For robust classification results, it is important to include about the same amount of instances for each class. For the case study this means to include about the same amount of true and false alarms. Also the inclusion of errorneous/noisy data samples help to increase the robustness. Usually, the selected data has to be preprocessed with the focus on data quality. Filtering or the handling of missing values are major issues during this step. The preprocessed data is then transformed into the feature space. Depending on the application this transformation usually reduces the amount of data to be processed. For example, in time series classification a mean value could be used to describe the data stream. Another common procedure in the transformation step is the conversion from numerical into nominal data (depending on the raw data type), known as discretization. DM, comprising feature selection and appropriate learning algorithms, is at the core of the KD process. From the transformed data those algorithms create and identify useful patterns. In the evaluation step these patterns are validated. In this part of the work this classical procedure is followed in order to classify patient monitoring data. Before applying DM algorithms in the medical domain one should be well aware of the uniqueness of biomedical data and applicable algorithms.

2.1. Data Mining in Medical Applications

DM in medicine must consider several issues quite different from other applications. In their position paper Cios and Moore [149] explain the uniqueness of medical DM and state, that medical data is the "most rewarding and difficult of all biological data to mine and analyze".
Among the key points to consider when mining medical data, Cios and Moor [149] identify the heterogenity of medical data, ethical, legal and social issues, as well as the special status of medicine in today's life. The unclear ownership of medical data, the fear of lawsuits by physicians, privacy and security, and the acceptance by the patients are the most significant challenges, apart from technical issues [144].
Medical data can be voluminous, complex and heterogenous. Patient data is usually acquired from different devices and sensors (e.g. ECG recordings and oxygen saturation). Managing all this data requires high capacity data storage devices and new tools to analyze such data [149]. The lack of a canonical form to describe medical data or events can be another hindering factor. Furthermore, machine learning is always based on ground truth data. In the medical domain these assessments are done by few domain experts. It can be shown, that the opinions of several physicians about the state of a patient can vary significantly [13].
Matheny and Ohno-Machado [150] criticize, that (i) data are simply not available or not structured enough to allow knowledge to be learned from them and that (ii) techniques to

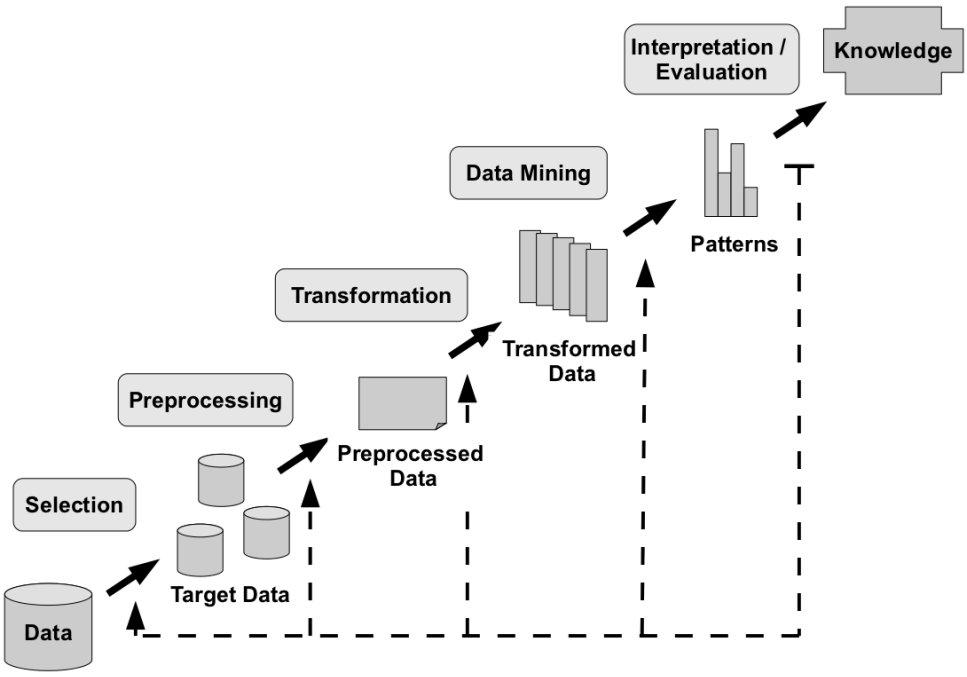

Figure VI-1.: The knowledge discovery process. From [144], redrawn after [147].

discover patterns from data are not well disseminated or not well evaluated in the biomedical community.
The fact, that every individual has different physiological characteristics, can be an obstacle for the application of DM algorithms or statistical analysis, when only taking crisp numerical values into account. Also the issue of missing values impedes medical data analysis [151]. Cios and Moore [149] claim, that "in a large medical database, almost every patient-record is lacking values for some feature, and almost every feature is lacking values for some patient-record". And also the nature of medical data itself can be an obstacle, since some events or diseases occur more frequently than others.
Mikut et al. [152] also identify the existence of hidden information, possible correlations between features and limited quality of data sets as difficulties when mining medical data. Furthermore, the extraction of useful features from time series, e.g. provided by ECG recordings, need special carefulness. Last but not least, Lavrač [153] states the need for effective and accurate prediction, as wrong results could cost lives. Only transparent and interpretable results from DM algorithms will find their way into clinical practice [149, 153].

2.2. Discretization Methods

Each instance used for DM is characterized by a feature or attribute. Depending on the domain of the features or attributes, discretization methods can be divided into two groups [154]. Numerical or quantitative attributes contain real numbers and have an infinite number of possible values. The other group is the nominal attributes, which are also known as qualitative ones. Their domain is limited to a finite and typically small number of possibilities. A special case of nominal attributes are binary ones [155] with only two possible values, "true" and "false". Some learning algorithms explicitly require nominal attributes.

While nominal attributes are more appropriate for most learning tasks, almost all measurements deliver numerical data. For that reason, some efforts have been made to find methods to convert numerical attributes into nominal ones.

2.2.a. Equal-Width Discretization

The simplest approach is the equal-width discretization. It is independent of the input data as the range of possible attribute values is divided into a predefined number of equal intervals [154]. Each of the intervals represents one value of the new nominal attribute. This method is fast, easy to understand, and requires only the number of intervals, the so-called bins, as a parameter. A drawback is, that the number of instances might not be equally distributed on the bins.

2.2.b. Equal-Frequency Discretization

To tackle the deficiency of unequal distribution on the bins, the procedure of equal-frequency discretization has been developed. Its idea is, that all instances are distributed uniformly on the fixed number of intervals [154]. This guarantees, that each value of the nominal attribute appears approximately as often as the other values. Indeed, the width of intervals can become tiny. Then, very similar values at the original numerical attribute can fall into different bins, which implies a substantial difference between them.

2.2.c. Supervised Discretization

The two illustrated discretization methods are also referred to as unsupervised approaches. This indicates, that they do not include a measure, how well they separate the instances with respect to the learning task. A different procedure is the entropy-based discretization. It is supervised and considers the prediction attribute in addition to the attribute which is to be discretized. The entropy measure describes the distribution of the values of the prediction attribute K in a set of instances m [155]. The entropy can be regarded as the sum of weighted probabilities p of the prediction values K, i.e., at which percentage the prediction value appears in the set m.

$$Entropy : -\sum_{k=1}^{K} \hat{p}_m k \ \log \hat{p}_m k \tag{VI.1}$$

Using this formula, the set of instances is iteratively split up to minimize the entropy in each step. The amount of entropy reduced is indicated by the information gain, which is the difference of the entropy before and after the split [154]. The information gain ensures, that neither bins contain a very unequal number of instances, nor very similar instances fall into different bins. Entropy-based discretization consciously accepts, that some intervals are wider and some contain more instances than others.

2.3. Feature Selection Approaches

A further important issue at the transformation step is the selection of appropriate features. Usually, many features are generated from the input data at first. In most cases it is unknown, which features are able to characterize instances belonging to one class. Some algorithms have an implicit feature selection. In general, selecting features improves the performance of the algorithms by dimensionality reduction. Moreover, less features mean better understandability [154].
The approaches to extract useful features, can be grouped into two different procedures. The wrapper methods on one hand include the usage of a learning algorithm and the prediction attribute. They are therefore known as supervised selection. In contrast, the filter methods do not involve a learning algorithm. Some authors refer to them as unsupervised selection.

2.3.a. Unsupervised Feature Selection: Filter Methods

Filter methods compute an index for ordering the features by importance. Kira and Rendell [156] proposed the Relief algorithm, which chooses the closest two neighbor instances and determines a relevance level through all neighbors. Hall [157] used the correlation as an indicator for the importance. He introduced the idea, that features with a very high correlation to another feature can be replaced by that one and are therefore redundant.

2.3.b. Supervised Feature Selection: Wrapper Methods

The wrapper approaches are based on executing the embedded learning algorithm with a different set of features. This implies more computational effort than just ranking the

features, but wrapper methods are considered to perform better in general. They can be distinguished by the direction for adapting the feature set. While forward selection starts with an empty set and adds features incrementally, the complete set of feature is the initial point for backward selection. Backward selection is regarded to output larger feature sets and better prediction accuracy than forward selection. It may stop early if the performance measure on the algorithm is not perfectly correct. The forward selection may also stop too early, having only few features selected and therefore worse accuracy [154]. At wrapper approaches, the error of the learning algorithm has to be kept in mind. If an algorithm tends to disregard a specific feature or a group for some reason, it is unsuitable for feature selection. This hazard can be tackled by applying several learning algorithms and use the intersection or union set for learning.

2.4. Data Mining Algorithms

Generally, DM algorithms can be divided into two groups, supervised and unsupervised learning algorithms. For supervised learning an extrinsic error measure is required for optimizing the output [155]. For example, the regression algorithm (see below) must be provided with information, how far a predicted value is from the optimal output to improve the results. Equally, classification algorithms need some class information in the training process. Unsupervised methods, such as cluster analysis, incorporate an explorative approach and group data without this extrinsic information. There are 4 groups of DM approaches, predominantly used.

Association Analysis: This method finds combinations of features, which appear relatively frequently together in instances [155]. It makes binary decisions (available or not available) for each feature resulting in feature patterns. This analysis often employed to discover customers' hidden sales patterns or relationships among items purchased [145]. It uses a so-called *a priori* property, i.e. if an attribute is not frequent among all instances, its descendants are also not frequent. By this, the efficiency of the algorithm is increased.

Cluster Analysis: Identifying groups of instances based on a similarity measure is the goal of clustering methods [155]. The members of the resulting clusters are more closely related to each other than to the remaining instances. It is a method of unsupervised learning, i.e., it has an explorative power and is frequently used in studies with a large amount of data but no, or very little, knowledge about that data. Clustering algorithms group objects into a predefined number of clusters. After clustering, objects in one group are similar to each others (in terms of attribute values) and distinct from other groups. Clustering methods can be subdivided into hierarchical and partional algorithms [158].

Classification: Classification methods belong to supervised learning strategies and aim at assigning a new instance to one of several classes [155]. Classification is a two-step process consisting of training and testing. The first step, training, builds a classification model, consisting of classifying rules, by analyzing training data containing class labels (...). The second step, testing, examines a classifier for accuracy (in which case the test data contains the class labels) or its ability to classify unknown objects (records) for prediction

[145]. In contrast to clustering, the classes have to be known beforehand for the training process.

Regression: Unlike the classification method, numerical data is predicted for a new instance instead of nominal data. The output of a regression model is therefore not a class, but a real number [155]. This number is calculated on the basis of a formula derived from the other instances.

In this work only classification algorithms are applied, since they are the core DM methods used in bioinformatics and biomedicine [145]. Therefore, the most prevalent algorithms are shortly introduced in the following.

2.4.a. Nearest-Neighbor Classification

The values of similar instances in the training set V are regarded for classifying the new instance $v*$. The approach of looking at the neighbors is referred to as k-Nearest-Neighbors (kNNs). The nearest neighbor of $v*$, denoted as $v_{min} \in V$, can be obtained by using the Euclidean distance in the feature space X and finding the instance with minimal distance:

$$v_{min} = v_i \in V : \min \left(\sqrt{\sum_{x=1}^{X} (v_{i,x} - \hat{v}_x)^2} \right) \tag{VI.2}$$

For numerical features the distance measure is obvious, nominal features have to be converted into a numerical representation. The only parameter, which has to be determined for this algorithm, is the number of neighbors k. Classifying an instance just by its nearest neighbor (k = 1) tends to be suboptimal, since an outlier may disturb the prediction. Therefore, the results can, in many scenarios, be improved by regarding k neighbors with $k>1$ [155]. Then, the majority class value from the k neighbors is assigned to $v*$. The challenge is to find an optimal k. There is a minimal error rate at a specific k which can be found by brute force search.

Despite its simplicity, kNN has showed to perform very successfully. A characteristic of the kNN algorithm is the absence of a model, which is trained once during the training phase. Instead, all training instances have to be used for classifying new instances. For that reason, the procedure is also known as instance-based learning. This approach is obviously not fast compared to model-based algorithms. In fact, the computational complexity is $O(dn^2)$ for d features (dimensions) and n instances [159].

2.4.b. Support Vector Machines

Like instance-based learning, Support Vector Machines (SVMs) are based on the proximity of instances with the same class value in the feature space. SVMs separate the classes by finding a hyperplane [154]. In contrast to instance-based learning, not all training instances have to be used repeatedly. The convex hull of the training instances per class is constructed instead [154]. The challenge for the training process is to find the hyperplane between the complex hulls with maximal margin, i.e. the distance to the hulls. Support vector machines are based on the assumption, that large margins mean clear separation and thus good classification [159]. From each convex hull, the instances, which are closest

to the hyperplane, are called "support vectors". Then, SVMs can formally be expressed by their hyperplane [154]:

$$x = \sum_{i=1}^{N} \alpha_i \, y_i \, a_i \, a + \beta \tag{VI.3}$$

The instance vectors a_i and their class information y_i contain the training data. They are provided with weights (α_i) and an offset (β) to position the hyperplane correctly in the feature space. The new classification x depends on the new instance vector a.

If the classes are linearly separable, and therefore the convex hulls of the classes are disjunct, the task is relatively easy. The Simplex algorithm from linear optimization can be utilized to find the most appropriate hyperplane [159]. The procedure includes a penalty term for misclassified instances. Aiming at the goal to minimize the penalty, the optimal hyperplane can be found [155]. However, if such a separation is not possible in the given feature space, the kernel trick is an approach to solve the problem. Its basic idea is to represent the data in a higher dimension. In this dimension, data of different classes should be linear separable. Obviously, finding an useful mapping function (kernel) is crucial. Including the transformation $K(x, x_i)$, the previous formula is extended to:

$$x = \sum_{i=1}^{N} \alpha_i \, y_i \, K(a_i, a) + \beta \tag{VI.4}$$

Popular kernel functions are polynomial and radial basis function (RBF) kernels [154]. The kernel trick often increases complexity, even if the original problem was quite simple. This may lead to overfitting, because many parameters can be perfectly fitted on the training data available. However, SVMs have a relatively inflexible decision boundary [154], which is useful against overfitting: the hyperplane is only modified, if the new instance is outside the convex hull of all instances of the same class. This makes SVMs robust to noisy data as well. In general, SVMs are considered as very accurate. Although the training process is slow for SVMs, they are fast in the testing phase. For evaluation, only the new instances have to be compared to the existing hyperplane.

2.4.c. Artificial Neural Networks

Although it is hard for humans to comprehend the specific behavior of a complex kernel transformation like in SVMs, the basic concept of a hyperplane dividing instances into two classes can be understood. Likewise, the Euclidean distance of kNN is easy to follow. In contrast, Artificial Neural Networks (ANNs) apply a black-box approach. They do not aim at interpretability, which is one of the reasons that they are hardly used in medical applications. The idea is to compare input values and classifications and reproduce the behavior with mathematical functions [155].
The structure of ANNs is inspired from the human brain [160]. The core idea is the distribution of workload onto a large number of small and relatively simple components. By the various combinations of those components, a decision is produced. In ANNs, these basic components are called nodes. A node is a simple function, which can be parameterized by a small number of factors. The nodes are connected by edges incorporating weights. This enables some nodes to have greater impact on the result than others. Hence, the whole

design of a neural network is a directed, acyclic graph. It can consist of several sequential layers, usually there are at least the input, the hidden, and the output layer [159]. A layer is a set of nodes with common predecessors and successors, but without edges between each other. If more layers are involved these networks are also called Multi-Layer Perceptron.

The functions of the nodes play a key role in artificial neural networks. Although they are simple by design, they are responsible for a complex output. Among the most popular functions is the nonlinear sigmoid (VI.5a), explained in detail by Duda [159]. Also the signum function (VI.5b) is frequently used [160], and last but not least the radial basis functions VI.5c [159].

$$f(x) = \frac{1}{1 + e^{-x}} \tag{VI.5a}$$

$$f(x) = \begin{cases} -1 & \forall x < 0 \\ 0 & \forall x = 0 \\ 1 & \forall x > 0 \end{cases} \tag{VI.5b}$$

$$f(x) = \sum_{i=1}^{c} \omega_i \, e^{-\frac{x-\mu_i}{\sigma_i}} \tag{VI.5c}$$

The weights of the edges are trained by the back-propagation algorithm. It is an iterative procedure, running through all layers. The algorithm starts with the adaption of the weights between the last hidden layer and the output layer. For the output layer, the values are given by the training instances. The weights are adapted in such a way, that they produce the available output values. Independent of the number of layers or nodes, the classification error is minimized by gradient descent on the weights [160]. The training phase belongs to the most expensive among all classification algorithms. This pays off at testing, which is fast. Although the overall accuracy is considered as very good [155], bad results are possible, if the model of the network does not fit the data. Also overfitting can occur, if the network consists of too many nodes.

2.4.d. Bayesian Learning with Naive Bayes

If the dimensionality of the feature space is high, distance-based procedures such as kNN or SVM are very expensive. Also ANNs incorporate serious costs for training. For that reason, probability-based methods exist. They are also known as Bayesian learning methods and use information about the distribution of a specific value per feature and class [154]. The basic formula behind Bayesian learning is the rule of Bayes (VI.6a). It is derived from the formula of conditional probability (VI.6b) determining $Pr[H \mid E]$.

$$Pr[H \mid E] = \frac{Pr[E \mid H] \, Pr[H]}{Pr[E]} \tag{VI.6a}$$

$$Pr[H \mid E] = \frac{Pr[H \cap E]}{Pr[E]} \tag{VI.6b}$$

The probability $Pr[H \mid E]$ states, how probable a certain hypothesis (or class) H occurs given evidence (instance data) E. Directly computing $Pr[H \mid E]$ is impossible due to the unknown joint probability $Pr[H \cap E]$. If this joint probability was known (for the case of

instance data and class value occurring together), the classification would be unnecessary. However, using the rule of Bayes, $Pr[H \mid E]$ can be computed on the basis of the overall probabilities of H and E and, in addition, the conditional probability $Pr[E \mid H]$. All these three can be obtained during the training phase. Usually, several probabilities $Pr[H \mid E]$ and $Pr[E]$ are computed for the different possibilities of E. For the actual classification, the appropriate (according to the present instance data E) $Pr[H \mid E]$ can be utilized to obtain the probabilities for the hypotheses (class values). E is in fact the tuple $(e_1, \ldots, e_n)$ and contains an instance value of all features. Regarding this, formula (VI.6a) can be written as:

$$Pr[H \mid \ e_1, \ldots, e_n] = \frac{Pr[e_1, \ldots, e_n \ \mid H] \, Pr[H]}{Pr[e_1, \ldots, e_n]} \tag{VI.6c}$$

While the joint probability $Pr[e_1, \ldots, e_n]$ in (VI.6c) is still possible to compute, the conditional probability $Pr[e_1, \ldots, e_n \mid H]$ can only be computed theoretically, but it would not be feasible in practice [160]. The solution is referred to as Naive Bayes (NB) and assumes the statistical independence of the features $e_1, \ldots, e_n$. Now the joint probabilities can be replaced by multiplications (VI.6d).

$$Pr[H \mid \ e_1, \ldots, e_n] = \frac{Pr[H] \prod_{i=1}^{n} Pr[e_i \ \mid H]}{\prod_{i=1}^{n} Pr[e_i]} \tag{VI.6d}$$

The NB classifier provides very good results in many cases [155] and is fast, since the class probabilities are computed during training. A mathematical problem in NB results from the multiplication. If one possible value of any e_i does not occur in the training data for any class, its probability is naturally 0. Consequently, all other probabilities become 0. The standard strategy against a division-by-zero error is adding a constant term to all probabilities in the nominator. The denominator has to be compensated by adding the constant term once for each possible value of the feature [154].

2.4.e. Decision Trees

Decision Trees (DTs) use entropy information to separate classes. The idea is simple: Because entropy is a measure for the disarrangement in a set of instances, the data set is well arranged, if the entropy is small. In a well-arranged set classification is easy by taking the majority class. However, this works obviously bad at an equally distributed data set for example. The goal is to group instances, which are well separable by one of the features. The original data set is split up according to the splitting attribute. From the theoretical perspective, they delimit subspaces of the feature space [159]. The main challenge is to find the best splitting attributes. This is a recursive process to reduce the entropy stepwise. The main method to select a splitting attribute is to utilize the information gain. It is defined as the difference of the entropy before the split (S) and the weighted sum of entropies after the split (S_v).

$$Gain(S, A) \equiv Entropy(S) - \sum_{v \in values(A)} \frac{|S_v|}{|S|} \, Entropy(S_v) \tag{VI.7}$$

Although meaningful splits are possible by the information gain, attributes with many values are preferred: They usually separate the instances better, because they have more alternatives. In the extreme case, values such as date or id allow a perfect split since only one instance is assigned to each class (entropy of 0 then). However, such a split does not provide useful information for the learning algorithm, because the idea is to assign new instances to the trained groups. The measure of gain ratio solves this problem: It divides each information gain by the sum of all information gains at that step [160]. In other words, it normalizes the information gain values. By this, splitting attributes are penalized, which split the data set into several small groups (e.g. id or time). [155] recommend even binary splits, because they try to avoid insufficient data at a lower level.
Again the problem of overfitting can occur if no adequate stopping criteria is applied. Another disadvantage of DTs is the instability. In theory, one additional instance could change the whole tree. For that reason, decision trees are not very suitable for online classification. Hastie [155] proposes averaging over many trees to impede continuous reorganizations, which is also known as bagging. In terms of computational complexity, DTs are quite expensive. Duda [159] determine the complexity with $O(dn\ (\log n)^2)$ for the training phase and O(log n) for testing. A distinct advantage of DTs is their interpretability. Whether the tree is visualized as graph structure with nodes and leafs or as logical IF-THEN rules, the splitting attributes and conditions are clear and easily accessible for domain experts.

2.4.f. Ensemble Methods

In contrast to the classification algorithms presented so far, ensemble methods involve a different type of proceeding: they classify instances by combining other classifiers and using the results of those in an elaborate manner. The driving hypothesis is, that considering several classifiers can improve the prediction accuracy. Three major ensemble methods will be described in this section: Bagging, boosting, and stacking.

For bagging, several subsets of the training set are constructed [154]. They may overlap, but should still be substantially different. Then, a classification algorithm is trained for each subset. The resulting classifiers usually vary in terms of the model or parameters. For relatively stable classification methods, these models tend to be similar. In this case, bagging might not improve the accuracy considerably. However, for unstable methods such as artificial neural networks or decision trees, bagging can be very useful [159]. Since small changes in the training data may change the models, the prediction accuracy can be increased by voting. From the computational perspective, bagging can be executed concurrently, as the different models are independent of each other.

In boosting, the process starts with constructing a subset as for bagging and continues with training a classifier of that subset. But in contrast to the other methods, the subset is mainly constructed based on the instances, which are not well represented by the first classifier [154]. Hence, the second classifier becomes an expert for data, on which the first classifier performed poorly. This procedure is repeated iteratively. The produced classifiers are usually weighted to determine their overall importance at the end. The most popular boosting algorithm is AdaBoost [159]. Its distinctive idea is to increase or decrease the probabilities for including an instance into a newly generated subset. By this, the instances, which are already well covered by the existing classifiers, are chosen less

	Class True	Class False
Classified as True	TP	FP
Classified as False	FN	TN

Table VI.1.: Different outcomes of a classification test, illustrated in a confusion matrix.

probably as training data for the new classifier. On the other hand, including instances that are badly represented are chosen with a higher probability.

Stacking does not combine the same type of classifier several times, but involves completely different learners. Basically any classification algorithms can be used as a level-0 classifier [154]. From the results of those, a level-1 or meta-classifier predicts the final outcome. The level-1 classifier could be as simple as voting (final class = majority of class values). Either predetermined rules could be involved or dynamic learning based on the error rate of the level-0 classifiers. Although any classification is allowed for the meta-classifier. It is a common procedure to use a rather simple method [154].

2.5. Performance Analysis

A common problem in machine learning is overfitting, i.e. the algorithms are designed to perform well on the training data, but perform badly in the general case, on arbitrary data [159]. Therefore, to evaluate DM algorithms, the data set is usually split into a training and a test set. Exemplarily, the data set is split into K=10 folds. Then, the algorithm is iteratively executed and each time another fold is taken as a test set, while the remaining $K-1$ folds are used for training [155]. This procedure is called "cross validation". The prediction error is averaged to obtain the overall performance measure [144].
Several other factors can be included in the performance evaluation. For instance, considerations about computational complexity. Algorithms, which cannot be computed within the available time and ressources, would be useless [159].
Especially in the medical domain transparency of the procedures and results of DM can be another evaluation criteria. For example, illustrations of a decision tree with leafs and connections in between are more comprehensible than weighting factors of an ANN and are probably better accepted in the medical community.

Apart from the qualitative evaluation, several quantitative factors are used to determine a DM algorithm's performance. A key factor in the machine learning domain is the accuracy:

$$\text{accuracy} = \frac{TP}{total} 100\%. \tag{VI.8}$$

It measures the percentage of correctly classified instances (TP =true positive) among all test instances ($total$). However, this measure can hide essential details of the achieved results and is therefore not acceptable in medicine [149]. A *sensitivity and specificity* analysis gives a more elaborate insight. In case of a binary class type, there are four possible outcomes: true positives (TP) and true negatives (TN) comprise the correct predictions for both classes. In contrast, false negatives (FN) and false positives (FP) combine the false predictions. This can be illustrated in a confusion matrix (Table VI.1). Following Cios and

Moore [149], three measure can be used for a thorough analysis:

$$\text{sensitivity} = \frac{TP}{TP + FN} 100\%, \tag{VI.9}$$

$$\text{specificity} = \frac{TN}{FP + TN} 100\%, \tag{VI.10}$$

$$\text{predictive accuracy} = \frac{TP + TN}{TP + TN + FP + FN} 100\%. \tag{VI.11}$$

The sensitivity measures how many of the positive test examples were correctly predicted. The specificity, on the other hand, is an indicator on how many of the negative examples were correclty excluded, and the predictive accuracy gives an overall evaluation. Only algorithms with high values in all three measures are assumed to perform well. It has to be noticed, that for an analysis based on sensitivity and specificity, the classification problem must be formulated as a yes-no-question, which can be challenging in medical investigations [149].

3. Related Work

Concerning the state of the art in medical DM, several categories have to be distinguished. This is due to the numerous interpretations of the term *DM*, as well as the broad range of possible applications in the healthcare domain. Yoo et al. [145] give a good overview of DM algorithms in the healthcare and biomedical domain. They generally differentiate between applications reported from the industry and DM applications in the research area. Studies can further be distinguished based on the DM approaches that were used (e.g. classification, statistical measures, clustering or comparative studies) or based on the particular application. Following Yoo et al. [145], efforts have exemplarily been made to classify DNA micro arrays [161, 162] or to give breast cancer prognosis [163, 164]. In this context the very recent work of Müller [165], examining DM algorithms for the diagnosis of brest cancer and alzheimer disease, shall be mentioned.
Also Matheny [150] gives an overview of the literature and includes two application areas relevant for this work, the prediction of ICU mortality and cardiovascular disease risk. Regarding the latter, Matheny lists prediction models primarily based on logistic regression methods [166–168] and states, that external validation of these models has shown good discrimination and calibration, with some limitations, when applied to populations with significantly different demographics and specific comorbidities [169, 170].
In the context of ICU mortality a huge amount of studies have been published over the last decades. Matheny [150] mentions a couple of studies to predict in-hospital mortality, based on a variety of physiological variables, with the comparative studies of Markgraf et al. [171], Beck et al. [172] and the review study of Ohno-Machado et al. [173] among the most recent ones. All these studies have a predictive nature and usually consider patient data from the last 24 hours. Therefore, they are not able to assess the current patient state without a long-term monitoring.
During the last couple of years several algorithms have been presented to classify online patient data. The intention is not to give predictions about future outcomes as in the studies presented before, but to increase patient safety and quality of care. Especially ECG

classification and Heart Rate Variability (HRV) analysis are predominant research areas in this category. Kampouraki et al. [174] applied Gaussian kernel-based SVM classification to differentiate between healthy and pathological cases based on HRV features. They used statistical features, such as standard deviation and autocorrelation values, as well as linear prediction and Haar wavelets as inputs for the classifier. Evaluation was done by leave-one-out cross validation and a 100% accuracy value was reported.
The study of Chin et al. [175] also examined ECG data. They focused on separating the ventricular tachycardia, ventricular fibrillation and normal sinus rhythm. They applied cross-correlation and a fuzzy kNN classifier and reported specificity and sensitivity values of 92.5% and 93.5%.
A different approach was chosen by Keogh et al. [176]. Instead of finding similar waves in the ECG record like Chin et al. [175], they aimed at detecting unusual sections [144]. However, there was no large-scale performance analysis of their algorithm.
Instead of analyzing ECG data, Wang et al. [177] used blood pressure waveforms to distinguish between normal and pathological cardiovascular behavior. Again a SVM classifier was applied and the blood pressure pulse waves were characterized by mean value, standard deviation and spectral energy ratios. They reported specificity and sensitivity values of 85% and 93%.
Chambrin et al. [178] examined high-frequency SpO_2 recordings and used a rule-based approach to classify deconnection, transient hypoxia and desaturation events. They reported good classification results, however, the data set was very limited with only 38 annotated events.
At the interface between the domains of DM and signal processing, Imhoff et al. [179] used low-order autoregressive and phase space models to detect qualitative patterns in monitoring data. They used 134 time series records and evaluated the performance in detecting the five patterns *no change*, *outlier*, *temporary level change*, *permanent level change* and *trend*. They reported a reliable detection rate, but constrain, that their methods are too sensitive for clinical use. Also Sharshar et al. [180] used regression models to describe trends, such as *increasing*, *decreasing*, *constant* and *transient*.

The work of Apiletti et al. [181] presents a framework for monitoring health conditions in any context. Particularly they focus on the generation of intuitive and sensible features in medical time series and the creation of a risk function, based on feature clusters. As risk components the authors extract the three measures *sharp changes*, *long-term trend* and *distance from normal behavior* from physiological signals, such as the ABP or HR curve. Apiletti et al. then apply different clustering algorithms (Simple K-Means, Farthest First, Expectation Maximization) and aggregate the clustering results in a risk function:

$$\text{risk}_x(t) = \frac{\sum_i k_{i,x} C_i(z_i(x))}{\sum_i k_{i,x}} \times \frac{n}{C_{max}} \qquad i = 1 \dots 3 \tag{VI.12}$$

$\text{risk}_x(t)$ determines the risk level $[0 \dots n]$ of signal x at time t. $C_i(z_i(x))$ indicates the risk level associated to the risk component z_i. Exemplarily, Figure VI-2 shows the risk levels on an ABP recording from the MIMIC Database [28], obtained with K-means clustering. Although the approach of Apiletti and coworkers is promising, it lacks a thorough evaluation, which was apparently done by visual inspection only. The reported accuracy values were acceptable with K-Means clustering, but omit the existing reports of false positive values. However, the features used in [181] are well-chosen and will be further evaluated

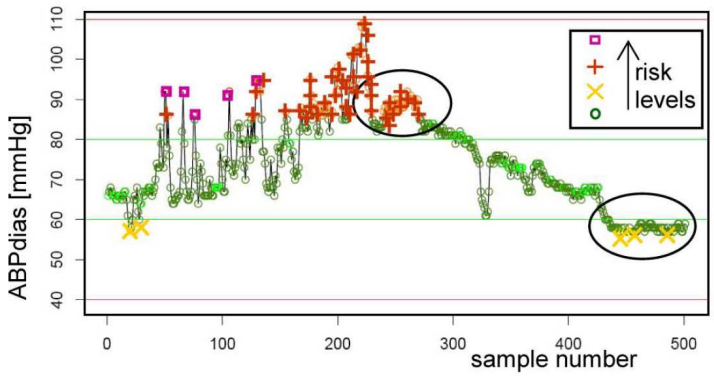

Figure VI-2.: Risk level assessment applying K-Means clustering on an ABP waveform. From Apiletti et al. [181].

in this work. Generally, clustering algorithms are used for finding unknown structures in large datasets. If intervals with high risk for the patients were known beforehand (training set), classification algorithms would probably be the method of choice.
The procedure of learning from labeled data was followed by Aboukhalil et al. [29]. Their work has two major contributions, (i) the creation of an annotated database for critical ECG alarms and (ii) an algorithm to reduce false alarm rates by combining features from ECG and ABP waveforms. Multiple expert reviews of 5386 critical ECG arrhythmia alarms from a total of 447 adult patient records in the MIMIC II [28] database were made [29]. An average of 42.7% of those alarms were found to be false. Aboukhalil et al. then introduce an algorithm leveraging the power of data fusion. Using morphological features of the ABP waveform, the ECG alarms triggered by bedside monitors, were validated. Alarms were suppressed, if the features of the ABP curve did not confirm the alarm. The processing distinguished between 5 alarm types: *Asystole, Bradycardia, Tachycardia, Ventricular Tachycardia*, and *Ventricular Fibrillation/Tachycardia*. On average, their algorithm reduced the incidence rate of false alarms from 42.7% to 17.2%, with an average FA suppression rate of 59.7%. The suppression rate of true alarms was all zero, except for ventricular tachycardia alarms (9.4%).
King et al. [182] evaluate smart alarms on a small clinical patient cohort. They started with interviewing ICU nurses to determine threshold ranges for the HR, blood pressure, SpO_2 and respiratory rate in post-operative patients after artery bypass graft. Using the expert information, fuzzy sets and a corresponding rulebase were established. A distinct feature in their reasoning is, that alarms are suppressed, if only one parameter is out of range, but the other 3 indicate a stable patient condition. King et al. reported a false alarm reduction rate of 55% with 1 missed true alarm.

Chapter VII

Case Study: False Alarm Rate Reduction of Patient Monitors

Contents

1	**Case Study: Reducing False Alarm Rates of Patient Monitors**	97
2	**Persitency of False Alarms in Patient Monitoring**	98
3	**Data Source and Selection Criteria**	99
4	**Preprocessing and Feature Design**	100
5	**Classification and Evaluation Criteria.**	104
6	**Results and Discussion**	104

1. Case Study: Reducing False Alarm Rates of Patient Monitors

In order to show the applicability and to evaluate the previously introduced DM concepts to assess a patient's health status, a well-defined real-world problem is tackled: the reduction of false alarm rates of patient monitors in ICUs. Although the main focus of this work deals with the automation of a portable HLM, there are several reasons why this application was chosen:

1. **Database availability:** Since the use of ECCSs outside a hospital is a rather new and specific application, there is no publicly available database. A large-scale and labeled database, however, is indispensable for the learning process of DM algorithms. On the other side, there are several databases available in the context of ICU monitoring. A labeled subset of the MIMIC II database [28] will be used here. Moreover, common patient parameters obtained during ECC, such as ECG, blood pressures or SpO_2, are also recorded in ICU databases.

2. **Evaluation:** During the last years intelligent monitoring and especially the reduction of false alarms have become a more and more popular research area. A broad range of studies (see section 2 and 3) employ DM approaches to increase patient safety and

quality of care on ICUs. Due to the established community in ICU research, results of this work are easier to compare and to evaluate with competing approaches if the challenge of alarm rate reduction is accepted.

3. **Contribution:** Last but not least, alarming is a predominant issue for all kinds of medical devices. The reliability of alarms is a major aspect, not only for the automation of a HLM. Therefore, the contribution of this part is not only limited to ICU research and HLM automation, but the findings can be helpful for other automation projects, such as automated medication [183] or automated Cardiopulmonary Resuscitation (CPR)[1] as well.

A summary of this section has been published by the IEEE Engineering in Medicine & Biology Society [12].

2. Persitency of False Alarms in Patient Monitoring

Patient monitors are indispensable in today's medicine. Especially in ICUs they are of significant importance. They support the staff in the assessment of a patient's health status and give acoustical warnings or alarms, if the physiological state of the patient needs attention or if there is a technical problem. However, several problems concerning those alarms have been reported. The produced noise can have a negative influence on both patients and staff. Gabor et al. [184] reported sleep disorders due to the noise on ICUs which led to a slowed recovery. Also Novaes et al. [185] emphazise the negative impact of the increased noise level in ICU and found, that machine alarms seem to disturb the members of the professional team even more than the patients themselves. Topf et al. [186] reported similar results, highlighting increased sound levels as an ambient stressor. Furthermore, high rates of alarms without any clinical relevance have been reported. Chambrin et al. [187] reported a false positive rate of 74.2%. Siebig et al. [188] stated, that only 17% of the alarms are clinically relevant and Görges et al. [189] identified up to 94% of the alarms as false. The high frequency of alarms, and especially of false alarms, also leads to a desensitization of the staff, as reported by the German Association for Electrical, Electronic and Information Technologies (VDE) [190]. Imhoff and Kuhls [191] state, that the rate of false alarms has basically not changed during the last 20 years, despite technological and methodological advances.
Usually, patient monitors display multiple signals such as ECG or blood pressures. Alarms are often triggered, if one parameter is out of range, e.g. increased HR. The motivation for this work is to reduce the rate of irrelevant alarms by not only looking at one parameter for its own, but to incorporate the knowledge from several sensors at the same time. This approach of data fusion is driven by human decision making: doctors or nurses assess the state of a patient by looking at multiple features at once and by relating them among each other, instead of just observing one parameter. This approach is supported by promising studies, using machine learning, artificial intelligence and knowledge-based methods

[1] Recently a cooperation between the *German Heart Center Munich* and the *Robotics and Embedded Systems, Dept. of Informatics, Technische Universität München* was established to research the automation of an electromechanical CPR.

Class	False Alarm	True Alarm	**Total**
Asystole	130	43	173
Brady	65	193	258
Tachy	169	802	971
V-Fib	92	33	125
V-Tach	315	282	597
Total	771	1353	**2124**

Table VII.1.: Distribution of the training set over class and alarm type.

[192–194]. Also Lipton et al. suggest to combine multiple monitoring devices to generate "smart alarms" [195].

3. Data Source and Selection Criteria

For training and test sets a subset of PhysioNet's MIMIC II Waveform Database [28] was used. The database comprises 4458 measurement records from 4099 patients. The number of signals within each record can vary. However, all records have a "Waveform" part containing up to four high-resolution signals (125 Hz). Furthermore, most of the records have a "Numerics" part with signals of low resolution (one value per minute). In addition to waveform and numerics data, metadata is available, providing age and sex information of the patients. Alarm notifications of the monitors are also included. They consist of a timestamp, the alarm type, the channel that caused the alarm and threshold information, if the alarm was caused by a parameter being out of range.
Aboukhalil et al. [29] selected a subset of the MIMIC II database for alarm labeling and classification that fulfilled two criteria: a critical ECG arrhythmia alarm was issued and one channel of ECG and an ABP waveform were present at the time of the alarm. They labeled five types of arrhythmia alarms: *asystole* (asystolic pause of 4 s), *bradycardia* (HR $<$40 bpm), *tachycardia* (HR $>$140 bpm), *ventricular tachycardia* (5 ventricular beats), and *ventricular fibrillation* (fibrillatory waveform lasting for 4 s). A group of experts reviewed those alarms and decided whether the alarm was true or false. Overall, 5386 alarms were labeled and considered as ground truth. Their labeled subset was chosen for training and testing in this work, but further requirements were imposed. Only records that contain the second Einthoven ECG derivation and the ABP signal were included. Furthermore, the signals had to persist continuously over a time window (alarm scope) of 20 seconds around the alarm event (15 s before and 5 s after). If available, the Pulmonary Arterial Pressure (PAP) was also part of the set. From the numerics part SpO_2, the CVP, age and sex of the patient were included. Only data with an associated alarm event and alarm label was included. The final set for training and testing contained 2124 labeled alarms. The set distribution, with respect to the alarm type and the alarm class (true/false alarm), is displayed in Table VII.1. Each alarm scope (20 s) in the set contains 7504 values: age, sex, CVP, SpO_2 and from the waveform part ABP, ECG and PAP sampled at 125 Hz each. Fig. VII-1 exemplarily shows an alarm scope retrieved from the database.

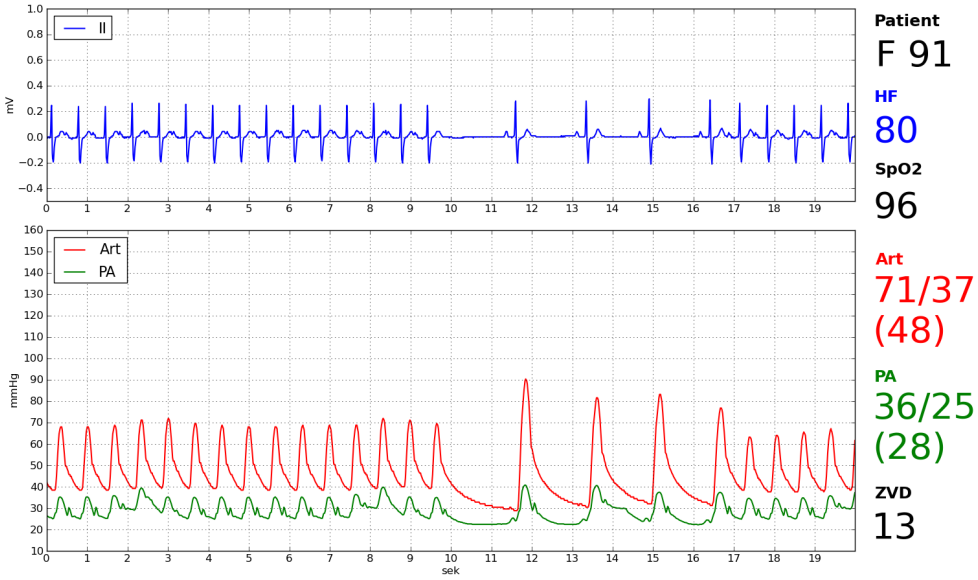

Figure VII-1.: Sample from the training set (alarm scope), showing ECG, arterial and pulmonary blood pressure as well as numerics data.

4. Preprocessing and Feature Design

By the transformation to feature space the characteristics of a particular alarm scope are extracted. Moreover, scaling issues are avoided and the dimension of the input data for classification is reduced.
For data from the numerics part of the set (Age, Sex, CVP, SpO_2) there was no further processing necessary, since those values did not change during an alarm scope. A QRS detection on the ECG signal located the cardiac intervals (I, beat-to-beat distance) in the scope. Based on those intervals, further time series, that were not present as raw data, were created: the HR in bpm, diastolic (BP_{dias}) and systolic (BP_{sys}) blood pressure time series (in mmHg) based on the min/max-values of the ABP and PAP data per interval:

$$HR(I) = \frac{60}{length(I)} \tag{VII.1}$$

$$BP_{sys}(I) = max(BP(I)) \tag{VII.2}$$

$$BP_{dias}(I) = min(BP(I)) \tag{VII.3}$$

In the following, 8 basic operations $f_{i=1,\ldots,8}$ are described to extract characteristics of the alarm scope X. The features were inspired by the work of Apiletti et al. [181] and have been designed in close collaboration with medical practitioners. The features can be divided into three groups: *scope-based*, *interval-based* and *sample-based* features. For interval- and sample-based operations the results are aggregated, such that the alarm scope is described by few single values.

4.1. Scope-based Features

The first two operations are calculated directly from the signal samples $x_{i=0,\dots,n}$ in the scope and don't need any further preprocessing:

Mean Value: Obvious features of the alarm scope are mean values of the vital parameters. The mean values help to easily distinguish several patient states such as bradycardia or tachycardia:

$$f_1(X) = \frac{1}{n} \sum_{i=0}^{n} x_i \tag{VII.4}$$

Dispersion: The second feature operation measures the dispersion of the waveforms and illustrates, how much the samples deviate from the average:

$$f_2(X) = \frac{\sum_{i=0}^{n} |x_i - f_1(X)|}{f_1(X)} \tag{VII.5}$$

The idea behind this operation is to detect strong variations in the sample values which would indicate some severe physiological state change or sensor movements. The dispersion was chosen instead of the standard deviation since it is independent of absolute values.

4.2. Interval-based Features

On the basis of cardiac intervals, the second feature group aims at characterising the ABP and PAP data morphologically. Therefore, the height, width and integral of each cardiac interval in the alarm scope is calculated:

Height: The height was computed as the difference of the maximum and the minimum signal value of a cardiac interval.

$$f_3(I) = x_{sys}(i) - x_{dias}(i) \tag{VII.6}$$

Width: The time difference between consecutive systolic values represents the width of the interval.

$$f_4(I) = t(x_{sys}(i+1)) - t(x_{sys}(i)) \tag{VII.7}$$

Area: The third feature extracted from the blood pressure signals is the area under the pressure waveform and is calculated as the integral of each interval.

$$f_5(I) = (t(x_{dias}(i+1)) - t(x_{dias}(i))) \cdot \sum_{t=t(x_{dias}(i))}^{t(x_{dias}(i+1))} x_t \tag{VII.8}$$

The interval-based operations f_3, f_4 and f_5 are aggregated for each alarm scope, by only considering the minimum, maximum and mean value of all intervals in the scope:

$$\boldsymbol{f}_i(X) = \begin{pmatrix} min(f_i(I)) \\ mean(f_i(I)) \\ max(f_i(I)) \end{pmatrix}, \quad i = 3, 4, 5 \tag{VII.9}$$

Exemplarily, in an alarm scope with 17 cardiac intervals, integral values for each interval are calculated. After the aggregation those 17 values are summarized by only 3, the minimum, mean and maximum values. By this aggregation the interval-based operations describe the complete alarm scope with only a few values, independent of the number of intervals within the scope. Figure VII-2 illustrates the interval-based features on a sample blood pressure curve.

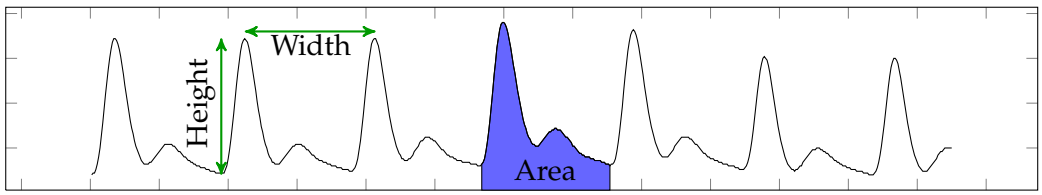

Figure VII-2.: Morphological features of blood pressure waveforms. Based on cardiac intervals, the height, width and integral of each interval are calculated and then aggregated over the complete alarm scope.

4.3. Sample-based Features

The last group of features is sample-based and includes a distance to normality, slope and an offset measure of the signal. This last group of features is applied to the HR, BP_{sys} and BP_{dias} signals only. Those signals provide one sample per cardiac interval.

Normality Distance: Since many alarms are caused by exceedence of thresholds, distance measure inspired by Apiletti et al. [181] is introduced. For each channel, critical thresholds c_1 and c_2 are defined, and, if exceeded, the distance to those limits is calculated:

$$f_6(x_i) = \begin{cases} c_1 - x_i \Leftrightarrow x_i < c_1 \\ x_i - c_2 \Leftrightarrow x_i > c_2 \\ 0 \Leftrightarrow c_1 \leq x_i \leq c_2 \end{cases} \tag{VII.10}$$

The signal-dependant thresholds were taken from [181] and are shown in Table VII.2. Again, the feature values were aggregated over the alarm scope. For the normality distance the sum and the maximum of $f_6(x_i)$ is considered:

$$\boldsymbol{f}_6(X) = \begin{pmatrix} sum(f_6(x_i)) \\ max(f_6(x_i)) \end{pmatrix} \tag{VII.11}$$

Signal	c_-	c_+
HR (bpm)	40	160
ABP_{sys} (mmHg)	80	200
ABP_{dias} (mmHg)	40	110
PAP_{sys} (mmHg)	15	30
PAP_{dias} (mmHg)	4	12

Table VII.2.: Thresholds for the normality range feature.

Slope: The slope of a curve is determined by the difference between the values of two consecutive intervals and aims at detecting sharp changes, that can indicate a dangerous situation for the patient. In contrast to the absolute measure of the normality distance, the slope operation considers the relative change between the intervals:

$$f_7(x_i) = x_i - x_{i-1} \tag{VII.12}$$

Offset: The offset feature, also inspired by [181], is similar to the slope. It does not regard a rapid change, but focuses on the trend over a few intervals. It calculates the difference between the current value and the average of the five previous intervals. For both slope and offset, several window sizes for the averaging were tried. A window of five intervals exhibited a good trade-off between balancing peak values and not blurring temporary signal aspects:

$$f_8(x_i) = |x_i - \frac{1}{5} \sum_{j=i-5}^{i-1} x_j| \tag{VII.13}$$

The slope and offset features are aggregated again to represent the complete alarm scope. The mean value and the maximum in the scope as well as the maximal sum of five consecutive intervals were considered:

$$\boldsymbol{f}_j(X) = \begin{pmatrix} mean(f_j(x_i)) \\ max(f_j(x_i)) \\ maxsum(f_j(x_i)) \end{pmatrix}, \quad j = 7, 8 \tag{VII.14}$$

4.4. Feature Overview

Table VII.3 summarizes the presented features together with the physiological signal they have been applied to. For the crisp values Age, Sex, CVP and SpO_2 no transformation is necessary and sensible, since they only provide one value per alarm scope. In total, 74 feature values are calculated per alarm scope. Since many classification algorithms don't yield better results when adding more and more features (accuracy can even get worse [154]), and with respect to resources and computational power, the maximum number of features was constrained to 20. Applying feature selection algorithms (see 2.3), heavy-weight features can be identified.

Feature		Signals
Crisp value		Age, Sex, CVP, SpO_2
Mean Value	$f_1(X)$	ECG, HR, ABP_{sys}, ABP_{dias}, PAP_{sys}, PAP_{dias}
Dispersion	$f_2(X)$	ECG, HR, ABP_{sys}, ABP_{dias}, PAP_{sys}, PAP_{dias}
Height	$\boldsymbol{f}_3(X)$	ABP, PAP
Width	$\boldsymbol{f}_4(X)$	ABP, PAP
Area	$\boldsymbol{f}_5(X)$	ABP, PAP
Normality Distance	$\boldsymbol{f}_6(X)$	HR, ABP_{sys}, ABP_{dias}, PAP_{sys}, PAP_{dias}
Slope	$\boldsymbol{f}_7(X)$	HR, ABP_{sys}, ABP_{dias}, PAP_{sys}, PAP_{dias}
Offset	$\boldsymbol{f}_8(X)$	HR, ABP_{sys}, ABP_{dias}, PAP_{sys}, PAP_{dias}

Table VII.3.: Physiological signals and applied features.

5. Classification and Evaluation Criteria

The Weka workbench [196] was used to design and evaluate the classifiers. Combinations of 5 discretization, 6 feature selection, and 9 classification methods were applied on the test set. The applied algorithms are enumerated in Table VII.4. In addition to the algorithmic feature selection, feature sets with less than 3 or more than 20 features were excluded. They were considered as either too small to be representative or too voluminous with respect to computation time. First, classifiers were trained and evaluated for the complete data set. In a second phase the data set was split with respect to the alarm types and again classifiers were trained and evaluated separately for each set. The classification was evaluated by a 10-fold cross validation and with respect to the evaluation guidelines of section 2.5.

6. Results and Discussion

Table VII.5 lists the most successful combinations of discretization, feature selection and classification methods for the different data sets in terms of classification accuracy. The accuracy for the complete set was 84.7% with a 6-bin equal frequency discretization, a Naive Bayes wrapper for feature selection and a SVM with standardized RBF (C=1,γ=0.01). 71.7% of false alarms were suppressed. This comes along with a rather high suppression of true alarms (7.9%).
The accuracy could be increased by splitting the data set with respect to the different alarm types with the best accuracy for asystole alarms (98.8%). Surprisingly, the accuracy for ventricular tachycardia alarms was worse than for the complete set (78.6%). Looking at the suppression rates, the results were also better with trained experts for each alarm type. The reduction rate of false asystole alarms was 99.2%. Again, ventricular tachycardia alarms were hard to classify with a rather low suppression rate of false alarms (75.2%), but a suppression of true alarms of 17.7%.

Compared to the work of Aboukhalil et al. [29] the reduction of false alarms was significantly better for tachycardia and ventricular-related alarms. However, they report a 0% suppression of true alarms except for ventricular tachycardia alarms.

Discretization Methods	Equal Width (6, 10 Bins), Equal Frequency (6, 10 Bins), Supervised Discrectization
Feature Selection Methods	Correlation-based Feature Selection (forward, backward), Supervised Feature Selection based on Information Gain, Relief Algorithm, Wrapper incl. Decision Trees, Wrapper incl. Naive Bayes
Classification Methods	Naive Bayes, kNN (1, 3, 5, 9 Neighbors), kNN + Distance Weighting (1, 3, 5, 9 Neighbors), Decision Tree (Confidence Level for Pruning: 0.2, 0.3, 0.5), Binary Decision Tree (Confidence Level for Pruning: 0.2, 0.3, 0.5), Unpruned Decision Tree, SVM incl. Polynomial Kernel (Classical, Standardized, Normalized, C=1, e=1), SVM incl. RBF Kernel (Classical, Standardized, Normalized, C=1, γ=0.01), Multi-Layer Perceptron (Learning Rate: 0.2, 0.3, 0.4, 40 nodes)

Table VII.4.: Applied discretization, feature selection and classification methods.

Training/ Test Set	Discretization	Feature Selection	Classification Algorithm	TP	FN	FP	TN	Accuracy (%)	Suppr. Rate TA(%)	Suppr. Rate FA(%)
Complete Set	Equal Frequency (6 Bins)	Wrapper incl. Naive Bayes	SVM RBF Standardized	1246	107	218	553	84.7	7.9 (2.4)	71.7 (59.7)
Asystole	Supervised Discretization	Wrapper incl. Naive Bayes	Naive Bayes	42	1	1	129	98.8	2.3 (0.0)	99.2 (93.5)
Brady	Supervised Discretization	Wrapper incl. Decision Tree	kNN (1)	188	5	12	53	93.4	2.6 (0.0)	81.5 (81.0)
Tachy	Equal Width (6 Bins)	Wrapper incl. Naive Bayes	Binary Decision Tree (0.3)	789	13	33	136	95.3	1.6 (0.0)	80.5 (63.7)
V-Fib	Supervised Discretization	Correlation-based, forward	Unpruned Decision Tree	91	1	8	25	92.8	1.1 (0.0)	75.8 (58.2)
V-Tach	Supervised Discretization	Wrapper incl. Decision Tree	Binary Decision Tree (0.5)	232	50	78	237	78.6	17.7 (9.4)	75.2 (33.0)

Table VII.5.: Classification results (10-fold cross validation) for different training and test sets. The last two columns show the suppression rates of true and false alarms and the corresponding values of [29] in parenthesis.

180 combinations of discretization, feature selection and classification algorithms have been tested. A distinct combination performing equally well on all data sets was not determined. However, several combinations appeared more frequently among the best results. The top 5 combinations for each alarm type are shown in Appendix A. Supervised discretization and correlation-based feature selection appeared most frequently. At the classification level SVMs performed best, followed by kNNs.

Training and testing classifiers on few instances can yield misleading results. In particular, this may apply to the classification of asystole (173) and ventricular fibrillation alarms (125). In addition, the class values of the training sets were unequally distributed (cmp. Table VII.1). This was intensified by the limited size of the data set. E.g. asystole alarms naturally occur less frequently than bradycardia alarms. Using only a subset of the training data to include the same number of alarms in every set solves the distribution problem, but limits the overall data size.
Additionally, the available data was a mix of true and false alarms, but did not include missed alarm events or sections without a triggered alarm. In future works such sections should be included. Identifying missed alarm events might be troublesome considering the vast amount of monitoring data, but adding random sections without alarms can be helpful for increasing the robustness of the classifiers.
The available data has further implications: all alarm labels were obtained manually and, even though they were declared gold standard by Aboukhalil et al., labels can be debatable, as results of a study at the German Heart center show [13]: In an online survey alarm events were presented (see Figure VII-1) and participants had to judge, whether the pa-

tient needed their attention, or if the alarm was false. Among the presented data were 486 events, that had already been labeled by Aboukhalil et al. It turned out, that 31.3% of the events were labeled differently. This result was confirmed by comparing the ratings among the group of participants (see [13], inter-institutional level), where the average consistency rate was 78.8%. This study also showed, that manual labeling is error-prone. Several alarm events were presented twice during the study and on average only 73.9% of those identical pairs were labeled equally by the 23 reviewers.
Except for ventricular tachycardia alarms, the accuracies for a particular alarm type were above the one for the complete set. All evaluated algorithms achieved an accuracy rate of at least 71% except for V-Tach alarms (57%). Also the results given by Aboukhalil et al. suggest particular problems in correctly classifying V-Tach events. The focus of this case study, however, is not to find an optimal method for alarm classification, but to illustrate the applicability of data mining to the problem of false alarm rate reduction and how data fusion can help to reduce the FP rates. The high values in all the three evaluation criteria, sensitivity ($1 -$ Suppr. Rate TA), specificity (Suppr. Rate FA) and accuracy justify the approach of smart alarms to combine information from several data streams at once. A larger database with equally distributed alarm types is desirable to foster the results.
After all, one should be aware that patient safety is the primary goal in ICU monitoring and that an alarm classification system as presented suppresses true alarms. Tuning the classification algorithms in order to achieve a 0% TA suppression rate decreases the suppression rate of false alarms, but would be the method of choice for a product in clinical use that still mitigates the reported high rates of false alarms.

The correct identification of monitoring alarms, and especially false alarms is of major relevance for automated medical devices, such as an automated HLM. Many alarms are threshold alarms, usually triggered by single parameters being out of range. Exemplarily, a sensor could get disconnected. If the control is based on that sensor data, it could lead to unwanted control behavior and set the patient at risk. Therefore, the data fusion approach of assessing the patient condition based on multiple parameters should be included in the control design. DM approaches, as presented before, already include this feature intrinsically and especially the presented use-case is of value, since many of the alarm events in the study are due to sensor errors or movements.
Another evaluation criteria for the DM algorithms is their computational complexity and realtime applicability. Generally, the learning process is more time and ressource consuming and should be performed offline. Online learning algorithms are useful for patient-specific therapy and care, but also need an offline initialization. In the presented application of false alarm reduction, the number of features to calculate from an alarm scope was limited to 20, ensuring a time-invariant calculation. The limiting factor are features based on time series analysis using windowing techniques. Exemplarily, the analysis of waveform trends naturally needs a certain amount of samples to be present. In the above application 5 s after the alarm were considered as sufficient. All tested algorithms were able to classify an alarm scope without significant delay during the evaluation phase and are therefore applicable in an online analysis.
Despite the promising results, one should keep in mind that DM approaches to classify monitoring data depend on the training data. ICU databases are publicly available, however, they often use different data formats or don't include meta-information about patient characteristics or ongoing therapy. Manual labeling is error-prone, as it was shown above,

however, indispensable for DM algorithms. Databases for the particular case of an ECCS application outside the hospital including patient and machine data, to the best of our knowledge, don't exist.
For using DM approaches in a real clinical setting a defensive procedure is suggested. At no circumstances, a critical situation shall be missed. Therefore, all algorithms should be tuned, such that the sensitivity value is 100%. Acceptance in the medical community is another key factor. Decision trees, exemplarily can be illustrated in a comprehensible way and are therefore better suited than ANNs with their black-box approach. DM and KD can be integrated into the automation of a HLM, exemplarily by adding additional rules to a FUZZYC.

Chapter VIII

Conclusion

Contents

1 **Summary** 109
2 **Future Work** 110

1. Summary

Preclinical applications of medical devices, such as HLMs or defibrillators, on patients with severe cardiac insufficiencies, have proved to increase the survivor rate. Automated defibrillators can even be used by untrained helpers in need. On the other hand, the use of a HLM in emergency situations is still sporadic, since sufficient knowledge for cannulation and additional staff for operating the device is needed. An automated device would increase the patient safety, quality of care and, at the same time, reduce the workload of the staff.
To investigate the potentials of an automated device, different approaches were followed. In animal experiments, patient and machine parameters were collected, and a prototype controller was tested with good results. Based on the aquired data and an extensive literature research, both a hydraulic and a virtual model of a patient under ECC was developed. In this work the focus was on the hydraulic model and its control. The model followed the three-element Windkessel model, which was found to give the best trade-off between accuracy and complexity. It comprises a cylindrical air chamber as a compliance element and two adjustable resistor elements, that change the tube diameter. A centrifugal pump with a static outlet resistance represents the HLM. A complete mathematical description was derived and transfered to a linear state space representation. Four concurrent control strategies for automated pump speed control, based on the pump flow and pressure, were implemented and evaluated in three scenarios. In scenario 1 all controllers were able to follow step changes in the target values with slight advantages for the PIC. In scenario 2, with additional noise, the MRAC outperformed its competitors in terms of the IAE. In experiment 3, the peripheral resistance was altered. The PIC achieved the lowest IAE for flow control, while the FUZZYC was ranked first in pressure control.

In general, all controllers lead to stable control and were able to solve the given tasks. It was demonstrated, that pump speed control of a HLM is feasible with high accuracy. However, qualitative factors such as design complexity and user acceptance should also be considered in the evaluation. Compared to its competitors, both the FUZZYC and the PIC are rather easy to design and to maintain. While the PIC design process requires an analytical system description, the FUZZYC is independent of a mathematical system model. This facilitates maintenance, because a redesign of the controller would not be necessary, if system components change. Also the natural language rulebase differentiates the FUZZYC from the other approaches. As long as the size of the rulebase is limited, the control behavior is transparent, even for untrained users. Furthermore, expert knowledge (from surgeons etc.) can be implemented directly. This increases the user acceptance, so that the FUZZYC is particularly suited for medical control applications.
As a major limitation, the hydraulic mock model is not able to replicate oxygen delivery or hypothermia, so that the control of the machine's gas blender or temperature regulation was not studied in the physical setup. Those tasks were evaluated in the simulation model (see [27]). In both the animal experiments and the tests with the hydraulic model it was observed, that the HLM was not always able to reach an appropriate blood flow. This is due to the femoral cannulation, which requires rather small cannulas. The small cannula diameters create a large resistance for the pump. A major advantage of the presented control approach is, that it is sufficient to measure the produced pump flow and the pressure difference between the pump outlet and inlet. Those parameters are obtained at the HLM. Data collection at the patient is therefore not required for pump speed control, even more, the patient can be considered as a black-box.

However, the patient state should be considered in a fully automated HLM for emergency applications. This is why the second aspect of this work examined DM methods for the automatic assessment of the patient's physiological constitution. Inspired from CDSS and considering the special challenges of medical DM, the well-known problem of false alarm rate reduction in patient monitoring was tackled. For the first time, a benchmark study, comparing several DM approaches, was done in this research area. A data fusion approach was followed, integrating information from several physiological variables, in order to validate an alarm. SVMs and kNNs yielded good results as alarm classifiers. Compared to competitive studies, higher specificity values were achieved, especially when training expert classifiers for specific alarm types. Accurate pump speed control and robust patient monitoring are two main aspects in preclinical ECC applications. This work elaborated their potentials and limitations and thereby contributes to workload reduction, patient safety and quality of care in emergency situations.

2. Future Work

The perception of contextual information, such as sensor reliablity, human intervention (e.g. manual control, medication) or a general assessment of the patient state, could enrich the quality and safety of a controlled HLM. If the patient state deteriorates during control, a human operator could be warned, or the control strategy could be changed directly. This thesis successfully demonstrated the feasibility of a pump speed control for HLMs, as well

as the applicability of DM methods for the assessment of the current patient state. Future work should combine these contributions in order to create a robust and reliable control system. This idea was already published in a previous work [5] and a conceptual integration profile is illustrated in Figure VIII-1. The bottom layer (Data Acquisition Layer) deals

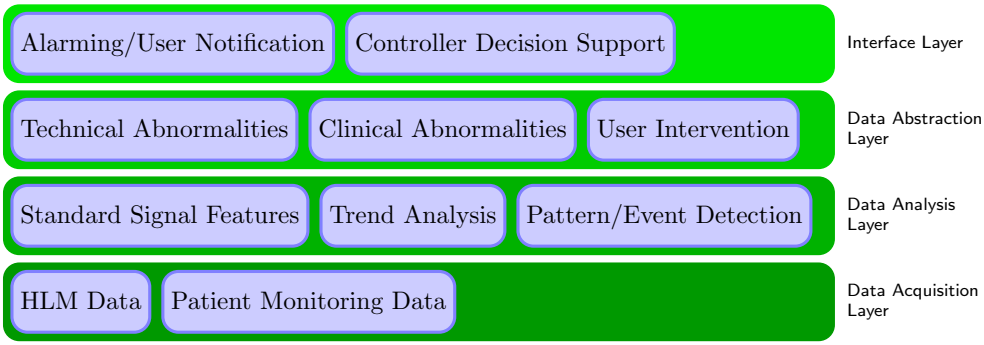

Figure VIII-1.: Conceptual layout of a SU, illustrating the required informational levels from sensoring to user interaction. From [5].

with the recording of crucial sensor data from both the HLM and the patient. This is already implemented in the co-developed AutoMedic Framework [2]. In the Data Analysis Layer, signal features are extracted and special events, such as kinking of the arterial line or sensor failure, should be detected. The third layer shifts the extracted features onto a semantic level.
Future work should research, how to integrate this contextual knowledge into the control strategy. For this, the implications of certain events need to be determined ("What happens if ...") and technical questions need to be resolved: Exemplarily, it is rather easy to extend a FUZZYC with additional rules, whereas a HINFC does not support semantic rules directly.
The knowledge acquired in this work is not restricted to HLM automation only. The developed tools and programs for data acquisition and control design can be used in other medical control applications as well. Projects dealing with CPR automation or automated medication [183] examine the interaction of the CVS and a medical device as well. The guidlines in control design and evaluation, presented in this work, can be adapted to those applications without much effort.

Concerning the presented approach for robust monitoring, classification results strongly depend on the given training and test sets. However, free, large-scale databases with labeled alarm situations are sparse. An online survey was designed, in which medical experts can label alarms [13]. Like this, more than 400 alarms were labeled during a relatively short period. The feedback of the participants was mainly positive, so it is suggested to extend this database in the future. Since the survey is web-based, it could include experts from all over the world. Still an unresolved issue is the imbalanced distribution of alarm types. Some alarms naturally appear more often than others. This implies, that classification results on different alarm types are hard to compare. Furthermore, it can be shown that human labeling of alarms is error-prone [13]. Therefore, each alarm situation should be labeled by 3 experts at least. With regards to the implemented DM approaches, fine-

tuning can be done, increasing the accuracy. Also the inclusion of monitoring data without particular events can increase the robustness of the classifiers.

Appendix A

Appendix

1. Classification of Complete Training Sets

Discretization	Feature Selection	Classification Algorithm	TP	FN	FP	TN	Accuracy (%)	Suppr. Rate TA(%)	Suppr. Rate FA(%)
Equal Frequency (6 Bins)	Wrapper incl. Naive Bayes	SVM RBF Standardized	1246	107	218	553	84.70	7.9	71.7
Supervised Discretization	Wrapper incl. Decision Tree	Decision Tree (0.2)	1230	123	213	558	84.18	9.1	72.4
Supervised Discretization	Wrapper incl. Decision Tree	Binary Decision Tree (0.3)	1218	135	211	560	83.71	10.0	72.6
Equal Frequency (6 Bins)	Wrapper incl. Naive Bayes	kNN (5), Dist. Weight	1222	131	220	551	83.48	9.7	71.5
Supervised Discretization	Correlation-based, backward	SVM RBF Standardized	1204	149	218	553	82.72	11.0	71.7

2. Classification of Asystole Alarms

Discretization	Feature Selection	Classification Algorithm	TP	FN	FP	TN	Accuracy (%)	Suppr. Rate TA(%)	Suppr. Rate FA(%)
Supervised Discretization	Wrapper incl. Naive Bayes	Naive Bayes	42	1	1	129	98.84	2.3	99.2
Equal Frequency (6 Bins)	Wrapper incl. Naive Bayes	Multi-Layer Perceptron (0.2)	38	5	0	130	97.11	11.6	100.0
Supervised Discretization	Correlation-based, forward	SVM Polynom. Standardized	39	4	3	127	95.95	9.3	97.7
Supervised Discretization	Correlation-based, backward	kNN (1)	37	6	2	128	95.38	14.0	98.5
Supervised Discretization	Wrapper incl. Naive Bayes	SVM Polynom. Standardized	36	7	2	128	94.80	16.3	98.5

3. Classification of Brady Alarms

Discretization	Feature Selection	Classification Algorithm	TP	FN	FP	TN	Accuracy (%)	Suppr. Rate TA(%)	Suppr. Rate FA(%)
Supervised Discretization	Wrapper incl. Decision Tree	kNN (1)	188	5	12	53	93.41	2.6	81.5
Supervised Discretization	Wrapper incl. Decision Tree	kNN (9), Dist. Weight.	188	5	12	53	93.41	2.6	81.5
Supervised Discretization	Wrapper incl. Decision Tree	Decision Tree (0.2)	188	5	12	53	93.41	2.6	81.5
Supervised Discretization	Wrapper incl. Decision Tree	Multi-Layer Perceptron (0.2)	188	5	12	53	93.41	2.6	81.5
Supervised Discretization	Wrapper incl. Decision Tree	SVM Polynom. Standardized	186	7	12	53	92.64	3.6	81.5

4. Classification of Tachy Alarms

Discretization	Feature Selection	Classification Algorithm	TP	FN	FP	TN	Accuracy (%)	Suppr. Rate TA(%)	Suppr. Rate FA(%)
Equal Width (6 Bins)	Wrapper incl. Naive Bayes	Binary Decision Tree (0.3)	789	13	33	136	95.26	1.6	80.5
Equal Frequency (6 Bins)	Wrapper incl. Naive Bayes	kNN (1)	788	14	33	136	95.16	1.7	80.5
Equal Frequency (6 Bins)	Wrapper incl. Naive Bayes	SVM Polynom.	783	19	35	134	94.44	2.4	79.3
Supervised Discretization	Correlation-based, backward	Multi-Layer Perceptron (0.2)	781	21	34	135	94.34	2.6	79.9
Equal Width (6 Bins)	Wrapper incl. Naive Bayes	Naive Bayes	782	20	38	131	94.03	2.5	77.5

5. Classification of V-Fib/Tach Alarms

Discretization	Feature Selection	Classification Algorithm	TP	FN	FP	TN	Accuracy (%)	Suppr. Rate TA(%)	Suppr. Rate FA(%)
Supervised Discretization	Correlation-based, forward	Unpruned Decision Tree	91	1	8	25	92.80	1.1	75.8
Supervised Discretization	Correlation-based, backward	kNN (5), Dist. Weight	90	2	7	26	92.80	2.2	78.8
Supervised Discretization	Correlation-based, forward	SVM RBF Standardized	91	1	9	24	92.00	1.1	72.7
Supervised Discretization	Correlation-based, backward	SVM Polynom. Normalized	87	5	5	28	92.00	5.4	84.8
Supervised Discretization	Correlation-based, forward	Naive Bayes	87	5	6	27	91.20	5.4	81.8

6. Classification of V-Tach Alarms

Discretization	Feature Selection	Classification Algorithm	TP	FN	FP	TN	Accuracy (%)	Suppr. Rate TA(%)	Suppr. Rate FA(%)
Supervised Discretization	Wrapper incl. Decision Tree	Binary Decision Tree (0.5)	232	50	78	237	78.56	17.7	75.2
Equal Frequency (6 Bins)	Wrapper incl. Decision Tree	Decision Tree (0.3)	209	73	58	257	78.06	25.9	81.6
Equal Frequency (10 Bins)	Wrapper incl. Naive Bayes	kNN (9) Dist. Weight	213	69	66	249	77.39	24.5	79.0
Equal Frequency (10 Bins)	Wrapper incl. Naive Bayes	Naive Bayes	227	55	83	232	76.88	19.5	73.7
Equal Frequency (10 Bins)	Wrapper incl. Naive Bayes	SVM RBF	213	69	71	244	76.55	24.5	77.5

Publications

[1] B. Baumgartner, A. Mendoza, U. Schreiber, S. Eichhorn, M. Krane, R. Bauernschmitt, and A. Knoll, "A simple fuzzy controller for an extra-corporeal circulation system - limitations and potentials," in *5th Russian-Bavarian Conference on Bio-Medical Engineering*, 2009.

[2] A. Mendoza García, B. Baumgartner, U. Schreiber, M. Krane, A. Knoll, and R. Bauernschmitt, "Automedic: Fuzzy control development platform for a mobile heart-lung machine," in *World Congress on Medical Physics and Biomedical Engineering*, ser. IFMBE Proceedings, vol. 25, 2009.

[3] U. Schreiber, S. Eichhorn, A. Mendoza, B. Baumgartner, R. Bauernschmitt, R. Lange, A. Knoll, and M. Krane, "A new fuzzy controlled extracorporeal circulation system. first results of an in-vitro investigation," in *Computers in Cardiology*, vol. 36, 2009.

[4] B. Baumgartner, A. Mendoza, U. Schreiber, S. Eichhorn, M. Krane, R. Bauernschmitt, and A. Knoll, "A comprehensive approach towards extra-corporal circulation control using fuzzy logic," in *IEEE International Conference on Fuzzy Systems*, 2010, pp. 1–5.

[5] ——, "A 4-layer supervising unit for extra-corporal circulation," in *Proceedings of the 4th International Conference on Bioinformatics and Biomedical Engineering*, June 2010.

[6] A. Mendoza García, B. Baumgartner, U. Schreiber, S. Eichhorn, M. Krane, R. Bauernschmitt, and A. Knoll, "Design of a fuzzy controller for the automation of an extracorporeal support system with the use of a simulation environment," in *International Conference of the IEEE Engineering in Medicine and Biology Society*, 2010.

[7] A. Mendoza García, B. Baumgartner, U. Schreiber, M. Krane, R. Bauernschmitt, and A. Knoll, "Simulation of extracorporeal circulation for the design of a fuzzy controlled perfusion," *IASTED Biomedical Engineering*, vol. 1&2, 2010.

[8] A. Mendoza García, S. Rösch, B. Baumgartner, U. Schreiber, M. Krane, A. Knoll, and R. Bauernschmitt, "Mathematical model of a portable extracorporeal life support system," *ASAIO Abstracts for the 56th Annual Conference*, vol. 56, pp. 81–118, 2010.

[9] B. Baumgartner, A. Mendoza, S. Eichhorn, U. Schreiber, and A. Knoll, "A comparative study on extra-corporal circulation control," in *International Conference of the IEEE Engineering in Medicine and Biology Society*, 2011, pp. 4287–4290.

[10] A. Mendoza García, M. Rodriguez, B. Baumgartner, U. Schreiber, and A. Knoll, "Embedded platform for automation of medical devices," in *Computing in Cardiology*, vol. 38, 2011, pp. 829–832.

[11] A. Mendoza García, N. Sprunk, B. Baumgartner, U. Schreiber, S. Eichhorn, R. Bauernschmitt, R. Lange, M. Krane, and A. Knoll, "Automation of an extracorporeal support system with adaptive fuzzy controllers," in *International Conference of the IEEE Engineering in Medicine and Biology Society*, 2011, pp. 1033–1036.

[12] B. Baumgartner, K. Rödel, and A. Knoll, "A data mining approach to reduce the false alarm rate of patient monitors," in *International Conference of the IEEE Engineering in Medicine and Biology Society*, 2012.

[13] B. Baumgartner, K. Rödel, U. Schreiber, and A. Knoll, "A web-based survey for expert review of monitor alarms," in *Computing in Cardiology*, vol. 39, 2012, pp. 209–212.

[14] A. Mendoza García, N. Sprunk, B. Baumgartner, A. Knoll, U. Schreiber, S. Eichhorn, M. Krane, and R. Lange, "Application of adaptive fuzzy controllers for the automation of medical devices," in *IEEE International Conference on Fuzzy Systems*, 2012.

[15] A. Mendoza García, M. Krane, B. Baumgartner, N. Sprunk, U. Schreiber, S. Eichhorn, R. Lange, and A. Knoll, "Automation of a portable extracorporeal circulatory support system with adaptive fuzzy controllers," *Medical Engineering & Physics*, 2013, to appear.

Bibliography

[16] C. Eberhard-Metzger, *Herz in Gefahr? Ursachen, Prävention, Therapie - Ergebnisse der Herzkreislaufforschung*. Bundesministerium für Bildung und Forschung, 2004.

[17] *Gesundheit - Todesursachen in Deutschland*. Statistisches Bundesamt Wiesbaden, 2012.

[18] M. Cheatham, E. Block, J. Promes, H. Smith, D. Dent, and D. Mueller, *Irwin and Rippe's Intensive Care Medicine*. Wolters Kluwer Health/Lippincott Williams & Wilkins, 2008, ch. 161. Shock: An overview, pp. 1831–1842.

[19] M. Krane, D. Mazzitelli, U. Schreiber, A. Mendoza Garzia, B. Voss, C. Badiu, R. Lange, and R. Bauernschmitt, "First experience with a new portable cardiopulmonary bypass system - lifebridge b2t with percutaneous femoral cannulation," in *Computers in Cardiology*, 2008, pp. 269–272.

[20] P. Feindt, C. Benk, U. Boeken, A. Bauer, U. Mehlhorn, J. Gehron, A. Markewitz, A. Beckmann, and F. Beyersdorf, "Use of extracorporeal circulation (ECC) outside the cardiac operating room: Indications, requirements and recommendations for routine practice," *Thorac Cardiovasc Surg*, vol. 59, no. 02, pp. 66–68, 2011.

[21] F. Boschetti, S. Mantero, F. Miglietta, M. L. Costantino, F. Montevecchi, and R. Fumero, "An approach to computer automation of the extracorporeal circulation," *Computers in Biology and Medicine*, vol. 32, no. 2, pp. 73–83, Mar. 2002.

[22] A. Schwarzhaupt, D. Torkzadeh, and U. Kiencke, "Signal analysis of the haemodynamics of extracorporeal circulation for the evaluation of patient status," *Biomedical Engineering*, vol. 44, pp. 120–128, 1999.

[23] "Lifebridge B2T," LIFEBRIDGE Medizintechnik AG. [Online]. Available: www.lifebridge.de

[24] G. Meyrowitz, "Automatisierung der Herz-Lungen-Maschine," Ph.D. dissertation, Universität Karlsruhe, 2005.

[25] B. Misgeld, "Automatic Control of the Heart-Lung Machine," Ph.D. dissertation, Ruhr-Universität Bochum, 2007.

[26] N. Westerhof, G. Elzinga, and P. Sipkema, "An artificial arterial system for pumping hearts," *Journal of Applied Physiology*, vol. 31, no. 5, pp. 776–781, Nov. 1971.

[27] A. Mendoza García, "Automation of an extracorporeal support system with the use of adaptive fuzzy controllers," Ph.D. dissertation, Technische Universität München, 2013, to appear.

[28] M. Saeed, M. Villarroel, A. Reisner, G. Clifford, L.-W. Lehman, G. Moody, T. Heldt, T. Kyaw, B. Moody, and R. Mark, "Multiparameter intelligent monitoring in intensive care ii: a public-access intensive care unit database." *Critical care medicine*, vol. 39, no. 5, pp. 952–960, May 2011.

[29] A. Aboukhalil, L. Nielsen, M. Saeed, R. G. Mark, and G. D. Clifford, "Reducing false alarm rates for critical arrhythmias using the arterial blood pressure waveform," *Journal of Biomedical Informatics*, vol. 41, no. 3, pp. 442–451, June 2008.

[30] A. Avolio, "Multi-branched model of the human arterial system," vol. 18, no. 6, pp. 709–718, 1980.

[31] A. Davies, A. Blakeley, C. Kidd, and J. McGeown, *Human Physiology*. Churchill Livingstone, 2001.

[32] R. Brandes and R. Busse, *Physiologie des Menschen*. Springer Berlin Heidelberg, 2011, ch. Kreislauf, pp. 572–626.

[33] L. Sherwood, *Human Physiology: From Cells to Systems*. Brooks/Cole, Cengage Learning, 2012.

[34] V. C. Rideout and D. E. Dick, "Difference-differential equations for fluid flow in distensible tubes," *Biomedical Engineering, IEEE Transactions on*, vol. 14, no. 3, pp. 171–177, 1967.

[35] W. Böttcher and H. Woysch, "Die erste erfolgreiche herzchirurgische Operation mit Hilfe der Herz-Lungen-Maschine," *Zeitschrift für Herz-, Thorax- und Gefäßchirurgie*, vol. 20, pp. 248–260, 2006.

[36] D. G. Melrose, "Cardiovascular disease - extracorporeal circulation," *Annual Review of Medicine*, vol. 12, pp. 67–76, 1961.

[37] J. Gibbon, "Application of a mechanical heart and lung apparatus to cardiac surgery," *Minnesota Med*, vol. 36, pp. 171–180, 1954.

[38] J. Werner, *Kooperative und autonome Systeme der Medizintechnik*. Oldenburg Wissenschaftsverlag, 2005.

[39] U. Böckler and A. Hahn, *Medizintechnik*. Springer Berlin Heidelberg, 2011, pp. 515–532.

[40] U. Mehlhorn, M. Brieske, U. M. Fischer, M. Ferrari, P. Brass, J. H. Fischer, and H.-R. Zerkowski, "Lifebridge: A portable, modular, rapidly available plug-and-play mechanical circulatory support system," *The Annals of Thoracic Surgery*, vol. 80, no. 5, pp. 1887–1892, Nov. 2005.

[41] "Sorin S5," Sorin Group Deutschland GmbH. [Online]. Available: www.sorin.com

[42] G. P. Gravlee, R. F. Davis, A. H. Stammers, and R. M. Ungerleider, Eds., *Cardiopulmonary Bypass: Principles and Practice*. Lippincott Williams & Wilkings, 2008.

[43] C. Schmid and A. Philipp, *Leitfaden extrakorporale Zirkulation*, C. Schmid and A. Philipp, Eds. Springer Berlin Heidelberg, 2011.

[44] H. Jakob, G. Hafner, C. Thelemann, A. Sturer, W. Prellwitz, and H. Oelert, "Routine extracorporeal circulation with a centrifugal or roller pump," *ASAIO Journal*, vol. 37, pp. 487–9, 1991.

[45] G. Lauterbach, *Handbuch der Kardiotechnik*. Urban & Fischer, 2002.

[46] L. K. von Segesser, M. Kalejs, E. Ferrari, S. Bommeli, O. Maunz, J. Horisberger, and P. Tozzi, "Superior flow for bridge to life with self-expanding venous cannulas," *European Journal of Cardio-Thoracic Surgery*, vol. 36, no. 4, pp. 665–669, Oct. 2009.

[47] G. S. Murphy, I. Hessel, Eugene A., and R. C. Groom, "Optimal perfusion during cardiopulmonary bypass: An evidence-based approach," *Anesth Analg*, vol. 108, no. 5, pp. 1394–1417, May 2009.

[48] E. Naujokat, *Ein Beobachtersystem für den Patientenzustand in der Herzchirurgie*. Shaker, 2003.

[49] B. Ji and A. Undar, "An evaluation of the benefits of pulsatile versus nonpulsatile perfusion during cardiopulmonary bypass procedures in pediatric and adult cardiac patients," *ASAIO Journal*, vol. 52, pp. 357–61, 2006.

[50] P. R. Hickey, M. J. Buckley, and D. M. Philbin, "Pulsatile and nonpulsatile cardiopulmonary bypass: Review of a counterproductive controversy," *Ann Thorac Surg*, vol. 36, no. 6, pp. 720–737, Dec. 1983.

[51] A. Ündar, "Myths and truths of pulsatile and nonpulsatile perfusion during acute and chronic cardiac support," *Artificial Organs*, vol. 28, no. 5, pp. 439–443, 2004.

[52] M. Krane, B. Voss, S. Braun, H. Schad, W. Heimisch, R. Lange, and R. Bauernschmitt, "A computer-controlled pulsatile pump system for cardiopulmonary bypass and its effects on regional blood flow, haemolysis and inflammatory response," in *Computers in Cardiology*, 2006, pp. 309–312.

[53] M. Newman, D. Kramer, N. Croughwell, I. Sanderson, J. Blumenthal, W. White, L. Smith, E. Towner, and J. Reves, "Differential age effects of mean arterial pressure and rewarming on cognitive dysfunction after cardiac surgery," *Anesth Analg*, vol. 81, pp. 236–42, 1995.

[54] R. M. Schell, F. H. Kern, W. J. Greeley, S. R. Schulman, P. E. Frasco, N. D. Croughwell, M. Newman, and J. G. Reves, "Cerebral blood flow and metabolism during cardiopulmonary bypass," *Anesthesia & Analgesia*, vol. 76, no. 4, pp. 849–865, 1993.

[55] N. Croughwell, M. Lyth, T. Quill, M. Newman, W. Greeley, L. Smith, and J. Reves, "Diabetic patients have abnormal cerebral autoregulation during cardiopulmonary bypass." *Circulation*, vol. 82, no. 5 Suppl, pp. IV407–12, Nov. 1990.

[56] G. S. Hartman, F. S. Yao, M. Bruefach, D. Barbut, J. C. Peterson, M. H. Purcell, M. E. Charlson, J. P. Gold, S. J. Thomas, and T. P. Szatrowski, "Severity of aortic atheromatous disease diagnosed by transesophageal echocardiography predicts stroke and other outcomes associated with coronary artery surgery: a prospective study," *Anesthesia & Analgesia*, vol. 83, no. 4, pp. 701–708, Oct. 1996.

[57] C. E. Eastridge and F. A. Hughes, "Central venous pressure monitoring: A useful aid in the management of shock," *The American Journal of Surgery*, vol. 114, no. 5, pp. 648–652, Nov. 1967.

[58] P. Feindt, F. Harig, and M. Weyand, Eds., *Empfehlungen zum Einsatz und zur Verwendung der Herz-Lungen-Maschine*. Steinkopff Verlag Darmstadt, 2006.

[59] D. J. Cook, J. A. Proper, T. A. Orszulak, R. C. Daly, and W. C. Oliver Jr, "Effect of pump flow rate on cerebral blood flow during hypothermic cardiopulmonary bypass in adults," *Journal of Cardiothoracic and Vascular Anesthesia*, vol. 11, no. 4, pp. 415–419, June 1997.

[60] W. Kolff, "Mock circulation to test pumps designed for permanent replacement of damaged hearts." *Cleve Clin Q*, vol. 26, pp. 223–226–, Oct. 1959.

[61] G. Mrava, "Mock circulation systems for artificial hearts," *Adv. Biomed. Eng. Med. Phys.*, vol. 3, pp. 115–130, 1970.

[62] W. Leliveld, *The Design of a Mock Circulation System*. Eindhoven University of Technology, 1974.

[63] H. Reul, H. Minamitani, and J. Runge, "A hydraulic analog of the systemic and pulmonary circulation for testing artificial hearts," *Proc. Eur. Soc. Artif. Organs*, vol. 2, pp. 120–126, 1975.

[64] K. M. High, J. A. Brighton, A. D. Brickman, and W. S. Pierce, "Analysis of an artificial ventricle and mock circulatory system," *J. Biomech. Eng.*, vol. 99, no. 4, pp. 184–188, Nov. 1977.

[65] J. Cornhill, "An aortic–left ventricular pulse duplicator used in testing prosthetic aortic heart valves," *The Journal of Thoracic and Cardiovascular Surgery*, vol. 73, no. 4, pp. 550–558, 1977.

[66] L. N. Scotten, D. K. Walker, and R. T. Brownlee, "Construction and evaluation of a hydromechanical simulation facility for the assessment of mitral valve prostheses," *Journal of Medical Engineering and Technology*, vol. 3, no. 1, pp. 11–18, Jan. 1979.

[67] A. C. Guyton, T. G. Coleman, and H. J. Granger, "Circulation: Overall regulation," *Annual Review of Physiology*, vol. 34, no. 1, pp. 13–44, Mar. 1972.

[68] C.-N. Nguyen, O. Simanski, R. Köhler, A. Schubert, M. Janda, J. Bajorat, and B. Lampe, "The benefits of using guyton's model in a hypotensive control system," *Computer Methods and Programs in Biomedicine*, vol. 89, no. 2, pp. 153–161, 2008.

[69] N. Westerhof, "Analog studies of human systemic arterial hemodynamics," Ph.D. dissertation, University of Pennsylvania, 1968.

[70] N. Stergiopulos, J.-J. Meister, and N. Westerhof, "Evaluation of methods for estimation of total arterial compliance." *American Journal of Physiology*, vol. 268, pp. H1540–8, 1995.

[71] G. P. Toorop, N. Westerhof, and G. Elzinga, "Beat-to-beat estimation of peripheral resistance and arterial compliance during pressure transients," *American Journal of Physiology - Heart and Circulatory Physiology*, vol. 252, no. 6, pp. H1275–H1283, June 1987.

[72] F. M. Donovan, "Design of a hydraulic analog of the circulatory system for evaluating artificial hearts," *Biomaterials, Medical Devices and Artificial Organs*, vol. 3, no. 0090-5488 (Linking), pp. 439–449, 1975.

[73] G. Rosenberg, M. P. Winfred, D. L. Landis, and W. S. Pierce, "Design and evaluation of the pennsylvania state university mock circulatory system," *ASAIO Journal*, vol. 4, pp. 41–49, 1981.

[74] S. Deutsch, J. M. Tarbell, K. B. Manning, G. Rosenberg, and A. A. Fontaine, "Experimental fluid mechanics of pulsatile artificial blood pumps," *Annual Review of Fluid Mechanics*, vol. 38, no. 1, pp. 65–86, Dec. 2006.

[75] M. Arabia and T. Akutsu, "A new test circulatory system for research in cardiovascular engineering," *Annals of Biomedical Engineering*, vol. 12, no. 1, pp. 29–48, 1984.

[76] P. Vermette, J. Thibault, and G. Laroche, "A continuous and pulsatile flow circulation system for evaluation of cardiovascular devices," *Artificial Organs*, vol. 22, no. 9, pp. 746–752, 1998.

[77] N. Stergiopulos, B. E. Westerhof, and N. Westerhof, "Total arterial inertance as the fourth element of the windkessel model," *American Journal of Physiology - Heart and Circulatory Physiology*, vol. 276, no. 1, pp. 81–88, Jan. 1999.

[78] R. Burattini and G. Gnudi, "Computer identification of models for the arterial tree input impedance: Comparison between two new simple models and first experimental results," *Medical and Biological Engineering and Computing*, vol. 20, no. 2, pp. 134–144, 1982.

[79] T. Kind, T. Faes, J.-W. Lankhaar, A. Vonk-Noordegraaf, and M. Verhaegen, "Estimation of three- and four-element windkessel parameters using subspace model identification," *IEEE Transactions on Biomedical Engineering*, vol. 57, no. 7, pp. 1531–1538, 2010.

[80] B. Lambermont, P. Gérard, O. Detry, P. Kolh, P. Potty, J. Defraigne, V. D'Orio, and R. Marcelle, "Comparison between three- and four-element windkessel models to characterize vascular properties of pulmonary circulation," *Archives of Physiology and Biochemistry*, vol. 105, no. 7, pp. 625–632, Jan. 1997.

[81] M. Sharp and R. Dharmalingam, "Development of a hydraulic model of the human systemic circulation," *ASAIO*, vol. 45, no. 6, pp. 535–540, 1999.

[82] W. W. Nichols, C. R. Conti, W. E. Walker, and W. R. Milnor, "Input impedance of the systemic circulation in man." *Circulation Research*, vol. 40, no. 5, pp. 451–8, 1977.

[83] M. Sharp, G. Thurston, and J. Moore Jr., "The effect of blood viscoelasticity on pulsatile flow in stationary and axially moving tubes," *Biorheology*, vol. 33, no. 3, pp. 185–208, May 1996.

[84] Y. Liu, P. Allaire, H. Wood, and D. Olsen, "Design and initial testing of a mock human circulatory loop for left ventricular assist device performance testing," *Artificial Organs*, vol. 29, no. 4, pp. 341–345, 2005.

[85] P. R. Verdonck, K. Dumont, P. Segers, S. Vandenberghe, and G. Van Nooten, "Mock loop testing of on-x prosthetic mitral valve with doppler echocardiography," *Artificial Organs*, vol. 26, no. 10, pp. 872–878, 2002.

[86] S. Vandenberghe, J. Van Loon, P. Segers, G. Rakhorst, and P. Verdonck, "In vitro evaluation of the puca ii intra-arterial lvad," *International Journal of Artificial Organs*, vol. 26, no. 8, pp. 743–52, 2003.

[87] G. M. Pantalos, S. C. Koenig, K. J. Gillars, G. A. Giridharan, and D. L. Ewert, "Characterization of an adult mock circulation for testing cardiac support devices," *ASAIO Journal*, vol. 50, no. 1, pp. 37–46, 2004.

[88] S. C. Koenig, G. M. Pantalos, K. J. Gillars, D. L. Ewert, K. N. Litwak, and S. W. Etoch, "Hemodynamic and pressure-volume responses to continuous and pulsatile ventricular assist in an adult mock circulation," *ASAIO Journal*, vol. 50, no. 1, pp. 15–24, 2004.

[89] J. Glower, R. Cheng, G. Giridharan, K. Gillars, G. Pantalos, K. Litwak, D. Ewert, and S. Koenig, "In vitro evaluation of control strategies for an artificial vasculature device," in *26th Annual International Conference of the IEEE Engineering in Medicine and Biology Society*, vol. 2, 2004, pp. 3773–3776.

[90] K. N. Litwak, S. C. Koenig, R. C. Cheng, G. A. Giridharan, K. J. Gillars, and G. M. Pantalos, "Ascending aorta outflow graft location and pulsatile ventricular assist provide optimal hemodynamic support in an adult mock circulation," *Artificial Organs*, vol. 29, no. 8, pp. 629–635, 2005.

[91] G. Ferrari, C. De Lazzari, M. Kozarski, F. Clemente, K. Górczynska, R. Mimmo, E. Monnanni, G. Tosti, and M. Guaragno, "A hybrid mock circulatory system: Testing a prototype under physiologic and pathological conditions," *ASAIO Journal*, vol. 48, no. 5, pp. 487–494, 2002.

[92] G. Ferrari, C. De Lazzari, R. Mimmo, G. Tosti, D. Ambrosi, and K. Gorczynska, "A computer controlled mock circulatory system for mono- and biventricular assist device testing," *International Journal of Artificial Organs*, vol. 21, no. 0391-3988, pp. 26–36, 1998.

[93] M. Kozarski, G. Ferrari, F. Clemente, K. Górczynska, C. De Lazzari, M. Darowski, R. Mimmo, G. Tosti, and M. Guaragno, "A hybrid mock circulatory system: development and testing of an electro-hydraulic impedance simulator," *International Journal of Artificial Organs*, vol. 26, no. 1, pp. 53–63, Jan. 2003.

[94] D. Timms, M. Hayne, K. McNeil, and A. Galbraith, "A complete mock circulation loop for the evaluation of left, right, and biventricular assist devices," *Artificial Organs*, vol. 29, no. 7, pp. 564–572, 2005.

[95] S. D. Gregory, "Simulation and development of a mock circulation loop with variable compliance," Master's thesis, Queensland University of Technology, 2009.

[96] D. L. Timms, S. D. Gregory, N. A. Greatrex, M. J. Pearcy, J. F. Fraser, and U. Steinseifer, "A compact mock circulation loop for the in vitro testing of cardiovascular devices," *Artificial Organs*, vol. 35, no. 4, pp. 384–391, 2011.

[97] S. D. Gregory, N. Greatrex, D. Timms, N. Gaddum, M. J. Pearcy, and J. F. Fraser, "Simulation and enhancement of a cardiovascular device test rig," *Journal of Simulation*, vol. 4, no. 1, pp. 34–41, Mar. 2010.

[98] D. Timms, M. Hayne, A. Tan, and M. Pearcy, "Evaluation of left ventricular assist device performance and hydraulic force in a complete mock circulation loop," *Artificial Organs*, vol. 29, no. 7, pp. 573–580, 2005.

[99] D. Timms, S. Gregory, M. Stevens, and J. Fraser, "Haemodynamic modeling of the cardiovascular system using mock circulation loops to test cardiovascular devices," in *Annual International Conference of the IEEE Engineering in Medicine and Biology Society*, 2011, pp. 4301–4304.

[100] M. Conlon, D. Russell, and T. Mussivand, "Development of a mathematical model of the human circulatory system," *Annals of Biomedical Engineering*, vol. 34, no. 9, pp. 1400–1413, Sept. 2006.

[101] A. Riesenberg, "Modellierung und Regelung des Herz-Kreislauf-Systems für Kreislaufunterstützungssysteme," Ph.D. dissertation, Universität Karlsruhe (TH), Karlsruhe, 1996.

[102] R. Bauernschmitt, E. Naujokat, H. Mehmanesh, S. Schulz, C. Vahl, S. Hagl, and R. Lange, "Mathematical modelling of extracorporeal circulation: simulation of different perfusion regimens," *Perfusion*, vol. 14, no. 5, pp. 321–330, 1999.

[103] X. Ding and P. Frank, "Modelling, control and monitoring of circulatory systems with an artificial heart," *International Journal of Quality and Reliability Management*, vol. 11, no. 2, pp. 41–50, 1994.

[104] M. Vollkron, H. Schima, L. Huber, and G. Wieselthaler, "Interaction of the cardiovascular system with an implanted rotary assist device: Simulation study with a refined computer model," *Artificial Organs*, vol. 26, no. 4, pp. 349–359, 2002.

[105] Y. Wu, P. Allaire, G. Tao, H. Wood, D. Olsen, and C. Tribble, "An advanced physiological controller design for a left ventricular assist device to prevent left ventricular collapse," *Artificial Organs*, vol. 27, no. 10, pp. 926–930, 2003.

[106] T. Korakianitis and Y. Shi, "A concentrated parameter model for the human cardiovascular system including heart valve dynamics and atrioventricular interaction," *Medical Engineering and Physics*, vol. 28, no. 7, pp. 613–628, Sept. 2006.

[107] H. Suga, K. Sagawa, and A. A. Shoukas, "Load independence of the instantaneous pressure-volume ratio of the canine left ventricle and effects of epinephrine and heart rate on the ratio," *Circulation Research*, vol. 32, no. 3, pp. 314–322, 1973.

[108] Y. Shi, T. Korakianitis, and C. Bowles, "Numerical simulation of cardiovascular dynamics with different types of vad assistance," *Journal of Biomechanics*, vol. 40, no. 13, pp. 2919–2933, 2007.

[109] M. Hassan, M. El-Brawany, and M. Sharaf, "A functional cardiovascular model with disorders," in *27th Annual International Conference of the Engineering in Medicine and Biology Society*, 2005, pp. 5089–5092.

[110] W. Shi and M.-S. Chew, "Mathematical and physical models of a total artificial heart," in *IEEE International Conference on Control and Automation*, 2009, pp. 637–642.

[111] L. Sheffer, W. Santamore, and O. Barnea, "Cardiovascular simulation toolbox," *Cardiovascular Engineering*, vol. 7, no. 2, pp. 81–88, 2007.

[112] K. Hassani, M. Navidbakhsh, and M. Rostami, "Simulation of the cardiovascular system using equivalent electronic system," *Biomedical Papers (Olomouc)*, vol. 150, no. 1, pp. 105–112, July 2006.

[113] ——, "Modeling of the aorta artery aneurysms and renal artery stenosis using cardiovascular electronic system," *BioMedical Engineering OnLine*, vol. 6, no. 1, p. 22, 2007.

[114] A. Schwarzhaupt, S. Schulz, R. Bauernschmitt, and U. Kiencke, "Simulation of human circulation at cardiopulmonary bypass." *Biomedical Sciences Instrumentation*, vol. 34, pp. 275–280, 1997.

[115] R. Bauernschmitt, S. Schulz, H. Mehmanesh, C. Vahl, and R. Lange, "Simulation of baroreflex control in a pulsatile mathematical model of the human arterial circulation," in *Computers in Cardiology*, 1999, pp. 229–232.

[116] G. Pennati, G. B. Fiore, K. Laganà, and R. Fumero, "Mathematical modeling of fluid dynamics in pulsatile cardiopulmonary bypass," *Artificial Organs*, vol. 28, no. 2, pp. 196–209, 2004.

[117] V. Prilutskii, S. Tropskii, V. Khrenov, and Y. Slavyak, "Analysis of control systems for extracorporeal-circulation equipment," *Biomedical Engineering*, vol. 12, no. 4, pp. 196–199, July 1978.

[118] T. Beppu, Y. Imai, and Y. Fukui, "A computerized control system for cardiopulmonary bypass," *The Journal of Thoracic and Cardiovascular Surgery*, vol. 109, no. 3, pp. 428–438, Mar. 1995.

[119] Y. Fukui, K. Tsuchiya, and Y. Imai, "Computer controlled extracorporeal circulation (ECC) with pulsatile perfusion for an infant," *ASAIO Journal*, vol. 28, pp. 133–137, 1982.

[120] N. Momose, R. Yamakoshi, R. Kokubo, T. Yasuda, N. Iwamoto, C. Umeda, I. Nakajima, M. Yanagisawa, and Y. Tomizawa, "Development of a new control device for stabilizing blood level in reservoir during extracorporeal circulation," *Perfusion*, vol. 25, no. 2, pp. 77–82, Mar. 2010.

[121] B. Misgeld, J. Werner, and M. Hexamer, "Robust and self-tuning blood flow control during extracorporeal circulation in the presence of system parameter uncertainties," *Medical and Biological Engineering and Computing*, vol. 43, no. 5, pp. 589–598, Oct. 2005.

[122] A. Schwarzhaupt, *Regelung der extrakorporalen Zirkulation auf der Basis eines Modells des menschlichen Kreislaufes*. Göttingen: Cuvillier, 1999.

[123] M. Nagel, "Aufbau eines Versuchsstandes zur Simulation des menschlichen Kreislaufs unter den Bedingungen der extrakorporalen Membranoxygenation (ECMO)," Master's thesis, Dortmund University, 2004.

[124] B. Misgeld, J. Werner, and M. Hexamer, "Automatisierung der extrakorporalen Zirkulation: Ein Vergleich verschiedener Regelansätze," in *Automatisierungstechnische Methoden und Systeme für die Medizin*, O. Simanski, Ed., 2006, pp. 55–56.

[125] L.-X. Wang, "Universal approximation by hierarchical fuzzy systems," *Fuzzy Sets and Systems*, vol. 93, no. 2, pp. 223–230, Jan. 1998.

[126] R. Isermann, *Mechatronic Systems Fundamentals*. Springer, 2005.

[127] J. Lunze, *Regelungstechnik 1&2*. Springer, 2007.

[128] J. Ackermann, *Robust Control: The Parameter Space Approach*. Springer, 2002.

[129] H. Geering and C. Roduner, "Entwurf Robuster Regler mit der H_∞-Methode," *Bulletin SEV/VSE*, vol. 3, pp. 55–58, 1999.

[130] F. Wienand, "Robuste regelung nichtlinearer prozesse nach der my-analyse und -synthese," Ph.D. dissertation, RWTH Aachen, 1997.

[131] B. Moore, "Principal component analysis in linear systems: Controllability, observability, and model reduction," *Automatic Control, IEEE Transactions on*, vol. 26, no. 1, pp. 17 – 32, Feb. 1981.

[132] P. Al Hokayem, *Adaptive Control*. Lecture Notes Nonlinear Systems and Control, Automatic Control Laboratory, ETH Zurich, 2011.

[133] P. Ioannou, *Robust Adaptive Control*. Prentice Hall, 1995.

[134] L. A. Zadeh, "Fuzzy sets," *Information and Control*, vol. 8, pp. 338–353, 1965.

[135] M. Ferrari and H. Figulla, "Circulatory assist devices in cardiology," *Deutsche Medizinische Wochenschrift*, vol. 130, no. 12, pp. 652–656, Mar. 2005.

[136] Institute of Medicine (U.S.). Committee on Quality of Health Care in America, *Crossing the Quality Chasm: A New Health System for the 21st Century*. National Academy Press, 2001.

[137] A. X. Garg, N. K. J. Adhikari, H. McDonald, M. P. Rosas-Arellano, P. J. Devereaux, J. Beyene, J. Sam, and R. B. Haynes, "Effects of computerized clinical decision support systems on practitioner performance and patient outcomes: A systematic review," *Journal of the American Medical Association*, vol. 293, no. 10, pp. 1223–1238, Mar. 2005.

[138] A. A. Montgomery, T. Fahey, T. J. Peters, C. MacIntosh, and D. J. Sharp, "Evaluation of computer based clinical decision support system and risk chart for management of hypertension in primary care: randomised controlled trial," *BMJ: British Medical Journal*, vol. 320, Mar. 2000.

[139] W. M. Tierney, J. M. Overhage, M. D. Murray, L. E. Harris, X.-H. Zhou, G. J. Eckert, F. E. Smith, N. Nienaber, C. J. McDonald, and F. D. Wolinsky, "Effects of computerized guidelines for managing heart disease in primary care," *Journal of General Internal Medicine*, vol. 18, no. 12, pp. 967–976, 2003.

[140] M. D. Murray, L. E. Harris, J. M. Overhage, X.-H. Zhou, G. J. Eckert, F. E. Smith, N. N. Buchanan, F. D. Wolinsky, C. J. McDonald, and W. M. Tierney, "Failure of computerized treatment suggestions to improve health outcomes of outpatients with uncomplicated hypertension: Results of a randomized controlled trial," *Pharmacotherapy: The Journal of Human Pharmacology and Drug Therapy*, vol. 24, no. 3, pp. 324–337, 2004.

[141] F. Chiarugi, S. Colantonio, D. Emmanouilidou, D. Moroni, and O. Salvetti, "Biomedical signal and image processing for decision support in heart failure," in *Lecture Notes in Computer Science*, P. Perner and O. Salvetti, Eds. Springer Berlin Heidelberg, 2008, vol. 5108, pp. 38–51.

[142] R. A. Greenes, "Definition, scope, and challenges," in *Clinical Decision Support*, R. A. Greenes, M.D., and P. Ph.D.A2 Robert A. Greenes, M.D., Eds. Burlington: Academic Press, 2007, pp. 3–29.

[143] ——, "Features of computer-based clinical decision support," in *Clinical Decision Support*, R. A. Greenes, M.D., and P. Ph.D.A2 Robert A. Greenes, M.D., Eds. Burlington: Academic Press, 2007, pp. 79–107.

[144] K. Rödel, "Physiological risk assessment for continuously monitored patients using data mining methods," Master's thesis, Technische Universität München, 2011.

[145] I. Yoo, P. Alafaireet, M. Marinov, K. Pena-Hernandez, R. Gopidi, J.-F. Chang, and L. Hua, "Data mining in healthcare and biomedicine: A survey of the literature," *Journal of Medical Systems*, vol. 36, no. 4, pp. 2431–2448, 2012.

[146] D. J. Hand, "Principles of data mining," *Drug Safety*, vol. 30, no. 7, pp. 621–622, 2007.

[147] U. Fayyad, G. Piatetsky-Shapiro, and P. Smyth, "From data mining to knowledge discovery in databases," *AI Magazine*, vol. 17, pp. 37–54, 1996.

[148] J. Han, *Data Mining: Concepts and Techniques*. San Francisco, CA, USA: Morgan Kaufmann Publishers Inc., 2005.

[149] K. J. Cios and W. Moore, "Uniqueness of medical data mining," *Artificial Intelligence in Medicine*, vol. 26, pp. 1–24, 2002.

[150] M. E. Matheny and L. Ohno-Machado, "Generation of knowledge for clinical decision support: Statistical and machine learning techniques," in *Clinical Decision Support*, R. A. Greenes, M.D., and P. Ph.D.A2 Robert A. Greenes, M.D., Eds. Burlington: Academic Press, 2007, pp. 227–248.

[151] R. Ichise and M. Numao, "Learning first-order rules to handle medical data," *NII Journal*, vol. 2, pp. 9–13, 2001.

[152] R. Mikut, M. Reischl, O. Burmeister, and T. Loose, "Data mining in medical time series," *Special Issue: Biosignal Processing (Part 2). Biomedizinische Technik*, vol. 51, pp. 288–293, 2006.

[153] N. Lavrač, "Machine learning for data mining in medicine," in *Artificial Intelligence in Medicine*, ser. Lecture Notes in Computer Science, W. Horn, Y. Shahar, G. Lindberg, S. Andreassen, and J. Wyatt, Eds. Springer Berlin / Heidelberg, 1999, vol. 1620, pp. 47–62.

[154] I. Witten and E. Frank, *Data Mining: Practical Machine Learning Tools and Techniques, Second Edition*, ser. Morgan Kaufmann Series in Data Management Systems. Elsevier Science, 2005.

[155] T. Hastie, R. Tibshirani, and J. Friedman, *The Elements of Statistical Learning: Data Mining, Inference, and Prediction*, 2nd ed. Springer, Aug. 2009.

[156] K. Kira and L. A. Rendell, "The feature selection problem: traditional methods and a new algorithm," in *Proceedings of the tenth national conference on Artificial intelligence*. San Jose, California: AAAI Press, 1992, pp. 129–134.

[157] M. A. Hall, "Correlation-based feature selection for machine learning," Ph.D. dissertation, University of Waikato, 1999.

[158] L. Kaufman and P. Rousseeuw, *Finding groups in data: an introduction to cluster analysis*, ser. Wiley series in probability and mathematical statistics: Applied probability and statistics. Wiley, 1990.

[159] R. Duda, P. Hart, and D. Stork, *Pattern classification*, ser. Pattern Classification and Scene Analysis: Pattern Classification. Wiley, 2001.

[160] T. Mitchell, *Machine Learning*. McGraw Hill, 1997.

[161] T. R. Golub, D. K. Slonim, P. Tamayo, C. Huard, M. Gaasenbeek, J. P. Mesirov, H. Coller, M. L. Loh, J. R. Downing, M. A. Caligiuri, C. D. Bloomfield, and E. S. Lander, "Molecular classification of cancer: class discovery and class prediction by gene expression monitoring," *Science*, vol. 286, no. 5439, pp. 531–537, 1999.

[162] H. Hu, J. Li, A. W. Plank, H. Wang, and G. Daggard, "A comparative study of classification methods for microarray data analysis." in *AusDM*, P. Christen, P. J. Kennedy, J. Li, S. J. Simoff, and G. J. Williams, Eds., vol. 61. Australian Computer Society, 2006, pp. 33–37.

[163] D. Delen, G. Walker, and A. Kadam, "Predicting breast cancer survivability: a comparison of three data mining methods," *Artificial Intelligence in Medicine*, vol. 34, no. 0933-3657 (Linking), pp. 113–127, 2005.

[164] R. Potter, "Comparison of classification algorithms applied to breast cancer diagnosis and prognosis." in *Industrial Conference on Data Mining - Posters and Workshops*, I. Bichindaritz and P. Perner, Eds., 2007, pp. 40–49.

[165] M. L. Mueller, "Data mining methods for medical diagnosis," Dissertation, Technische Universität München, München, 2012.

[166] E. J. Wallis, L. E. Ramsay, I. U. Haq, P. Ghahramani, P. R. Jackson, K. R. Yeo, and W. W. Yeo, "Coronary and cardiovascular risk estimation for primary prevention:validation of a new sheffield table in the 1995 scottish health survey population," *BMJ: British Medical Journal*, vol. 320, no. 7236, pp. 671–676, 2000.

[167] R. J. Stevens, V. Kothari, A. I. Adler, and I. M. Stratton, "The ukpds risk engine: a model for the risk of coronary heart disease in type ii diabetes (ukpds 56)." *Clinical Science*, vol. 101, no. 6, pp. 671–679, 2001.

[168] R. Conroy, K. Pyörälä, A. Fitzgerald, S. Sans, A. Menotti, G. De Backer, D. De Bacquer, P. Ducimetière, P. Jousilahti, U. Keil, I. Njølstad, R. Oganov, T. Thomsen, H. Tunstall-Pedoe, A. Tverdal, H. Wedel, P. Whincup, L. Wilhelmsen, and I. Graham, "Estimation of ten-year risk of fatal cardiovascular disease in europe: the score project," *European Heart Journal*, vol. 24, no. 11, pp. 987–1003, June 2003.

[169] M. Lenz and I. Mühlhauser, "Cardiovascular risk assessment for informed decision making. validity of prediction tools," *Medizinische Klinik*, vol. 99, no. 11, pp. 651–661, Nov. 2004.

[170] J. W. Stephens, G. Ambler, P. Vallance, D. J. Betteridge, S. E. Humphries, and S. J. Hurel, "Cardiovascular risk and diabetes. are the methods of risk prediction satisfactory?" *European Journal of Cardiovascular Prevention & Rehabilitation*, vol. 11, no. 6, pp. 521–528, Dec. 2004.

[171] R. Markgraf, G. Deutschinoff, L. Pientka, and T. Scholten, "Comparison of acute physiology and chronic health evaluations ii and iii and simplified acute physiology score ii: A prospective cohort study evaluating these methods to predict outcome in a german interdisciplinary intensive care unit," *Critical Care Medicine*, vol. 28, no. 1, pp. 26–33, 2000.

[172] D. H. Beck, G. B. Smith, J. V. Pappachan, and B. Millar, "External validation of the saps ii, apache ii and apache iii prognostic models in south england: a multicentre study," *Intensive Care Medicine*, vol. 29, no. 2, pp. 249–256, 2003.

[173] L. Ohno-Machado, F. Resnic, and M. Matheny, "Prognosis in critical care," *Annual Review of Biomedical Engineering*, vol. 8, pp. 567–599, 2006.

[174] A. Kampouraki, G. Manis, and C. Nikou, "Heartbeat time series classification with support vector machines," *IEEE Transactions on Information Technology in Biomedicine*, vol. 13, no. 4, pp. 512–518, 2009.

[175] F. J. Chin, Q. Fang, T. Zhang, and I. Cosic, "A fast critical arrhythmic ecg waveform identification method using cross-correlation and multiple template matching," in *Annual International Conference of the IEEE Engineering in Medicine and Biology Society*, 2010, pp. 1922–1925.

[176] E. Keogh, J. Lin, A. W. Fu, and H. Van Herle, "Finding unusual medical time-series subsequences: Algorithms and applications," *IEEE Transactions on Information Technology in Biomedicine*, vol. 10, no. 3, pp. 429–439, 2006.

[177] K. Wang, L. Wang, D. Wang, and L. Xu, "Svm classification for discriminating cardiovascular disease patients from non-cardiovascular disease controls using pulse waveform variability analysis," in *Lecture Notes in Computer Science*, G. Webb and X. Yu, Eds. Springer Berlin Heidelberg, 2005, vol. 3339, pp. 109–119.

[178] M. Chambrin, S. Charbonnier, S. Sharshar, G. Becq, and L. Badji, "Automatic characterization of events on spo2 signal : comparison of two methods," in *26th Annual International Conference of the IEEE Engineering in Medicine and Biology Society*, vol. 2, 2004, pp. 3474–3477.

[179] M. Imhoff, M. Bauer, U. Gather, and D. Löhlein, "Statistical pattern detection in univariate time series of intensive care on-line monitoring data," *Intensive Care Medicine*, vol. 24, no. 12, pp. 1305–1314, Dec. 1998.

[180] S. Sharshar, L. Allart, and M.-C. Chambrin, "A new approach to the abstraction of monitoring data in intensive care," *Artificial Intelligence in Medicine*, pp. 13–22, 2005.

[181] D. Apiletti, E. Baralis, G. Bruno, and T. Cerquitelli, "Real-time analysis of physiological data to support medical applications," *IEEE Transactions on Information Technology in Biomedicine*, vol. 13, no. 3, pp. 313–321, 2009.

[182] A. King, K. Fortino, N. Stevens, S. Shah, M. Fortino-Mullen, and I. Lee, "Evaluation of smart alarm for intensive care using clinical data," in *International Conference of the IEEE Engineering in Medicine and Biology Society*, 2012.

[183] N. Sprunk, A. Mendoza G, A. Knoll, U. Schreiber, S. Eichhorn, J. Horer, and R. Bauernschmitt, "Hemodynamic regulation using fuzzy logic," in *8th International Conference on Fuzzy Systems and Knowledge Discovery*, vol. 1, 2011, pp. 515–519.

[184] J. Y. Gabor, A. B. Cooper, S. A. Crombach, B. Lee, N. Kadikar, H. E. Bettger, and P. J. Hanly, "Contribution of the intensive care unit environment to sleep disruption in mechanically ventilated patients and healthy subjects," *American Journal of Respiratory and Critical Care Medicine*, vol. 167, no. 5, pp. 708–715, Mar. 2003.

[185] M. A. F. P. Novaes, E. Knobel, A. M. Bork, O. F. Pavão, L. A. Nogueira-Martins, and M. Bosi Ferraz, "Stressors in icu: perception of the patient, relatives and health care team," *Intensive Care Medicine*, vol. 25, no. 12, pp. 1421–1426, 1999.

[186] M. Topf, "Hospital noise pollution: an environmental stress model to guide research and clinical interventions," *Journal of Advanced Nursing*, vol. 31, no. 3, pp. 520–528, 2000.

[187] M.-C. Chambrin, P. Ravaux, D. Calvelo-Aros, A. Jaborska, C. Chopin, and B. Boniface, "Multicentric study of monitoring alarms in the adult intensive care unit (icu): a descriptive analysis," *Intensive Care Medicine*, vol. 25, no. 12, pp. 1360–1366, 1999.

[188] S. Siebig, S. Kuhls, M. Imhoff, J. Langgartner, M. Reng, J. Schölmerich, U. Gather, and C. E. Wrede, "Collection of annotated data in a clinical validation study for alarm algorithms in intensive care – a methodologic framework," *Journal of Critical Care*, vol. 25, no. 1, pp. 128–135, Mar. 2010.

[189] M. Görges, B. A. Markewitz, and D. R. Westenskow, "Improving alarm performance in the medical intensive care unit using delays and clinical context," *Anesthesia & Analgesia*, vol. 108, no. 5, pp. 1546–1552, 2009.

[190] VDE, Ed., *Alarmgebung medizinischer Geräte*, 2010.

[191] M. Imhoff and S. Kuhls, "Alarm algorithms in critical care monitoring," *Anesthesia and Analgesia*, vol. 102, no. 5, pp. 1525–1537, May 2006.

[192] E. Koski, T. Sukuvaara, A. Mäkivirta, and A. Kari, "A knowledge-based alarm system for monitoring cardiac operated patients-assessment of clinical performance," *International Journal of Clinical Monitoring and Computing*, vol. 11, no. 2, pp. 79–83, 1994.

[193] C. Oberli, J. Urzua, C. Saez, M. Guarini, A. Cipriano, B. Garayar, G. Lema, R. Canessa, C. Sacco, and M. Irarrazaval, "An expert system for monitor alarm integration," *Journal of Clinical Monitoring and Computing*, vol. 15, no. 1, pp. 29–35, 1999.

[194] C. L. Tsien, "Event discovery in medical time series data," in *In American Medical Informatics Association (AMIA) Symposium*, 2000.

[195] J. Lipton, M. van Ettinger, R. Barendse, T. van Dam, N. van der Putten, and S. Nelwan, "Alarms on the intensive cardiac care unit," in *Computers in Cardiology*, sept. 2009, pp. 253 –256.

[196] M. Hall, E. Frank, G. Holmes, B. Pfahringer, P. Reutemann, and I. H. Witten, "The weka data mining software: an update," *Special Interest Group on Knowledge Discovery and Data Mining Explorations*, vol. 11, no. 1, pp. 10–18, 2009.